ANALYSIS OF VARIOUS LOADS ON VISCOTHERMOELASTIC STRUCTURES

Thesis Submitted for the Award of the Degree of

DOCTOR OF PHILOSOPHY

in

Mathematics

By

Deepti

Registration Number: 41800444

Supervised By

Dr. Prince (16092)

DEPARTMENT OF MATHEMATICS (Professor)

LOVELY PROFESSIONAL UNIVERSITY, PUNJAB

2025

DECLARATION

I, hereby declare that the presented work in the thesis entitled "**Analysis of Various Loads On Viscothermoelastic Structures**" in fulfilment of the degree of Doctor of Philosophy (Ph.D.) is the outcome of research work carried out by me under the supervision of **Dr. Prince**, working as **Professor**, in the **Department of Mathematics, School of Chemical Engineering and Physical Sciences** of Lovely Professional University, Punjab, India.

In keeping with the general practise of reporting scientific observations, due acknowledgements have been made whenever work described here has been based on the findings of other investigators. This work has not been submitted in part or full to any other University or Institute for the award of any degree.

(Signature of Scholar)

Deepti
Reg. No.: 41800444
Mathematics
School of Chemical Engineering and Physical Sciences
Lovely Professional University,
Punjab, India

CERTIFICATE

This is to certify that the work reported in the Ph.D. thesis entitled "**Analysis of Various Loads On Viscothermoelastic Structures**" submitted in fulfillment of the requirement for the award of degree of Doctor of Philosophy (Ph.D.) in the **Department of Mathematics, School of Chemical Engineering and Physical Sciences**, is a research work carried out by **Deepti**, **41800444**, and is a bonafide record of his/her original work carried out under my supervision and that no part of the thesis has been submitted for any other degree, diploma or equivalent course.

(Signature of Supervisor)

Dr. Prince
Professor
Department of Mathematics
School of Chemical Engineering and Physical Sciences
Lovely Professional University, Punjab

Abstract

The need of structural components, working under thermal and mechanical loading, is rising in the modern engineering. It is essential to understand the performance of these components under transient and steady state conditions. Visco-thermoelastic materials, which exhibit time-dependent deformation due to viscosity and thermal relaxation effects, provide a realistic framework for modeling such conditions. Visco-thermoelastic structures, such as beam and plate resonators, are widely used in microelectromechanical systems (MEMS), and high-precision instrumentation, where both thermal and mechanical fields interact under dynamic service conditions. Traditional elastic or purely thermoelastic models frequently make inaccurate predictions about deflection because they do not account for the effects of material viscosity and finite thermal wave propagation. Through the incorporation of thermal relaxation time, the Lord–Shulman (LS) generalized thermoelasticity framework offers a more accurate description, facilitating improved modeling of both transient and steady-state responses.

The primary objective of this study is to develop and assess mathematical models for predicting deflection in visco-thermoelastic plate and beam resonators under varied loading scenarios. Taking into account the interaction of thermal, mechanical, and viscoelastic effects, the study aims to investigate the deflections of beam resonators and plate resonators under harmonic and uniform loads. The study also highlights the evaluation of mode shapes and their variations for higher modes, tracking the evolution of deflection profiles over time, and examining spatial patterns of deflection across the structure. To create a strong foundation for precise performance prediction in resonator applications, the impact of boundary conditions on the spatial response is evaluated. The thesis is divided into five chapters.

First chapter includes the basics of classical theory of elasticity, viscothermoelasticity and basics of the Lord Shulman (LS) theory of thermoelasticity. The chapter further discusses about transverse vibrations and bending theory in different structures. Also, brief literature survey in the area under study is given.

Second chapter includes the discussion about deflection induced in one-dimensional beam under uniform loading in the framework of LS theory. Displacement vector is

written in accordance with Euler-Bernoulli beam theory. The study is carried out under two cases of static deflection and dynamic deflection by using L.T. w.r.t. spatial variable x and time variable t. Three types of boundary conditions are considered: CC, SS and CF. Method of residues is used for inverse L.T. Graphical results are used to depict the behaviour of deflection across the length of beam and at different time. The static and dynamic deflections are compared in terms of response ratio and is demonstrated graphically also.

Third chapter includes the discussion about deflection in beam under time harmonic load in the context of LS model. Euler-Bernoulli beam theory is employed to write bending moments for viscothermoelastic beams. Temperature distribution function, bending moment and hence deflection are derived post non-dimensionalisation with the use of L.T. Specific types of boundary conditions such as CC, SS and CF are taken. Method of residues is applied for inverse L.T. The numerical results of deflection are demonstrated for different modes using graphical illustration.

Fourth chapter is an extension of work carried out in second chapter. It includes the study of deflection in viscothermoelastic rectangular plate under uniform loading in the framework of LS theory. Displacement vector is written in accordance with Kirchhoff-Love plate theory. Governing equations of heat conduction and bending moments in dimensionless form are solved using L.T. w.r.t. time variable t and FFST w.r.t. spatial variable y. Method of Residues is used for inverse L.T. The study of deflection is carried out under two boundary conditions of CSCS and SSSS plate. Numerical computation and graphical interpretation is carried out using MATLAB. The graphs depict the variation of deflection along the edges of plate at different time and for different modes.

Fifth chapter is an extension of work carried out in third chapter. It includes the study of deflection in viscothermoelastic rectangular plate under time harmonic load. Governing equations of heat conduction and bending moments are written using LS theory and Kirchhoff-Love plate theory. After non-dimensionalisation, the equations are further solved using L.T. w.r.t. time variable t, FFST w.r.t. spatial variable y and method of residues for inverse L.T. The results are displayed graphically using MATLAB, explaining the behaviour of deflection along the edges of SSSS and CSCS rectangular plate.

ACKNOWLEDGEMENT

First and foremost, I want to express my deepest gratitude to my esteemed supervisor, **Dr. Prince**, for his leadership, compassion, determination, inspiration, and unwavering support during my research project. He helped me with every facet of my PhD research.

I would like to extend my sincere thanks to the Head of the Department of Mathematics and the faculty members for providing a supportive and resourceful research environment.

I am indebted to my family for their unconditional love, encouragement, and support. Their belief and confidence in me kept me motivated during challenging times. A special word of thanks to my parents for their innumerable sacrifices and unwavering faith in my academic journey. I am eternally thankful to my colleagues for their love, support, and encouragement throughout my research.

Finally, I thank the Almighty for granting me strength, health, and perseverance to accomplish this work.

Deepti

Contents

List of Symbols and Abbreviations

Symbol	Description
σ_{ij}	Components of stress tensor
e_{ij}	Components of strain tensor
λ and μ	Lames parameters of an elastic material
λ^* and μ^*	Lames parameters of a viscoelastic material
β	Coupling coefficient linking the temperature field to the velocity field
β^*	Coupling coefficient for viscoelastic material
E	Young's Modulus
ν	Poisson ratio
ρ	Density of medium
α_0 and α_1	Viscoelastic relaxation times
t_0	Thermal relaxation time
α_T	Linear thermal expansion coefficient
K	Thermal conductivity
C_e	Specific heat
δ_{ij}	Kronecker's delta function
$u\,(u_1, u_2, u_3)$	Displacement vector
w	Transverse deflection
M	Bending moment
Q_0	Heat source term
L.T.	Laplace Transform
FFST	Finite Fourier Sine Transform
CC	Clamped-Clamped
SS	Simply supported-Simply supported
CF	Clamped-Free
CS	Clamped-Simply supported

List of Figures

List of Tables

Chapter 1

Introduction

1.1 Background

In today's era, driven by advancements in science and technology, the role of materials in supporting various mathematical applications has become increasingly significant. Engineering materials mostly include polycrystalline solids, polymers for various technological developments. These materials are widely utilized as structural components, with their vibrational properties being crucial for practical applications across diverse fields such as aerospace, navigation, medicine, and resonators.

Solid mechanics focuses on understanding how solid materials, particularly elastic ones, behave under the influence of external forces, loads, temperature changes, and other factors. Elasticity specifically examines a material's capacity to return to its original shape once the external forces are removed. The response of elastic materials is analysed in terms of deformation, stress, and strain components. The linear theory of elasticity based on Hooke's Law, is employed to investigate the effects produced by external forces.

Thermoelasticity is an extension of elasticity theory that investigates how temperature changes affect material behaviour. When a material experiences a change in temperature, the thermal energy alters the vibrations of its atoms or molecules. An increase in temperature intensifies these vibrations, which lengthens molecular bonds and causes the material to expand. This thermal expansion or contraction leads to thermal stresses within the material. Additionally, volume changes due to mechanical stress result in temperature changes: compression heats the material, while dilation cools it. Thermoelasticity focuses on understanding how deformation affects temperature distribution and, conversely, how temperature changes influence stress and strain in elastic solids. It examines the dynamic system involving both mechanical work and thermal effects to determine thermomechanical behaviour. Under typical conditions, deformation-induced heat flux creates unsteady heating. For small temperature changes, inertia terms

in elastic equations can be disregarded, but for large or sudden temperature changes, these terms must be considered in the equations of motion.

Viscoelastic materials play a crucial role in solid mechanics. Modern engineering structures are often constructed from materials with complex internal structures, such as polycrystalline materials, amorphous polymers, and fibrous composites. Viscoelastic substances combine both viscous and elastic properties, meaning they exhibit time-dependent strain rates due to their viscosity. When a load is applied and then removed, viscoelastic materials dissipate energy. Their properties change with variations in temperature, as thermal motion influences the deformation of polymers. Consequently, polymer science and the use of plastic materials are essential in applications involving high temperatures.

In the modern material science and engineering, the study and application of thermoelastic and viscothermoelastic materials have become increasingly essential due to their unique ability to dynamically respond to mechanical and thermal factors. Thermoelastic materials exhibit elastic behaviour influenced by temperature changes, while viscothermoelastic materials combine viscous, elastic, and thermal properties. These materials are critical in designing durable, high-performance components across various industries, including aerospace, automotive, civil engineering, and biomedical fields, where components are frequently subjected to fluctuating temperatures and mechanical loads. Understanding the behaviour of these materials helps predict changes in mechanical properties with temperature and responses under different loading conditions over time. This knowledge enables engineers to create accurate models for predicting material performance, leading to better design and optimization of components. Materials with well-understood viscoelastic and thermoelastic properties can be designed for longer life, improved performance, and lower maintenance, ultimately reducing costs and environmental impact.

In the context of elasticity and material science, "Stress is the intensity of internal force acting at a point in a body, defined as the force per unit area." [1]. This internal force per cross section arises to counteract and distribute the external pressures or forces, ensuring the material's equilibrium. "Strain is the relative change in length or angle, produced by stress." [1]. It is a dimensionless quantity. Sokolnikoff [2] studied the deformable bodies and provided the conceptual foundations in the field of elasticity and also derived the relation between stress and strain. Stress tensors σ_{ij} and strain tensors e_{kl} are related through constitutive equations that describe the material's response to deformation. In the context of linear elasticity, this relationship is given by Hooke's Law for isotropic materials. For anisotropic materials having have no symmetry restrictions, the relationship between stress and strain tensors is more complex and involves a

fourth-order stiffness tensor C_{ijkl} with 81 constants.

$$\sigma_{ij} = C_{ijkl} e_{kl}. \tag{1.1}$$

But due to symmetry of stress and strain tensors, these reduces to 21 independent elastic constants. Orthotropic materials, with three mutually perpendicular planes of symmetry, require 9 independent elastic constants: Transversely isotropic material having one axis of symmetry require 5 independent elastic constants. For isotropic materials having same properties in all directions, only 2 independent elastic constants (Young's Modulus E, Poisson ratio ν) are needed. These elastic constants are expressed in terms of Lame' parameters λ and μ as

$$E = \mu \left(\frac{3\lambda + 2\mu}{\lambda + \mu} \right), \quad \nu = \frac{\lambda}{\lambda + \mu}. \tag{1.2}$$

Strain tensor is related to displacement $u = (u_1, u_2, u_3)$ of elastic body and is given by

$$e_{ij} = \left(\frac{u_{i,j} + u_{j,i}}{2} \right), \qquad i, j = 1, 2, 3, ... \tag{1.3}$$

Eliminating the stress tensor using displacement field, we get

$$(\lambda + \mu) \nabla (\nabla . u) + \mu \nabla^2 u = \rho \frac{\partial^2 u}{\partial t^2}. \tag{1.4}$$

The theory contributed significantly in understanding the bending in different types of structures. Elastic beams, plates, vibrating strings and vibrating membranes, can be studied using above model under different initial and boundary conditions. Thermal gradients can cause stress in a material, while elastic waves can lead to heat dissipation. Modelling of such devices is done by combining the theories of heat conduction and linear elasticity. So theory of thermoelasticity is developed. Equation of heat conduction is modified as

$$K \nabla^2 T = \rho C_e \frac{\partial T}{\partial t} + \alpha T_0 (3\lambda + 2\mu) \nabla . \dot{u}. \tag{1.5}$$

Stress tensor is modified as

$$\sigma_{ij} = 2\mu e_{ij} + \lambda \delta_{ij} e_{kk} - \delta_{ij} \alpha (3\lambda + 2\mu)(T - T_0), \tag{1.6}$$

where T_0 is the initial temperature. Biot [3] validated the solutions of thermoelasticity equations for an isotropic homogeneous medium and also calculated the internal damping by taking minimum entropy in account. The theory although has a limitation of

an infinite speed of heat waves. Three types of theories on Thermoelasticity have been developed:

1. Theory of Uncoupled Thermoelasticity,
2. Coupled theory of Thermoelasticity,
3. Generalized theory of Thermoelasticity.

Five models have been introduced in generalized theory of thermoelasticity:

- Lord-Shulman Model (L-S Model),
- Green-Lindsay Model (G-L Model),
- Green-Nagdhi Model (GN Model),
- Chandrasekharaiah Model,
- Tzou (Dual Phase Lag).

1.1.1 Lord-Shulman Model (L-S Model)

Lord and Shulman [5] removed the limitation of [3]. The theory successfully explained the finite rate of propagation of heat waves by involving single relaxation time. The theory formulated the solution using generalized theory and also discussed the effect of relaxation time and coupling constant. The Lord and Shulman model, developed in 1967, presents the first theory of generalized thermoelasticity. The Lord and Shulman model stands out in thermoelasticity by integrating thermal effects and elasticity into a cohesive framework. This theory is significant because it allows for finite speed of propagation by removing the constraint of infinite speed of heat propagation in classical Fourier's law of heat conduction. This model assumes the hyperbolic nature of the heat equation by introducing a relaxation time parameter, which accounts for the delay in heat flow response due to a thermal gradient, meaning the time required to get back to equilibrium after sudden thermal gradient. Considering a single relaxation time, the resulting equation of motion accounts for these small strains and temperature changes. These characteristics make this theory as foundational theory in the study of thermoelastic materials and their dynamic behaviour. This relaxation time is crucial for accurately predicting the behaviour of materials under rapid thermal changes. Under the assumptions of small strains and temperature changes, the equations governing the thermoelastic behaviour are derived. The primary equations involve the displacement field and temperature distribution within the material, coupled through the constitutive

relations that incorporate the thermal and elastic effects.

Lord Shulman model derivation

The fundamental heat equation, based on Fourier's law and energy conservation, is:

$$\rho C_e \frac{\partial T}{\partial t} = K\nabla^2 T + Q_0.$$

To account for thermal relaxation, we can modify Fourier's law by introducing a relaxation time τ:

$$q + \tau\left(\frac{\partial q}{\partial t}\right) = -K\nabla T,$$

where q is the heat flux vector. Combining this with the energy conservation equation leads to the Cattaneo-Vernotte equation, which includes a second-order time derivative of temperature:

$$\rho C_e \left(\frac{\partial T}{\partial t} + \tau\frac{\partial^2 T}{\partial t^2}\right) = K\nabla^2 T + Q_0.$$

In thermoelasticity, temperature changes can induce strains, and conversely, strains can affect the temperature field. This coupling is often represented by a term proportional to the divergence of the displacement or velocity field $\nabla \cdot u$.

Considering further generalization of the Cattaneo-Vernotte equation, including characteristic time, coupling parameter of temperature and velocity field. Also, introducing a heat source term (Q_0) that is dependent on the velocity field:

$$Q_0 = -\beta T_0 \left(\frac{\partial}{\partial t} + t_0\frac{\partial^2}{\partial t^2}\right)(\nabla \cdot u).$$

This form suggests that the heat source is not only influenced by the rate of deformation $\frac{\partial}{\partial t}$ but also by its acceleration $\frac{\partial^2}{\partial t^2}$, possibly reflecting inertial effects in the material's response. Substituting this expression for Q into the Cattaneo-Vernotte equation and replacing τ with t_0:

$$\rho C_e \left(\frac{\partial T}{\partial t} + t_0\frac{\partial^2 T}{\partial t^2}\right) = K\nabla^2 T - \beta T_0 \left(\frac{\partial}{\partial t} + t_0\frac{\partial^2}{\partial t^2}\right)(\nabla \cdot u).$$

The equation governing the heat transfer is

$$K\nabla^2 T = \rho C_e \left(\frac{\partial T}{\partial t} + t_0\frac{\partial^2 T}{\partial t^2}\right) + \beta T_0 \left(\frac{\partial}{\partial t} + t_0\frac{\partial^2}{\partial t^2}\right)\nabla.u. \tag{1.7}$$

The equation of motion subjected to small strains and temperature changes is

$$(\lambda+\mu)\nabla(\nabla.u)+\mu\nabla^2u-\beta\nabla T=\rho\frac{\partial^2u}{\partial t^2}. \tag{1.8}$$

It has been shown in the theory that at considerable high temperature, the relaxation constant becomes very less, so theory reduces to coupled theory of thermoelasticity. Also around absolute temperature, the coupling between temperature and strain becomes insignificant. Solution obtained from generalized theory of elasticity is almost same as obtained from coupled theory with the exception that generalized theory gives a thermal wave front having finite velocity of propagation.

1.1.2 Viscothermoelasticity

Viscothermoelastic materials have great applications in engineering and are found very commonly in the form of rubbers, polymers, tissues, fibre-reinforced materials etc. The properties of viscothermoelastic materials such as time-dependent, temperature-dependent behaviour, heat generation during deformation, response to loads make it an essential part of modern engineering applications. The various fields in which viscothermoelastic materials are being used include aerospace engineering, biomedical engineering and automotive engineering. Researchers are studying these materials for developing more accurate, creative and efficient models. Viscoelastic properties vary with increasing or decreasing temperature, so thermal motion is one factor contributing to the deformation of polymers. Thus polymer science and plastic materials has found wide use in materials under high temperature. Drozdov [11] derived a model for thermoviscoelastic materials and explained the response of viscoelastic materials with respect to temperature changes. Time-dependent stress-strain connections under various thermal circumstances are dealt in the model, considering the impacts of mechanical and thermal interactions. For visco-thermoelastic material, heat equation and equation of motion will be modified as:

$$K\nabla^2T=\rho C_e\left(\frac{\partial T}{\partial t}+t_0\frac{\partial^2T}{\partial t^2}\right)+\beta^*T_0\left(\frac{\partial}{\partial t}+t_0\frac{\partial^2}{\partial t^2}\right)\nabla.u, \tag{1.9}$$

$$\sigma_{ij}=2\mu^*e_{ij}+\lambda^*\delta_{ij}e_{kk}-\beta^*T\delta_{ij},$$

$$(\lambda^*+\mu^*)\nabla(\nabla.u)+\mu^*\nabla^2u-\beta^*\nabla T=\rho\frac{\partial^2u}{\partial t^2}, \tag{1.10}$$

where $\lambda^* = \lambda\left(1+\alpha_0\frac{\partial}{\partial t}\right)$, $\mu^* = \mu\left(1+\alpha_1\frac{\partial}{\partial t}\right)$, $\beta^* = \beta\left(1+\beta_0\frac{\partial}{\partial t}\right)$, and $\beta_0 = (3\lambda\alpha_0 + 2\mu\alpha_1)\frac{\alpha_T}{\beta}$

1.1.3 Transverse Vibrations

The Lord-Shulman (LS) model, which includes the effect of finite thermal wave speed, provides a framework for the analysis of transverse vibrations induced in viscothermoelastic structures. Along with the strings and membranes, beams and plates are also the significant part of the engineering elastic structures. Beam is defined as a structure with its one dimension larger than the other. The one with larger length is defined as axis of beam and cross section normal to the axis is assumed to vary evenly along the length of beam. Beams, in particular, serve as the cornerstone of most physical constructions, forming the backbone of machine parts, automotive frames, girders, and aircraft components. Beam theory provides a better understanding of complex structures at initial stage. The study of transverse vibrations in beams is a vital aspect of structural dynamics, as it is essential for the design and analysis of engineering structures to ensure their safety and efficiency. Transverse vibrations occur when a beam experiences oscillatory motion perpendicular to its longitudinal axis. These vibrations are significant because they can impact the structural integrity and serviceability of the beam. The study of transverse vibrations provides the details of resonant conditions. Beams are designed to oppose bending when subjected to loads. Each beam has its own set of natural frequencies at which it tends to vibrate when disturbed. These frequencies correspond to specific mode shapes, which describe the beam's deformation patterns. The vibration characteristics, including the natural frequencies and mode shapes, are influenced by the beam's boundary conditions. Typical boundary conditions include simply supported, clamped, and free ends, each of which affects the beam's vibrational behaviour differently. Euler-Bernoulli beam theory is commonly used to analyse their transverse vibrations. This theory assumes that sections of the beam maintain a planar configuration and remain normal to the axis throughout the deformation. The displacement in transverse vibrations is perpendicular to the beam's length, and it can be triggered by various factors, such as external forces, initial displacements, or dynamic loading. In contrast to strings and membranes with thickness infinitely small compared to lateral dimensions, in beams and plates the thickness of the structure, cannot be ignored. One of the most useful theories to study beam models is given by Euler and Bernoulli named as Euler-Bernoulli beam theory.

1.1.4 Euler-Bernoulli Beam Theory

Bauchau and Craig [22] provided a thorough explanation of beam structures by providing detailed derivations of the basic equations, boundary conditions, and analytical solutions for a range of loading and support circumstances. When analyzing structures with two dimensions that are significantly smaller than the third, Euler-Bernoulli beam theory is employed. The beam is oriented with its axis aligned along its dominant dimension and the cross-section, which is perpendicular to this axis, is presumed to change gradually in the direction of beam axis. Additionally, it is expected that the cross-section of the beam is symmetric and the bending occurs within this plane of symmetry. Since the bending moment and the material properties of the beam are uniform throughout its length, the beam's deformation is consistent at every point along its axis. The beam just bends to support the weight. According to this notion, the beam cannot twist. Few assumptions that have been made in the theory.

1. The cross-section is infinitely rigid in its own plane, i.e., no deformation occurs in plane of cross-section.

2. The cross-section of a beam remains plane after deformation.

3. The cross-section remains normal to the deformed axis of the beam.

Two rigid body translations and one rigid body rotation are allowed under the first assumption, which relates to the in-plane displacement field. The direct result of it is the loss of the in-plane strain field. The out-of-plane displacement field is covered by the second and third assumptions. A direct result of assumption 3 is the loss of transverse shearing strain. Additionally, assumption 2 directly leads to the variation of axial strains in a linear manner across the cross-section. Combining these three presumptions yields the following expression for the Euler-Bernoulli beam's total displacement field:

$$\left.\begin{aligned} u_1(x,y,z) &= \bar{u}(x) - z\frac{d\bar{w}(x)}{dx} - y\frac{d\bar{v}(x)}{dx}, \\ u_2(x,y,z) &= \bar{v}(x), \\ u_3(x,y,z) &= \bar{w}(x), \end{aligned}\right\} \tag{1.11}$$

where $u_1(x,y,z)$, $u_2(x,y,z)$, $u_3(x,y,z)$ represent displacement of any arbitrary point (x,y,z) along three axes and $\bar{u}(x)$, $\bar{v}(x)$, $\bar{w}(x)$ represent displacement of neutral axis

along three axes. Using displacement field components, strain tensor can be written as:

$$\left.\begin{aligned} e_{yy} &= e_{zz} = e_{yz} = 0, \\ e_{xy} &= e_{xz} = 0, \\ e_{xx} &= \frac{\partial u_1}{\partial x} = \frac{d\bar{u}}{dx} - z\frac{d^2\bar{w}}{dx^2} - y\frac{d^2\bar{v}}{dx^2}. \end{aligned}\right\} \tag{1.12}$$

Stress field in the beam is described by the force and bending moments:

$$\left.\begin{aligned} F_1(x) &= \int_A \sigma_{xx}\, dA, \\ F_2(x) &= \int_A \sigma_{xy}\, dA, \\ F_3(x) &= \int_A \sigma_{xz}\, dA, \end{aligned}\right\} \tag{1.13}$$

$$\left.\begin{aligned} M_2(x) &= -\int_A z\sigma_{xx}\, dA, \\ M_3(x) &= -\int_A y\sigma_{xx}\, dA, \end{aligned}\right\} \tag{1.14}$$

where F_1 is the axial force and $F_2,\ F_3$ are the two transverse shearing forces. $M_2,\ M_3$ are the bending moments acting along normal axes.

According to this theory, the beam's slopes and deflections are minimal. It outlines the way internal and external forces contribute to cause a beam's deflection to vary over time. The beam's equation of motion in the vertical direction is as follows:

$$\frac{\partial^2 M}{\partial x^2} + q = \rho A \frac{\partial^2 w}{\partial t^2}. \tag{1.15}$$

Here M, w and $q(x,t)$ represents the bending moment, transverse deflection and external force respectively in the thin beam undergoing the transverse motion.

1.1.5 Kirchhoff-Love Plate Theory

Bauchau and Craig [22] provided a thorough explanation of plate mechanics by presenting the basic equations, boundary conditions, and analytical solutions for a range of loading and support circumstances. Kirchhoff-Love plate theory is one of the best theories for studying another kind of structure, known as plate or flat structure, which has one dimension that is significantly smaller than the other two. The theory is based on few assumptions.

1. The direction orthogonal to the plate's mid-plane, i.e., normal material line, experience no deformation, making it infinitely rigid across its length.

2. After deformation, the plate's normal material line stays straight and normal to the plate's deformed mid-plane.

Employing the above assumptions, the complete displacement field for plate is given as:

$$\left.\begin{aligned} u_1(x,y,z) &= \bar{u}(x,y) - z\frac{\partial \bar{w}(x)}{\partial x}, \\ u_2(x,y,z) &= \bar{v}(x,y) - z\frac{\partial \bar{w}(x)}{\partial y}, \\ u_3(x,y,z) &= \bar{w}(x,y), \end{aligned}\right\} \tag{1.16}$$

where $u_1(x,y,z)$, $u_2(x,y,z)$ represent in-plane displacement and $u_3(x,y,z)$ represents the transverse dislacement of any arbitrary point of the plate. $\bar{u}(x,y)$, $\bar{v}(x,y)$ represent the in-plane displacement and $\bar{w}(x,y)$ represents the transverse displacement of mid point of normal material line. Using displacement field components, strain tensor can be written as:

$$\left.\begin{aligned} &e_{xz} = e_{yz} = e_{zz} = 0, \\ &2e_{xy} = \frac{\partial \bar{u}}{\partial y} + \frac{\partial \bar{v}}{\partial x} - 2z\frac{\partial^2 \bar{w}}{\partial x \partial y}, \\ &e_{xx} = \frac{\partial \bar{u}}{\partial x} - z\frac{\partial^2 \bar{w}}{\partial x^2},\ e_{yy} = \frac{\partial \bar{v}}{\partial y} - z\frac{\partial^2 \bar{w}}{\partial y^2}. \end{aligned}\right\} \tag{1.17}$$

The strain components diminish in the direction normal to the plate in accordance with first assumption. The diminishing of transverse shear strain components is in line with second assumption.
Stress field in the plate is described by:

$$\left.\begin{aligned} M_1(x,y) &= -\int_A z\sigma_{yy}dA, \\ M_2(x,y) &= -\int_A z\sigma_{xx}dA, \\ M_{12}(x) &= -\int_A z\sigma_{xy}dA, \end{aligned}\right\} \tag{1.18}$$

where M_1, M_2 known as bending moments, are the first moment of in-plane stress components. M_{12} is the first moment of in-plane shear stress component and is known as twisting moment.

1.2 Literature Review

Timoshenko et al. [4] set up the necessary basis for studying the stability, vibration, and bending of shell and plate structures. The theory incorporates shear deformation and rotary inertia effects, which are particularly significant when analyzing thick plates and beams. Nowacki [7] provided the theoretical formulations for the materials with microstructural effects. The author modified the classical elasticity by combining the effects of stresses and micro-rotation. Nowacki [9] outlined the various models for coupled and uncoupled thermoelastic effects and also explored the time-dependent loads. The author offered a thorough analysis of interaction between thermal and mechanical effects under dynamic conditions and analysed the different characteristics.

Chandrasekharaiah [10] outlined the thermoelastic theories which explained the finite speed of thermal waves by replacing the parabolic nature of heat equation by hyperbolic nature. The author has discussed Lord-Shulman model and Green-Lindsay theories in view of above point. These theories introduced the temperature rate or flux rate in the heat equation for accomplishing the finite speed of heat propagation. The review has significantly contributed in the engineering applications. A few limitations where the experimental data is unavailable for useful insights have been mentioned by the author. Drozdov [11] derived a model for thermoviscoelastic materials and explained the response of viscoelastic materials with respect to temperature changes. Time-dependent stress-strain connections under various thermal circumstances are dealt in the model, considering the impacts of mechanical and thermal interactions. Lifshitz [12] explained the damping in thin rectangular beam of micro-scale by offering theoretical basis for conceptualizing energy dissipation caused by irreversible heat flow between compressed and expanded areas. The author also explained the importance of quality factor for designing of resonators at micro-scale.

Ezzat and El-Karamany[13] examined the relaxation effects of volume in viscoelastic material in context of Lord Shulman and Green–Lindsay theory. The authors have used the model to examine the stress distribution and wave propagation in one dimensional problem in the absence or presence of heat sources. Ezzat et al. [14] studied the impact of viscoelastic volume relaxation on thermoelastic responses. The authors utilized a generalized thermoelastic framework that incorporates thermal relaxation time to estimate the behaviour of temperature distribution and wave characteristics due to volume viscosity. Guo and Rogerson [15] explained the impact of thermoelastic coupling on micro-machined resonators. The model developed by author discussed the quality factor, heat flow-induced energy dissipation. Also the model discussed the change in frequency ratio when coupling is ignored. Nayfeh and Younis [16] discussed the

influence of thermoelastic damping on efficiency of MEMS through a numerical and analytical study. The authors explained the impact of geometrical parameters, mode shapes, and material properties on damping by using modal analysis and classical thermoelasticity. Kumar and Choudhary [17] examined the deformation induced in orthotropic micropolar viscoelastic medium due to time-harmonic source. The authors acknowledged the rotational and couple stress effects and derived the analytic solution explaining the deformation fields and wave propagation. Vengallatore [19] investigated the thermoelastic damping and energy dissipation in three-layered laminated composite micro beam resonators and studied the material properties, frequency range for less damping. Kumar and Choudhary [18] demonstrated the importance of Anisotropy and microstructure's effects on wave properties in an orthotropic micropolar viscoelastic medium. The authors made significant observations on micro rotation, displacement, and stress distributions in medium under time-harmonic source.

Sun et al. [20] analysed the thermoelastic damping in micro beam using integral transforms and for different boundary and temperature conditions. The authors discussed the change in deflection, thermal moment and frequency with respect to coupling effect and thickness of beam. Prabhakar and Vengallatore [21] offered valuable insights for enhancing the performance and decreasing damping in view of the changes in material properties and layer interactions. The authors computed the magnitude of damping at different frequencies and computed it to significant at high frequency and negligible at low frequency. Guo et al. [23] examined the dynamic behaviour of axially moving beam with respect to thermoelastic factors. Taking into account variables including axial motion, temperature gradients, and material qualities, the authors solved a mathematical model to study the effect of ratio of length to height, moving speed on beam's stability using the differential quadrature method.

Prabhakar [24] explored the effect of thermoelastic coupling on two-dimensional frequency shifts using Galerkin technique. The authors gave insights on effect of scale, dimensions and material properties. Sun and Saka [25] derived the analytical expressions of thermoelastic damping in circular plate resonator under various boundary conditions and plate dimensions for out-of-plane vibrations. The dimension that corresponds to maximal damping was identified by the authors. The research advances the design of high-Q circular plate resonators. Yanping and Yilong [26] studied the micro-cantilever beam for the static deflection by examining 24 symmetric beams with different dimensions. The impact of size was examined when the neural network is subjected to transverse loading. The study explored the type of relation between vertical bending and beam dimensions and variation. Sharma and Grover [28] investigated the thermoelastic damping in beams with voids, taking into account the coupling of thermal

and mechanical effects, at small scale dimensions. Behaviour of transverse deflection and frequency ratio and critical thickness were discussed by deriving the expressions. Also the authors compared the critical thickness under different boundary conditions. Grover and Sharma [32] examined the behaviour of vibrations in piezothermoelastic beam by developing a model that includes the coupled effect of mechanical, thermal and electrical force. The authors studied the variation in thermal relaxation time, critical thickness and extreme damping. The analysis was represented graphically with the help of MATLAB for different nodes.

Pustan et al. [27] employed finite element analysis and thoroughly examined the impact of geometrical parameters, material characteristics on the mechanical behaviour of flexible MEMS parts. The authors also discussed the deformation induced due to mechanical loading. Youssef and Elsibai [29] examined the impact on the dynamic response of nanoscale structures due to ramp type thermal loading and also highlighted the more accuracy by including the size-dependent effects and thermal relaxation. Grover [31] derived a theoretical model by integrating the mechanical and thermal dissipation mechanisms and also taken beam thickness variations into consideration. The author offered insights into the effect of thickness on the damping and frequency shift. The author made many observations on change in critical thickness due to different modes and under different boundary conditions in view of coupled theory of thermoelasticity and LS model of generalized thermoelasticity. Sharma and Grover [36] examined the thermoelastic effects on the damping due to presence of voids. The authors derived the expressions depicting the effect of voids. The authors highlighted the points indicating the change in peak damping, critical thickness due to voids for different modes and under various boundary conditions. Li et al. [35] shed light on behaviour of damping function under different types of geometry. affects damping properties and quality parameters by contrasting circular and rectangular microplates. The authors developed the model by deriving the expressions for thermoelastic damping for two different shapes.

Guo et al. [33] employed the dual phase lag model to investigate the thermoelastic damping at the micro and nano scale. The authors developed a more precise model for high frequency resonators by taking into account the impact of phase delays in thermal relaxation time and heat conduction. The authors investigated behaviour of heat flux with respect to beam dimensions, aspect ratio and relaxation time. The authors remarked the important observation that at the nanoscale, thermoelastic damping is strongly influenced by the values of thermal relaxation constants and their ratio. Kumar et al. [34] studied the effect of viscosity on wave propagation in an anisotropic thermoelastic media. The authors developed a theoretical framework to understand the wave propagation by taking into account the three phase lag model. The authors com-

puted the different wave characteristics such as phase velocity, attenuation coefficient, specific loss and penetration depth graphically. Xu and Zhou [37] developed theoretical model to study the impact of varying thickness and thermo-mechanical loads on thermal distribution. The authors offered insights on beam deformation and stress profile due to geometry and loading. Ali and Mohammadi [30] investigated the impact of thermoelastic damping on annular microplate vibrational behaviour under CC boundary conditions. The governing equations of the model discussed the effect of material characteristics and geometric features on quality factor. The authors represented the outcomes graphically.

Christensen [38] provided a fundamental resource for examining viscoelastic materials. The study offered a thorough investigation of time dependent deformation and stress relaxation in solids. The author shed light on basic ideas, constitutive models, and analytical methods to study the behaviour of viscoelastic materials behave under varied loading scenarios.Sharma and Grover [41] incorporated both viscosity and thermal influences to study wave propagation in viscothermoelastic material. The author used Kibel number parameter for understanding the behaviour of velocity, attenuation coefficient, specific loss graphically. The authors used correlation coefficient for evaluating the effects of viscosity and also used statistical tools to examine wave behaviour.

Grover [39] investigated the implications of thermoelasticity and viscosity on the transverse vibrational dynamics of micro-scale beam resonators. The model developed by author threw light on effect of quality factor and frequency response due to viscosity and heat conduction. Also the authors made few important highlights about critical thickness, peak damping for different modes in view of coupled theory of thermoelasticity and LS model of generalized thermoelasticity. Lal and Kumar [40] examined the vibrational characteristics of rectangular plate with changing thickness. The authors used Rayleigh-Ritz method to study the responses of natural frequencies and mode shape due to non-homogeneity.

Sharma and Kaur [44] analysed the vibration characteristics in anisotropic thermoelastic beam when exposed to time harmonic load at micro-scale. The study discussed the deflection curve and thermal moment under different boundary conditions and for different modes. The graphs interpreted the deflection curve profile. Sharma and Kaur [43] derived a model that investigate the significant effects of thermal and diffusive relaxation parameters on resonance frequency, mass diffusion, thermomechanical coupling and damping properties. The author analysed the energy dissipation induced by different surface conditions and beam dimensions. The author made important highlights on variation in frequency shift and critical thickness at higher modes.

Zenkour and Abouelregal [45] examined the vibrational behaviour of nanobeams

affected by harmonically fluctuating thermal loads, considering temperature-dependent thermal conductivity and nonlocal elasticity into picture. The authors investigated the effect on temperature, displacement, bending moment, and lateral vibration induced by changes in thermal conductivity and phase lags. The authors identified the nonlocal theories of coupled thermoelasticity and generalized thermoelasticity with a single relaxation time as special case of the present model. Zenkour and Abouelregal [46] investigated the effects of material gradation, sinusoidal pulse-heat conduction, small-scale effects and thermal pulses on vibration characteristics in view of nonlocal thermoelastic model. For a variety of pulse width parameters, the authors compared the LS model of generalized thermoelasticity with the Coupled Theory of Thermoelasticity.

Guo et al. [42] utilized the DPL model of generalized thermoelasticity to investigate the damping and energy dissipation in circular plate resonators. The authors also highlighted the better results due to DPL model by demonstrating the great impact of relaxation time on resonance characteristics. Lal and Saini [50] used generalized differential quadrature (GDQ) method and Kirchhoff's plate theory to create a mathematical model for investigating the vibrational behaviour by taking into account material inhomogeneity and varying thickness. The governing equations obtained by solving the model examined the influence of structural characteristics on natural frequencies and mode shapes. The authors made observations on changes in frequency parameter with nonhomogeneity and thickness parameters. Sharma and Kaur [52] developed a mathematical model that incorporates mechanical and thermal interactions to examine the response of micro-beam to time-dependent external influences. The authors investigated the impact of anisotropy, thermal relaxation, and micro-scale factors on vibration characteristics. The authors made the highlights on resonance criteria and observed the oscillatory response corresponding to dynamic character of loading. Parayil et al. [51] derived analytical and numerical models that investigate impact of beam shape and thermal relaxation parameters on vibration response by employing analytical techniques and finite element simulation. The authors compared the findings derived from analytical approach and numerical technique SEM. The authors analysed the agreement of results from both methods for higher aspect ratio.

Zenkour and Abouelregal [53] addressed the impacts of beam velocity, small-scale effects, and thermal relaxation on vibration characteristics by deriving a mathematical model which takes into account the axial motion, sinusoidal pulse heating, and nonlocal elasticity. The authors examined the response of axially rotating beam under recurring thermal loading. The various observations were made on effect of phase lag, width of pulse and speed of resonator. Also the authors represented the accuracy of results with DPL model by comparing with results with Lord and Shulman (LS) theory, GN theory

and coupled thermoelasticity theory (CTE). Rana and Robin [55] explored the vibrational behaviour of rectangular plates with different thicknesses and inhomogeneous materials under damping effects. The authors derived a model which addressed the vibrations in plate with parabolically varying thickness and studied the effect of damping, non-homogeneity, elastic foundation and taperness.

Grover [48] created a mathematical model to study the energy dissipation in circular plate with a strong focus on the interaction of thermal, elastic and viscous factors. The author investigated the impact of material properties, thickness and relaxation parameters on vibration characteristics. The author made important observations on significant effect of relaxation time, surface conditions on damping. Hoang [49] created a theoretical framework that includes nonlocal elasticity and thermal relaxation effects to examine energy dissipation mechanisms. The author investigated the effects of mode shapes, material characteristics, and temperature parameters on frequency response and damping behaviour. The author evaluated the quality factor and the conditions to improve it.

Abbas [47] utilized Green and Naghdi theory (GNIII) to analyse the free vibrations in a generalized thermoelastic nano beam resonator. Analytical expressions were provided for the deflection, thermal change, frequency changes, and thermoelastic damping. The author offered insights into graphical representation of natural frequencies, damping and frequency shift. Bland [54] provided a reference for complex research on thermoelasticity and viscoelasticity and also discussed the analytical framework for analyzing the damping and deformation in different kind of structures. Zhang et al. [56] explored the effect of size on thermoelastic damping. The authors accounted the material length scale parameter, the phonon mean-free route, and the relaxation time to address the impact of size. The authors used complex-frequency technique and compared the results of damping with pre-existing models. The authors demonstrated the insignificance of nonlocal effect due to length scale parameter. Mashat et al. [59] discussed the effect of viscosity term, laser intensity parameter on thermoelastic field using theory of phase lags. The authors compared the results of different models of thermoelasticity and showed the closeness of results of different models. The authors shed the light on significant role of phase lags on characteristics. The study involved use of L.T. to discuss the effect of sinusoidal pulse heating.

Partap and Chugh [60] thoroughly analysed deflection behaviour of micro-scale beam resonators considering thermoelastic and microstretch effects into account. The authors studied thermal fields and microstructural deformations due to time harmonic load by utilizing micro continuum mechanics and a generalized thermoelasticity model in the thin beam resonators. The authors examined the deflections and dynamic re-

sponse for various boundary conditions. The authors used MATLAB's graphical interpretations to make significant observations about the deflection profiles for various modes. Partap and Chugh [61] examined the microstretch continuum-based rectangular plate structures in relation to thermoelastic damping. The authors explored the impact of plate geometry and microstretch variables on damping characteristics. The authors used Kirchhoff theory to derive the expressions for transverse vibrations in plate under different cases of boundary conditions. Li et al. [58] utilized generalized thermoelastic theories to study the damping behaviour in beam resonators with functionally graded materials. The authors used the layer-wise homogenization technique. and examined the vibration characteristics, thermal and mechanical coupling in the materials with varying properties.

Alghamdi [57] investigated the impact of voids in the framework of DPL thermoelasticity theory. The author offered insights on effect on vibration characteristics due to voids and phase lags and explored the damping under these factors. Liu et al. [63] established a theoretical framework in three dimensions for analyzing thermoelastic damping in resonators made of laminated composite plates. The framework incorporated the effects of anisotropy, multilayered configuration, and thermal-mechanical coupling to determine the expressions of damping. The authors offered insights into the effect of thickness, mode and material properties on the damping. The authors demonstrated the extreme values of damping under different boundary conditions. Grover and Seth [62] developed the study to examine the thermoelastic damping and frequency shift by taking into consideration the viscosity and thermal relaxation. The authors used dual-phase lagging theory to investigate the impact on deflection and wave characteristics due to viscosity and phase lags. Partap and Chugh [67] investigated the damping mechanisms and deflection profile in micro beam resonators within the framework of microstretch thermoelasticity theory. The authors examined the influence of material gradients, microstructural effects like micro-rotations, microstretch parameters and modes on the magnitude of damping for various boundary conditions.

Rao [68] offered a thorough analysis of vibration behaviour in different structures like plates, shells, beams, strings, rods, and membranes. The author developed the conceptual foundations and solution techniques under various boundary and loading conditions. The author shed light on the relevant design practical applications in engineering. Grover and Seth [66] used the dual-phase-lagging theory to present an extensive study of damping behaviour in circular micro-plate resonators. The authors used the micro-scale thermo-mechanical interactions in circular plate and took thermal relaxation and viscous effects into consideration to represent model precisely. The authors examined the impact of time delay, plate dimensions and mechanical relaxation

on the resonance conditions and damping. Zhang et al. [69] focused on the effect of temperature-sensitive mechanical and thermal properties on damping behaviour. The authors discussed the temperature dependence and substantial deviations from classical models at high temperatures. Grover [65] examined the effects of anisotropy, thermoelastic coupling on the damping and resonance characteristics. By considering the CF boundary conditions, the author discussed the change in extreme values of damping and critical thickness through analytical formulations.

Alghamdi [64] investigated the vibration characteristics of circular micro-ceramic plate in the framework of DPL viscothermoelasticity theory. The author explored the effect of viscous and thermal relaxation on damping. Zuo et al. [70] offered a thorough analysis of energy dissipation in microplate resonators made up of three different layers. The authors investigated the effect of temperature distribution, material layering on the damping and also shed light onto difference in energy dissipations among three layers. Pierro [74] explored the efficient combination of viscoelasticity and external control methods to modify the vibration characteristics and studied the vibration suppression by including damping parameters. The author considered the viscoelastic beam under different boundary conditions and shed light on response of beam with respect to dimensionless dimensions and material properties. Youssef [76] took damage parameters and variable thermal conductivity into account and used GN-II theory to study the vibration characteristics. The author demonstrated the significant impact of the parameters. Alghamdi [73] studied the damping and lagging effects in nanoscale structures using DPL model. The author demonstrated the impact on mechanical relaxation time. Abouelrega and Mohammed [71] studied the effect of nonlocal thermoelasticity parameters on mechanical and thermal responses. The author shed light on the dynamic behaviour under these factors. Saeed et al. [75] implemented Green–Lindsay (GL) model to study the thermo-mechanical effects in porous material. The authors adopted finite element method and demonstrated the significant observations on stress and thermal distribution. Alcheikh et al. [72] developed a numerical model to investigate the in-plane air damping in MEMS/NEMS resonators, embedded between two electrodes, to understand the profile of quality factor. Gu and He [79] explored the wave characteristics in Euler–Bernoulli beams within the combined framework of nonlocal theory and Green–Naghdi (GN) theory. The study demonstrated the effects of nonlocal and strain gradient parameters on wave speed and attenuation. Chugh and Partap [78] performed a comprehensive study on thermoelastic damping in microstretch thermoelastic thin circular plates under various boundary conditions. The authors indicated the relation of thermal relaxation time and microstretch parameters with the critical damping value.

Youssef [82] used DPL model to developed a model for studying interactions be-

tween viscosity and thermal conductivity. The authors demonstrated the impact of thickness on thermal conductivity. Abouelregal [77] utilized fractional derivative approach to study the damping in a viscoelastic micro beam, which was exposed to axial load and periodically varying heat. The author analysed the response of beam with respect to mechanical and thermal induced effects. Youssef and El-Bary [81] investigated the vibration characteristics in circular viscothermoelastic microplate resonators due to material degradation in context of DPL theory. The authors discussed the significant effect of ramp heating parameter. Kumar and Kumar [80] implemented two-temperature model to study thermoelastic vibration characteristics, damping in MEMS/NEMS resonators. Alghamdi and Alosaimi [83] investigated the thermal and mechanical reactions in a simply supported silicon nitride visco-thermoelastic nano-beam which was subjected to thermal shock. The authors assessed the characteristics of material, effects of parameters and illustrated the results through figures. Qi et al. [84] used size effects and memory-dependent effects to estimate the thermoelastic responses. The authors derived the analytical solutions to calculate the displacement and stress after considering thermal loading. Grover [86] developed a model to investigate the damping in piezothermoelastic plate resonators with voids. The author assesses the effect of material porosity, piezoelectric effect on damping characteristics. Guha et al. [87] followed the beam theory by Euler-Bernoulli and examined the damping, frequency shift in a micro-scale piezoelectro-magneto-thermoelastic beam. The authors presented the analytical solutions which considered coupling of thermal, magnetic and piezo effects using numerical methods. Singh [89] concentrated on dynamic behaviour of isotropic viscoelastic beam and used GN-III theory, memory-derivative approach to study the effects on vibration characteristics such as deflection, damping and frequency shift. Mungle et al. [88] derived a mathematical formula of deflection in rectangular body under mechanical body. The authors added insights into effect of geometrical parameters on the deflection.

Abouelregal [85] investigated the responses of functionally graded nanobeams subjected to periodic thermal flux using memory-dependent heat conduction models. The author used generalized thermoelasticity theory to explain the effects of thermal memory effects, non-Fourier heat conduction, and material gradation on deflection and stress responses. Youssef and El-Bary [91] studied the effect of mechanical damage on vibrational response of viscothermoelastic rectangular nanobeam subjected to thermal loading. The authors demonstrated the significant effect of these parameters in view of GN-II theory. Duhan et al. [92] evaluated the deflection, volume fraction, temperature distribution by incorporating voids and piezothermoelastic factors. The authors focused on accuracy of MEMS/NEMS applications by discussing void-induced imper-

fections and size-dependent features. Srivastava and Mukhopadhyay [90] thoroughly investigated the piezothermoelastic micro beam resonators by incorporating thermal relaxation effects in dual-phase-lag (DPL) model. The authors studied the effects of coupled mechanical, thermal, and piezoelectric fields and demonstrated the significant change in dynamic responses and thermal wave propagation by DPL model.

Srivastava and Mukhopadhyay[95] offered an analysis of beam resonators using DPL model, nonlocal strain gradient theory and by incorporating transverse isotropy. The authors studied vibration responses in piezothermoelastic beams considering size-dependent mechanical and thermal effects. The authors shed light on the impact on vibration characteristics. Mondal and Sur [93] thoroughly analysed piezothermoelastic microbeams by incorporating memory-dependent effects. The authors studied the effect of mechanical, electrical, and thermal coupling on vibrational behaviour of beam. The authors gave important observations on steady-state and transient responses. Mondal and Sur [94] took size-dependent behaviors into consideration to analyse the dynamic behaviour of piezoelectric microbeams. The authors combined memory-dependent heat conduction with nonlocal elasticity theory and gave significant insights on frequency shifts and damping mechanisms.

1.3 Organization of Thesis

This work aims to find the deflection in different visco-thermoelastic structures under different loading and boundary conditions in the context of Lord-Shulman model of generalized thermoelasticity using L.T., FFST and method of residues.

The first chapter provides an introduction to theory of generalized thermoelasticity along with the bending theory in different structures.

In the second chapter, static and dynamic deflection are derived for visco-thermoelastic beam, in the context of LS model, under uniform loading by using Euler-Bernoulli beam theory. The static and dynamic deflections are compared in terms of response ratio and the results are demonstrated graphically to depict the behaviour of deflection across the length of beam and at different time for different types of boundary conditions such as CC, SS and CF.

In the third chapter, the analytical expression of deflection in visco-thermoelastic beam under harmonic load is derived in the framework of LS model of generalized thermoelasticity. L.T. is used to solve the governing equations of transverse motion of beam and heat conduction. The numerical results of deflection are demonstrated graphically for different modes using MATLAB.

In the fourth chapter, deflection in visco-thermoelastic rectangular plate is studied

under uniform loading in the framework of LS theory. The equations of transverse motion in plate and heat conduction are written by using displacement vector in accordance with Kirchhoff-Love plate theory. L.T. and FFST is used to solve the governing equations. Graphical interpretation is done for deflection under SSSS and CSCS boundary conditions for different modes.

In the fifth chapter, the analytic expression for deflection in visco-thermoelastic rectangular plate under harmonic loading is derived in the framework of LS theory. Kirchhoff-Love plate theory is used to define displacement vector, which is further used in the equation of transverse motion in plate and heat conduction. Integral transforms such as L.T. and FFST are used to derive the deflection. MATLAB is used to demonstrate the deflection profiles under SSSS and CSCS boundary conditions for different modes.

Chapter 2

Static and Dynamic Analysis of Uniform Load on Transverse Vibrations in Visco-thermoelastic Beam

2.1 Introduction

Beam resonators have a significant role in various engineering fields, including micro-electromechanical systems (MEMS), nano-scale sensors and biomedical devices. The study of deflection in viscothermoelastic beams is helpful in understanding the performance, stability and durability of beams which is crucial for estimating the response of beams in the field of manufacturing and construction engineering under different loading scenarios. Designing solid frameworks that can effectively withstand dynamic and thermal stresses requires an understanding of how mechanical forces, temperature changes, and viscoelastic characteristics interact. Viscothermoelastic beams has a vital role as these incorporate the interactions between mechanical stress, temperature effects, and time-dependent formation due to viscous nature, and the beams further exhibit different behaviour under different types of loading.

Ezzat and El-Karamany [13] derived a model for problems involving viscoelastic materials in one-dimension, in the presence or absence of heat sources, in context of generalized thermoelasticity theory, which accounted for relaxation effects. The authors have shared perspectives about volume changes which were driven by thermal effects. Yanping and Hao [26] provided the understanding of the static deflections in beam under transverse loading and compared the static and dynamic deflection. Grover [31] explored the viscothermoelastic micro-scale beam resonators with a focus on beams with linearly varying thickness and provided the crucial insights on the effects of relaxation times, beam dimensions on transverse vibrations under different boundary conditions. Pierro [74] studied the transverse vibrations in viscoelastic beam for controlling the damping.

Existing research has conducted the studies on thermoelastic beam under the dif-

ferent loading conditions for different set of boundary conditions. Some studies have explored the viscothermoelastic beams without considering the influence of external loading. Also some studies depend on classical Fourier heat conduction model, which assumes infinite thermal wave propagation speed. These limitations mandate a theoretical framework that explains the response of viscothermoelastic beam under external loading. This chapter uses the generalized thermoelasticity theory put forth by Lord and Shulman to examine the deflection response of viscothermoelastic resonators under spatially uniform loading. By getting around the drawbacks of the traditional Fourier law, the Lord–Shulman (LS) model adds a single thermal relaxation time, enabling a more accurate depiction of heat transmission. Using the Kelvin–Voigt viscoelastic model, which captures time-dependent material damping effects, the mechanical behaviour is further described. The amalgamation of viscoelasticity and the LS model facilitates a more precise analysis of coupled thermo-mechanical responses, particularly in materials where thermal and mechanical fields develop simultaneously.

2.2 Primary Equations

With the z-axis oriented orthogonal to the plane of isotropy and aligned to the material's axis of symmetry, we examine a homogeneous, transversely isotropic, viscothermoelastic media in a Cartesian coordinate system that was undeformed in the beginning and at a constant temperature T_0. The fundamental equations of motion and heat conduction, along with the fundamental relations derived from the Lord and Shulman (LS) model of generalized thermoelasticity, are analysed under the assumption of no body forces or heat sources. These equations govern the displacement vector $u(x,y,z,t) = (u_1, u_2, u_3)$ and the temperature change $T(x,y,z,t)$ as described:

$$\left.\begin{aligned} \frac{\partial \sigma_{xx}}{\partial x} + \frac{\partial \sigma_{xy}}{\partial y} + \frac{\partial \sigma_{xz}}{\partial z} &= \rho \frac{\partial^2 u_1}{\partial t^2}, \\ \frac{\partial \sigma_{yx}}{\partial x} + \frac{\partial \sigma_{yy}}{\partial y} + \frac{\partial \sigma_{yz}}{\partial z} &= \rho \frac{\partial^2 u_2}{\partial t^2}, \\ \frac{\partial \sigma_{zx}}{\partial x} + \frac{\partial \sigma_{zy}}{\partial y} + \frac{\partial \sigma_{zz}}{\partial z} &= \rho \frac{\partial^2 u_3}{\partial t^2}. \end{aligned}\right\} \tag{2.1}$$

$$\sigma_{ij} = \lambda^* \delta_{ij} e_{kk} + 2\mu^* e_{ij} - \beta^* T \delta_{ij}. \tag{2.2}$$

$$K\nabla^2 T = \rho C_e \left(\frac{\partial T}{\partial t} + t_0 \frac{\partial^2 T}{\partial t^2} \right) + \beta^* T_0 \left(\frac{\partial}{\partial t} + t_0 \frac{\partial^2}{\partial t^2} \right) \nabla . u, \tag{2.3}$$

where

$$\left.\begin{aligned} \lambda^* &= \lambda\left(1+\alpha_0\frac{\partial}{\partial t}\right) \qquad & \mu^* &= \mu\left(1+\alpha_1\frac{\partial}{\partial t}\right) \\ \beta^* &= \beta\left(1+\beta_0\frac{\partial}{\partial t}\right) \qquad & \beta_0 &= \left(3\lambda\alpha_0+2\mu\alpha_1\right)\frac{\alpha_T}{\beta} \end{aligned}\right\} \tag{2.4}$$

Here $\lambda,\ \mu$ represents Lame parameters. $\alpha_0,\ \alpha_1$ are viscoelastic relaxation times, α_T is linear thermal expansion coefficient and $C_e,\ \delta_{ij}$ represent specific heat and Kronecker's delta function respectively.

2.3 Modelling of Beam Structure

Considering a homogeneous, isotropic and viscothermoelastic beam of length L, width b, and thickness h, where $(0 \le x \le L)$, $\left(\frac{-b}{2} \le y \le \frac{b}{2}\right)$, $\left(\frac{-h}{2} \le z \le \frac{h}{2}\right)$ and is examined for flexural deflection induced in it due to uniform load. In its equilibrium state, the beam experiences no stress or strain and is maintained at a stable temperature T_0. Euler-Bernoulli beam theory is used to determine the transverse deflection. In accordance with Euler-Bernoulli assumptions,

1. Being rigid, plane of cross section experience no deformation.

2. After deformation, every beam cross section that was initially normal to the beam's axis stays flat and normal.

The beam experiences deflection about the $x-$ axis only. The width of the beam is extremely small as compared to the other two dimensions. So the deflection along this axis is insignificant, i.e. $u_2 = 0$. The beam does not undergo shear deformation in accordance with second assumption i.e., γ_{xz}, γ_{yz} are insignificant. Also normal strain e_{zz} can be ignored since the deflection is primarily due to bending strains. Considering the above assumptions, the relation between strain and displacement can be reduced to:

$$u_1 = -z\frac{\partial w}{\partial x},\ u_2 = 0,\ u_3 = w(x,t),\ T = T(x,z,t) \tag{2.5}$$

The displacement vector u, temperature function T variables characterize the mechanical and thermal response of beam under the given loading and boundary conditions. Now by substituting the equation (2.5) in equations (2.2) and (2.3), consequently, the resulting equations are as follows:

$$\sigma_{xx} = (\lambda+2\mu)\left(-z\frac{\partial^2 w}{\partial x^2}\right) + (\lambda\alpha_0+2\mu\alpha_1)\left(-z\frac{\partial^3 w}{\partial t\partial x^2}\right) - \beta\left(T+\beta_0\frac{\partial T}{\partial t}\right). \tag{2.6}$$

$$K\left(\frac{\partial^2 T}{\partial x^2}+\frac{\partial^2 T}{\partial z^2}\right)=\rho C_e\left(\frac{\partial T}{\partial t}+t_0\frac{\partial^2 T}{\partial t^2}\right)-\beta^* z T_0\left(\frac{\partial^3 w}{\partial x^2\partial t}+t_0\frac{\partial^4 w}{\partial x^2\partial t^2}\right). \tag{2.7}$$

Also, the flexural moment of cross section $M(x,t)$ due to normal stress σ_{xx} is given as:

$$M(x,t)=-\int_{-h/2}^{h/2} b\sigma_{xx} z dz.$$

Using equation (2.6)

$$M(x,t)=(\lambda+2\mu)\frac{\partial^2 w}{\partial x^2}I+(\lambda\alpha_0+2\mu\alpha_1)\frac{\partial^3 w}{\partial t\partial x^2}I+\beta\left(M_T+\beta_0\frac{\partial M_T}{\partial t}\right). \tag{2.8}$$

Now addressing equation of the beam's transverse motion

$$\frac{\partial^2 M}{\partial x^2}+\rho A\frac{\partial^2 w}{\partial t^2}=q(x,t). \tag{2.9}$$

Using the notations $A=bh$; for the cross-sectional area, $I=\dfrac{bh^3}{12}$; for the moment of inertia of the cross section and $M_T=\displaystyle\int_{-h/2}^{h/2} bTzdz$; for moment of beam due to thermal effects, and using the uniform loading as $q(x,t)=-q_0$. Consequently, arriving at the reduced form of equation of motion for the beam:

$$(\lambda+2\mu)I\frac{\partial^4 w}{\partial x^4}+(\lambda\alpha_0+2\mu\alpha_1)I\frac{\partial^5 w}{\partial t\partial x^4}+\beta\left(\frac{\partial^2 M_T}{\partial x^2}+\beta_0\frac{\partial^3 M_T}{\partial t\partial x^2}\right)+\rho A\frac{\partial^2 w}{\partial t^2}=-q_0. \tag{2.10}$$

Considering non-dimensional quantities

$$x'=\frac{x}{L},\ w'=\frac{w}{h},\ z'=\frac{z}{h},\ t'=\frac{c_1}{L}t,\ {t_0}'=\frac{c_1}{L}t_0,\ T'=\frac{T-T_0}{T_0}.$$

Using the non-dimensional quantities in equations (2.7) and (2.10), we get

$$\frac{1}{12{A_R}^2}\left(\frac{\partial^4 w}{\partial x^4}+\left(\frac{\lambda\alpha_0+2\mu\alpha_1}{\lambda+2\mu}\right)\frac{c_1}{L}\frac{\partial^5 w}{\partial t\partial x^4}\right)+\left(\frac{\beta T_0}{\rho c_1^2}\right)\left(\frac{\partial^2 M_T}{\partial x^2}+\frac{c_1\beta_0}{L}\frac{\partial^3 M_T}{\partial t\partial x^2}\right)+\frac{\partial^2 w}{\partial t^2}=-q_0, \tag{2.11}$$

$$where\quad M_T=\int_{-1/2}^{1/2} Tzdz.$$

$$\left(\frac{\partial^2 T}{\partial x^2}+{A_R}^2\frac{\partial^2 T}{\partial z^2}\right)=\frac{\rho C_e c_1 L}{K}\left(\frac{\partial T}{\partial t}+t_0\frac{\partial^2 T}{\partial t^2}\right)-\frac{zh^2 c_1\beta}{LK}\left(1+\frac{\beta_0 c_1}{L}\frac{\partial}{\partial t}\right)\left(\frac{\partial^3 w}{\partial x^2\partial t}+t_0\frac{\partial^4 w}{\partial x^2\partial t^2}\right), \tag{2.12}$$

where

$$A_R = \frac{L}{h}, {c_1}^2 = \frac{\lambda + 2\mu}{\rho}, q' = \frac{q_0 A_R^2}{b\rho {c_1}^2}. \tag{2.13}$$

(For the sake of convenience, primes are omitted.)

2.4 Preliminary and Boundary Conditions

A beam with both ends either clamped (CC), both simply supported (SS), or one end clamped and the other free (CF) has been considered and the following boundary conditions have been incorporated from [8].

Case I: For CC beam

$$(w(x,t))_{x=0} = \left(\frac{\partial w(x,t)}{\partial x}\right)_{x=0} = 0 \quad \text{and} \quad (w(x,t))_{x=1} = \left(\frac{\partial w(x,t)}{\partial x}\right)_{x=1} = 0, \tag{2.14}$$

Case II: For SS beam

$$(w(x,t))_{x=0} = \left(\frac{\partial^2 w(x,t)}{\partial x^2}\right)_{x=0} = 0 \quad \text{and} \quad (w(x,t))_{x=1} = \left(\frac{\partial^2 w(x,t)}{\partial x^2}\right)_{x=1} = 0, \tag{2.15}$$

Case III: For CF beam

$$(w(x,t))_{x=0} = \left(\frac{\partial w(x,t)}{\partial x}\right)_{x=0} = 0 \quad \text{and} \quad \left(\frac{\partial^2 w(x,t)}{\partial x^2}\right)_{x=1} = \left(\frac{\partial^3 w(x,t)}{\partial x^3}\right)_{x=1} = 0, \tag{2.16}$$

and the initial conditions are considered as

$$(w(x,t))_{t=0} = \left(\frac{\partial w(x,t)}{\partial t}\right)_{t=0} = \left(\frac{\partial^2 w(x,t)}{\partial t^2}\right)_{t=0} = 0, (T(x,z,t))_{t=0} = \left(\frac{\partial T(x,z,t)}{\partial t}\right)_{t=0} = 0. \tag{2.17}$$

2.5 Laplace Transform Technique

Adopting L.T. to the equations (2.11) and (2.12) w.r.t the time domain, defined as:

$$\bar{w}(x,s) = \int_0^\infty e^{-st} w(x,t)\, dt \qquad \text{and} \qquad \bar{T}(x,z,s) = \int_0^\infty e^{-st} T(x,z,t)\, dt,$$

which gives the set of following equations:

$$\frac{1}{12{A_R}^2}\left(1+\frac{(\lambda\alpha_0+2\mu\alpha_1)\,c_1 s}{(\lambda+2\mu)\,L}\right)\frac{\partial^4\bar{w}}{\partial x^4}+\frac{\beta T_0}{\rho{c_1}^2}\left(1+\frac{c_1\beta_0 s}{L}\right)\frac{\partial^2 M_{\bar{T}}}{\partial x^2}+s^2\bar{w}=-\frac{q_0}{s}. \tag{2.18}$$

$$\left(\frac{\partial^2\bar{T}}{\partial x^2}+{A_R}^2\frac{\partial^2\bar{T}}{\partial z^2}\right)=\frac{\rho C_e c_1 L s\,(1+st_0)}{K}\bar{T}-\frac{zh^2c_1\beta s\,(1+st_0)\left(1+\frac{sc_1\beta_0}{L}\right)}{LK}\frac{\partial^2\bar{w}}{\partial x^2}, \tag{2.19}$$

and

$$M_{\bar{T}}=\int_{-h/2}^{h/2}\bar{T}z\,dz. \tag{2.20}$$

Considering the fact that the thermal gradients are much larger along thickness direction than along the axis of beams, i.e., $\dfrac{\partial^2\bar{T}}{\partial x^2}=0$. Also, no heat exchange occurs through the top and bottom exposed areas of the beam.

$$\frac{\partial\bar{T}}{\partial z}=0 \quad \text{at} \quad z=\pm\frac{1}{2}.$$

Under above mentioned conditions, solution of equation (2.19) reduces to

$$\bar{T}(x,z,s)=\frac{\beta\left(1+\frac{sc_1\beta_0}{L}\right)}{C_e\rho A_R^2}\left(z-\frac{\sin pz}{p\cos\left(\frac{p}{2}\right)}\right)\frac{\partial^2\bar{w}}{\partial x^2} \quad \text{where} \quad p^2=-\frac{\rho C_e c_1 L s\,(1+st_0)}{K{A_R}^2}. \tag{2.21}$$

Using equation (2.20) to find $M_{\bar{T}}$ and differentiating twice w.r.t. x

$$\frac{\partial^2 M_{\bar{T}}}{\partial x^2}=\frac{\beta\left(1+\frac{sc_1\beta_0}{L}\right)}{12C_e\rho A_R^2}\left(1+\frac{24}{p^3}\left(\frac{p}{2}-\tan\left(\frac{p}{2}\right)\right)\right)\frac{\partial^4\bar{w}}{\partial x^4}. \tag{2.22}$$

Using the equation (2.22) in (2.18), we get

$$F_s\frac{\partial^4\bar{w}}{\partial x^4}+s^2\bar{w}=-\frac{q_0}{s},$$

where $1+st_0=\gamma_0,\ 1+\frac{sc_1\beta_0}{L}=\gamma_1,\ f(p)=\frac{24}{p^3}\left(\frac{p}{2}-\tan\left(\frac{p}{2}\right)\right),\ \varepsilon_0=\left(\frac{\lambda\alpha_0+2\mu\alpha_1}{\lambda+2\mu}\right)\frac{c_1}{L},$
$\varepsilon_1=\frac{\beta^2T_0}{\rho^2{c_1}^2C_e},\ F_s=\frac{1}{12{A_R}^2}\left(1+\varepsilon_0 s+\varepsilon_1\gamma_1^2\left(1+f(p)\right)\right).$

$$\frac{\partial^4\bar{w}}{\partial x^4}-\eta^4\bar{w}=-\frac{q_0}{sF_s} \quad \text{where} \quad \eta^4=-\frac{s^2}{F_s}. \tag{2.23}$$

2.5.1 Static Analysis

In this scenario, the deflection does not vary with time, implying that $\frac{\partial}{\partial t} = 0$. As a result, the loads applied to the beam under the uniform loading can be expressed $q(x) = -q_0$, so the equation (2.23) reduces to

$$\frac{\partial^4 w_{static}}{\partial x^4} = -\frac{q_0}{F},$$

where $F = \frac{1}{12A_R^2}$.
Partially integrating the above equation four times w.r.t x, we get

$$w_{static} = -\frac{q_0 x^4}{4!\,F} + a_1\frac{x^3}{3!} + a_2\frac{x^2}{2!} + a_3 x + a_4.$$

Using the boundary conditions from $(2.14) - (2.16)$, we get

Case I

$$w_{static} = -\frac{q_0 A_R^2 x^2 (1-x)^2}{2}, \tag{2.24}$$

Case II

$$w_{static} = -\frac{q_0 A_R^2 x \left(x^3 - 2x^2 + 1\right)}{2}, \tag{2.25}$$

Case III

$$w_{static} = -\frac{q_0 A_R^2 x^2 \left(x^2 - 4x + 6\right)}{2}. \tag{2.26}$$

2.5.2 Dynamic Analysis

This section delves into the analysis of beam deflection caused by loads that change over time. Applying L.T. with respect to space domain defined as $\bar{W}(\xi, s) = \int_0^\infty e^{-\xi x}\bar{w}(x,s)\,dx$, equation (2.23) reduces to

$$\left[\xi^4\bar{W} - \xi^3\bar{w}(0,s) - \xi^2\bar{w}'(0,s) - \xi^3\bar{w}''(0,s) - \bar{w}'''(0,s)\right] - \eta^4\bar{W} = -\frac{q_0}{sF_s\xi}. \tag{2.27}$$

Incorporating the conditions at $x = 0$ outlined by equations $(2.14) - (2.16)$ and performing the inverse L.T. w.r.t. space domain

Case I

$$\bar{w}(x,s) = \frac{k_1 C_-(\eta x)}{2\eta^2} + \frac{k_2 S_-(\eta x)s}{2\eta^3} - \frac{q_0}{sF_s}\frac{C_+(\eta x) - 2}{2\eta^4}, \tag{2.28}$$

Case II

$$\bar{w}(x,s) = \frac{k_3 S_+(\eta x)}{2\eta} + \frac{k_4 S_-(\eta x)}{2\eta^3} - \frac{q_0}{sF_s}\frac{C_+(\eta x) - 2}{2\eta^4}, \tag{2.29}$$

Case III

$$\bar{w}(x,s) = \frac{k_5 C_-(\eta x)}{2\eta^2} + \frac{k_6 S_-(\eta x)}{2\eta^3} - \frac{q_0}{sF_s}\frac{C_+(\eta x)-2}{2\eta^4}, \tag{2.30}$$

where

$$C_-(\eta x) = \cosh(\eta x) - \cos(\eta x), \quad S_-(\eta x) = \sinh(\eta x) - \sin(\eta x),$$

$$C_+(\eta x) = \cosh(\eta x) + \cos(\eta x), \quad S_+(\eta x) = \sinh(\eta x) + \sin(\eta x).$$

A system of non-homogeneous linear equations is obtained on incorporating the conditions at $x = 1$ outlined by equations $(2.14) - (2.16)$, and the requirements for ensuring infinite solutions is:

Case I

$$\cos\eta \cosh\eta = 1, \tag{2.31}$$

Case II

$$\sin\eta \sinh\eta = 0, \tag{2.32}$$

Case III

$$\cos\eta \cosh\eta = -1. \tag{2.33}$$

The respective roots of the equations $(2.31) - (2.33)$ are given by:

Case I

$$\eta_1 = 4.730,\ \eta_2 = 7.8532,\ \eta_m = \left(m + \frac{1}{2}\right)\pi, m \geq 3, \tag{2.34}$$

Case II

$$\eta_1 = 3.1416,\ \eta_2 = 6.2832,\ \eta_m = m\pi, m \geq 3, \tag{2.35}$$

Case III

$$\eta_1 = 1.8751,\ \eta_2 = 4.6941,\ \eta_m = \left(m - \frac{1}{2}\right)\pi, m \geq 3. \tag{2.36}$$

and solutions for all the cases of boundary conditions are provided by:

Case I

$$\bar{w}(x,s) = -\frac{q_0}{2s\eta^4 F_s}\left(\frac{A_1(\eta)C_-(\eta x) + B_1(\eta)S_-(\eta x) + G_1(\eta)\left(C_+(\eta x)-2\right)}{G_1(\eta)}\right), \tag{2.37}$$

Case II

$$\bar{w}(x,s) = -\frac{q_0}{4s\eta^4 F_s}\left(\frac{A_2(\eta)S_+(\eta x) + B_2(\eta)S_-(\eta x) + 2G_2(\eta)\left(C_+(\eta x)-2\right)}{G_2(\eta)}\right), \tag{2.38}$$

Case III

$$\bar{w}(x,s) = -\frac{q_0}{2s\eta^4 F_s}\left(\frac{A_3(\eta)C_-(\eta x)+B_3(\eta)S_-(\eta x)+G_3(\eta)\left(C_+(\eta x)-2\right)}{G_3(\eta)}\right), \quad (2.39)$$

where
$A_1(\eta) = \cosh\eta - \cos\eta - \sinh\eta\sin\eta, B_1(\eta) = \sinh\eta\left(\cos\eta - 1\right) + \sin\eta\left(\cosh\eta - 1\right),$
$A_2(\eta) = \sinh\eta\left(1-\cos\eta\right) + \sin\eta\left(1-\cosh\eta\right), B_2(\eta) = \sinh\eta\left(\cos\eta - 1\right) + \sin\eta\left(1-\cosh\eta\right),$
$A_3(\eta) = \sinh\eta\sin\eta, B_3(\eta) = -\left(\cosh\eta\sin\eta + \sinh\eta\cos\eta\right),$
$G_1(\eta) = 1 - \cosh\eta\cos\eta, G_2(\eta) = \sinh\eta\sin\eta, G_3(\eta) = \cosh\eta\cos\eta + 1.$
Making use of method of residues for evaluating Inverse L.T. w.r.t. time domain defined as:

$$w(x,t) = \sum \text{Residues of } e^{st}\bar{w}(x,s). \quad (2.40)$$

Case I

$s = 0$ is simple pole.
Residue at $s = 0$ is given as

$$-\frac{q_0 A_R^2\left(1-x\right)^2 x^2}{2}.$$

Singularities corresponding to $G_1(\eta) = 0$ are also simple poles given by (2.34).
Also, using the relation $\eta^4 = -\frac{s^2}{F_s}, s = \pm\imath {\eta_m}^2\sqrt{F_s} = \pm i s_m,$
Residue at $s = \pm\imath s_m$ is

$$-\frac{q_0 e^{\pm\imath s_m t}}{\pm 2\imath s_m \eta_m^4}\left(\frac{H_1\left(\eta_m x\right)}{F_s G_1'\left(\eta_m\right)\frac{d\eta}{ds}}\right)_{s=\pm\imath s_m}.$$

Solution of deflection in CC beam is given as:

$$w_{dynamic}(x,t) = -\frac{q_0}{2}\left[A_R^2\left(1-x\right)^2 x^2 \mp \imath\frac{e^{\pm\imath s_m t}}{s_m\eta_m^4}\left(\frac{H_1\left(\eta_m x\right)}{F_s G_1'\left(\eta_m\right)\frac{d\eta}{ds}}\right)_{s=\pm\imath s_m}\right], \quad (2.41)$$

where
$s_m = s_0\left(1 + \frac{\varepsilon_0 s_0}{2} + \frac{\varepsilon_1\gamma_{10}^2}{2}\left(1+f_{P0}\right)\right),$
$H_1\left(\eta_m x\right) = A_1(\eta_m)C_-(\eta_m x) + B_1(\eta_m)S_-(\eta_m x) + G_1(\eta_m)(C_+(\eta_m x) - 2),$
$s_0 = \frac{{\eta_m}^2}{2\sqrt{3}A_R},\ \gamma_{10} = \left(1 + \frac{s_0\beta_0 c}{L}\right),\ P_0^2 = \frac{\rho C_e c L s_0\gamma_{10}}{K{A_R}^2}, 1 + f_{P0} = 1 - \frac{12}{P_0^2} + \frac{24\tanh\left(\frac{P_0}{2}\right)}{P_0^3}.$

Case II

$s = 0$ is simple pole.

Residue at $s=0$ is

$$-\frac{q_0 A_R^2 x\left(x^3-2x^2+1\right)}{2}.$$

Singularities corresponding to $G_2(\eta)=0$ are simple poles given by (2.35).
Residue at $s=\pm\iota s_m$ is

$$-\frac{q_0 e^{\pm\iota s_m t}}{\pm 4\iota s_m \eta_m^4}\left(\frac{H_2(\eta_m x)}{F_s G_2'(\eta_m)\frac{d\eta}{ds}}\right)_{s=\pm\iota s_m}.$$

Solution of deflection in SS beam is given as:

$$w_{dynamic}(x,t)=-\frac{q_0}{2}\left[A_R^2 x\left(x^3-2x^2+1\right)\mp\iota\frac{e^{\pm\iota s_m t}}{2s_m\eta_m^4}\left(\frac{H_2(\eta_m x)}{F_s G_2'(\eta_m)\frac{d\eta}{ds}}\right)_{s=\pm\iota s_m}\right], \tag{2.42}$$

where $H_2(\eta_m x)=A_2(\eta_m)S_+(\eta_m x)+B_2(\eta_m)S_-(\eta_m x)+2G_2(\eta_m)(C_+(\eta_m x)-2)$.

Case III

$s=0$ is simple pole,
Residue at $s=0$ is given as:

$$-\frac{q_0 A_R^2\left(x^2-4x+6\right)x^2}{2}.$$

Singularities corresponding to $G_3(\eta)=0$ are also simple poles given by (2.36).
Residue at $s=\pm\iota s_m$ is

$$-\frac{q_0 e^{\pm\iota s_m t}}{\pm 2\iota s_m \eta_m^4}\left(\frac{H_3(\eta_m x)}{F_s G_3'(\eta_m)\frac{d\eta}{ds}}\right)_{s=\pm\iota s_m}.$$

Solution of deflection in CF beam is given as:

$$w_{dynamic}(x,t)=-\frac{q_0}{2}\left[A_R^2\left(x^2-4x+6\right)x^2\mp\iota\frac{e^{\pm\iota s_m t}}{s_m\eta_m^4}\left(\frac{H_3(\eta_m x)}{F_s G_3'(\eta_m)\frac{d\eta}{ds}}\right)_{s=\pm\iota s_m}\right], \tag{2.43}$$

where
$H_3(\eta_m x)=A_3(\eta_m)C_-(\eta_m x)+B_3(\eta_m)S_-(\eta_m x)+G_3(\eta_m)(C_+(\eta_m x)-2)$.
(Values of η_m for SS and CF beams are taken from 2.35 and 2.36 resp.)

2.6 Response Ratio

We can also examine the response ratios for all the cases of boundary condition on beams. The response ratio of the beam have been defined as:

$$R(t) = \frac{w_{dynamic}}{w_{static}}. \tag{2.44}$$

The values of w_{static} and $w_{dynamic}$ have been defined in equations (2.24), (2.41) for CC beam; (2.25), (2.42) for SS beam; and (2.26), (2.43) for CF beam resp.

2.7 Numerical Results and Graphical Explanations

In this section, we give numerical results to investigate the effects of dimensions and boundary conditions on the deflection of a viscothermoelastic beam at different places and times. Viscothermoelastic solid like magnesium has been selected as the material for the beam with its physical properties listed in Table 2.1 from [28].

λ	$2.17 \times 10^{10} N/m^2$
μ	$1.639 \times 10^{10} N/m^2$
ρ	$1.74 \times 10^{3} Kg/m^3$
C_e	$1.04 \times 10^{3} JKg^{-1}deg^{-1}$
T	$298^o K$
K	$170 Wm^{-1}deg^{-1}$
$\alpha_0 = \alpha_1$	0.779×10^{-9}
β	2.68×10^{6}
q_0	2×10^{-7}

Table 2.1: Physical properties of magnesium

For the numerical computations, beam specifications are taken as $L = 100\mu m$, $b = 5\mu m$ and $h = 2\mu m$. Using the relation $t_0 = s_0^{-1}$, the non-dimensional relaxation time value is calculated. The values are given as $t_0 = 7.7417, 17.5493, 49.262$ for the first mode and $2.8084, 4.3873, 7.8606$ for the second mode, and $1.4326, 1.9499, 2.8073$ for the third mode, for the above considered boundary conditions, respectively. The equations $(2.41) - (2.44)$ have been used to evaluate the non-dimensional deflection and response ratio for few modes. The MATLAB program has been used for carrying out

the numerical calculations. The response ratio and deflection visualizations have been shown in Figures $[2.1 - 2.12]$.

2.7.1 Case I

Figure $[2.1]$ reveals the behaviour of deflection in CC beam, analysed over various axial distances (x) at different times. The variation for deflection v/s axial distance has been obtained at the time $t = 7.7417, 10, 18$. The deflection curves are symmetrical around the beam's midpoint, and extremities of the beam are observed to give significant responses. It is noted that the maximum deflection w_{max} increases as the time increases. Figure $[2.2]$ depicts the change in deflection in CC beam, analysed over time (t). The variation for deflection v/s time has been obtained at the points $x = 0.15, 0.30, 0.50, 0.75$. The deflection curves are symmetrical around the beam's midpoint, and significant responses are observed at the ends of the beam. Deflection curves follow periodic pattern with time. It is found that the maximum deflection w_{max} grows as the time grows. It has been remarked that deflection curve attains its peak value at middle spot of beam and deflection reduces as it shifts away from it in either direction. Figure $[2.3]$ shows the deflection curves over axial distance for first three modes at $t = 7.7417$. The difference in deflection values is more significant from first to second as compared to when we go from second mode to third mode. Figure $[2.4]$ depicts the variation of response-ratio v/s time at the middle point of beam $x = 0.5$. The curve follows oscillatory behaviour. The peaks in Figure $[2.2]$ and $[2.4]$ has been observed at same time.

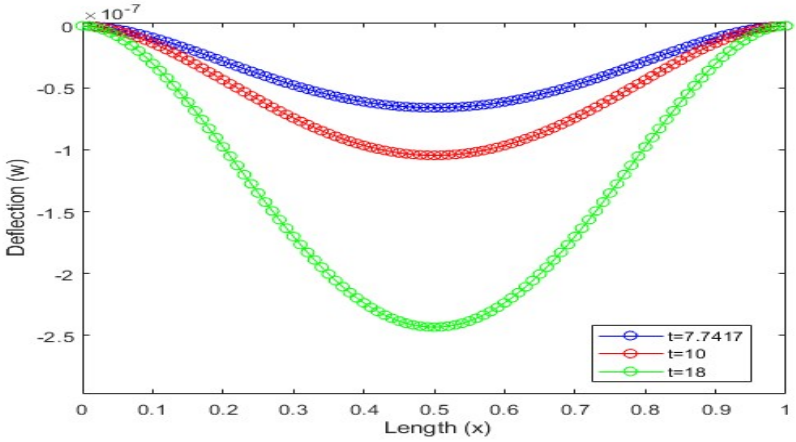

Figure 2.1: Deflection (w) in CC Viscothermoelastic beam vs length (x) at various times for first mode.

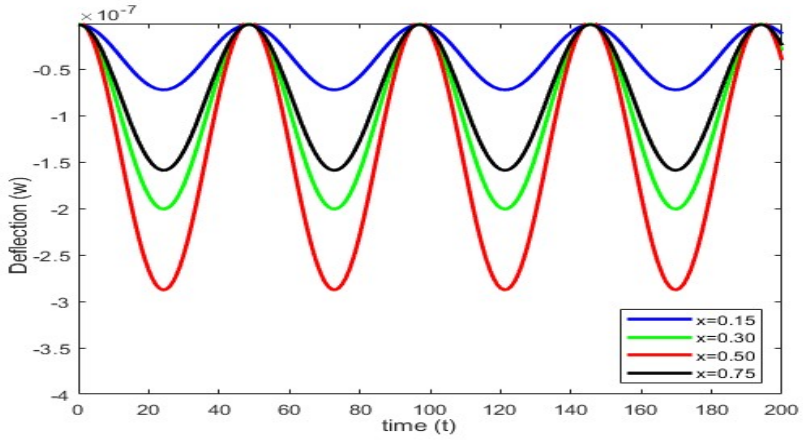

Figure 2.2: Deflection (w) in CC Viscothermoelastic beam vs time (t) at various lengths for first mode.

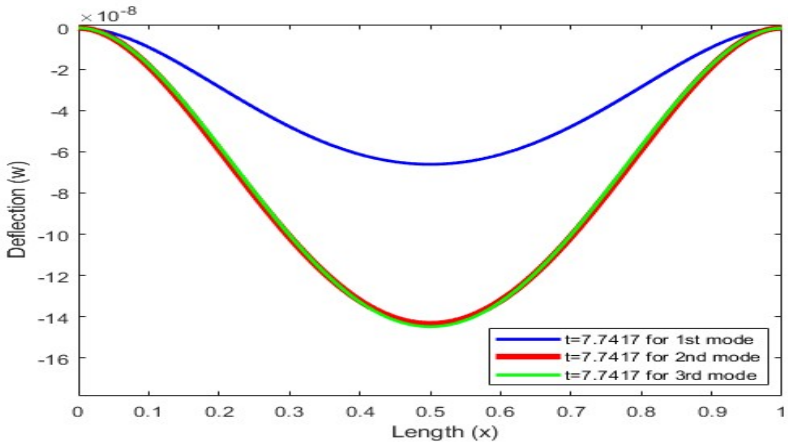

Figure 2.3: Deflection (w) in CC Viscothermoelastic beam vs length (x) for first three modes.

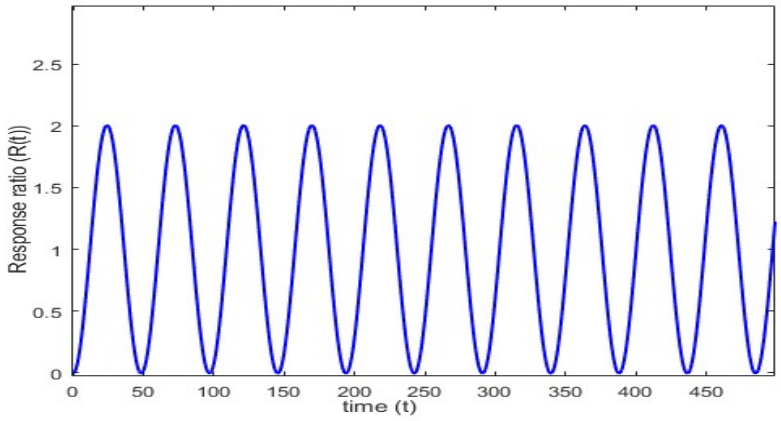

Figure 2.4: Response-ratio $(R(t))$ in CC Viscothermoelastic beam vs time (t) at mid point of beam for first mode.

2.7.2 Case II

Figure$[2.5-2.8]$ illustrate the transition of deflection and response ratio in a viscothermoelastic beam under SS boundary conditions. The variation for deflection v/s axial distance has been obtained at the time $t = 10, 17.5493, 30$. The deflection curves are found almost same as the CC beam except that more symmetry is observed in SS beam and deflection is more pronounced at the ends of beam in CC beam as compared to SS beam. Figure $[2.7]$ shows the deflection curves over axial distance for first three modes at $t = 17.5493$. Here also, it has been remarked that changes in deflection are insignificant for higher modes. Figure $[2.8]$ depicts the same oscillatory pattern as that was in CC beam except that period of curve is changed. Here also, the peaks of Figure $[2.6]$ and $[2.8]$ has been observed at same time.

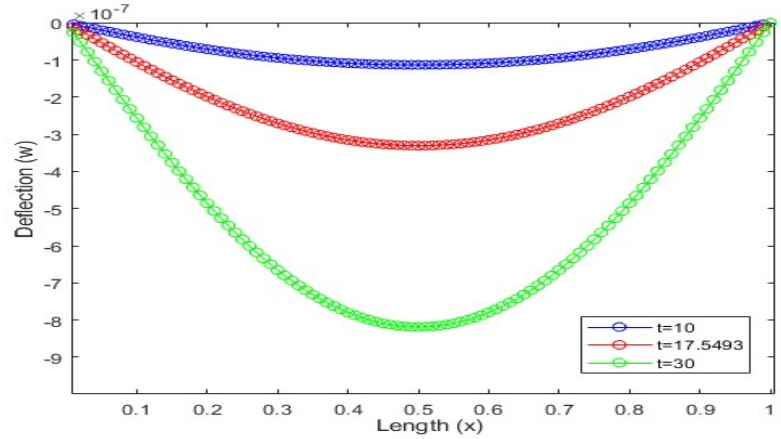

Figure 2.5: Deflection (w) in SS Viscothermoelastic beam vs length (x) at various times for first mode.

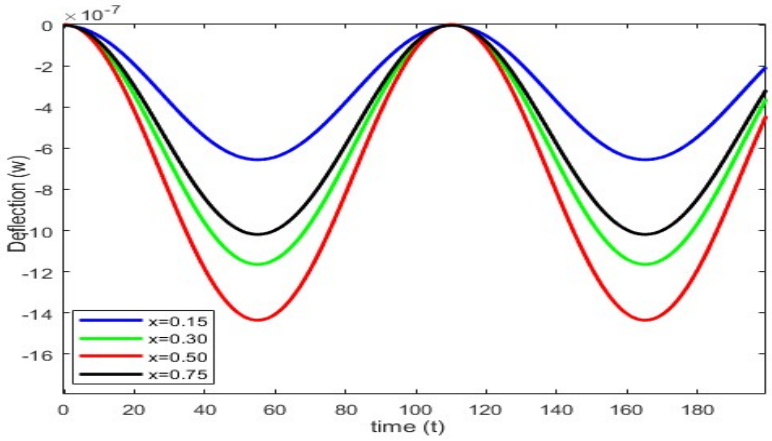

Figure 2.6: Deflection (w) in SS Viscothermoelastic beam vs time (t) at various lengths for first mode.

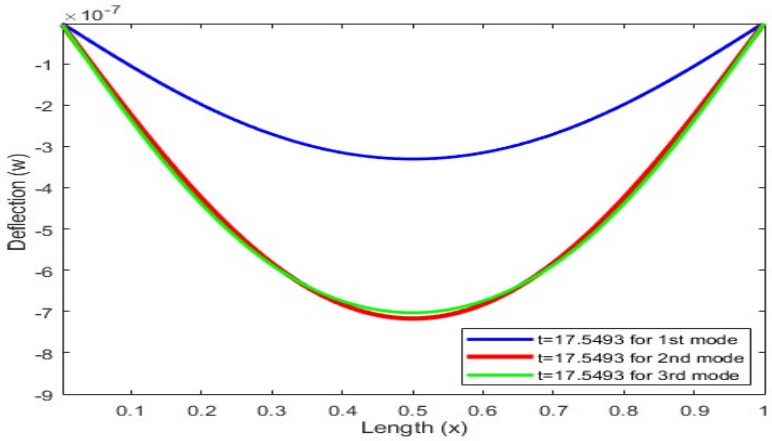

Figure 2.7: Deflection (w) in SS Viscothermoelastic beam vs length (x) for first three modes.

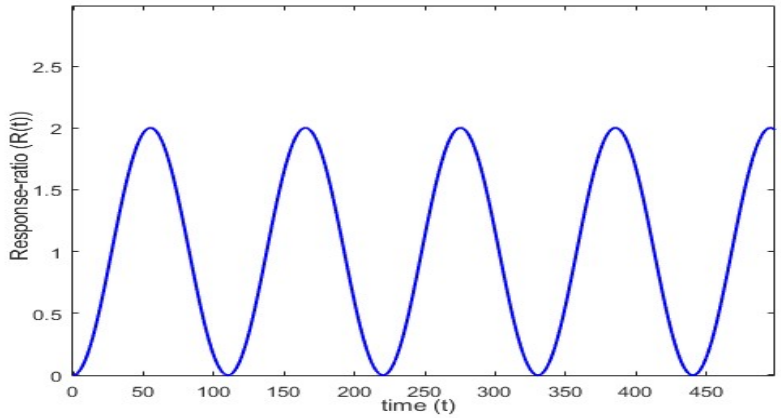

Figure 2.8: Response-ratio $(R(t))$ in SS Viscothermoelastic beam vs time (t) at mid point of beam for first mode.

2.7.3 Case III

Figure $[2.9-2.12]$ reveals the transition of deflection and response ratio in a viscothermoelastic beam under CF boundary conditions. The variation for deflection v/s axial distance has been obtained at the time $t = 20, 49.262, 60$. Deflection profile observes different pattern in case of CF beam. The deflection increases with axial distance and found to attain maximum value at the right (free) end of beam. Figure $[2.11]$ shows the deflection curves over axial distance for first three modes at $t = 49.262$. Figure $[2.12]$ depicts the same oscillatory pattern with larger time period.

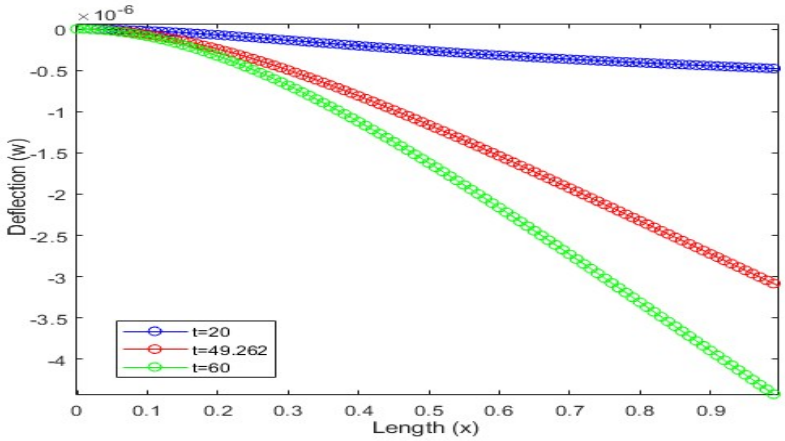

Figure 2.9: Deflection (w) in CF Viscothermoelastic beam vs length (x) at various times for first mode.

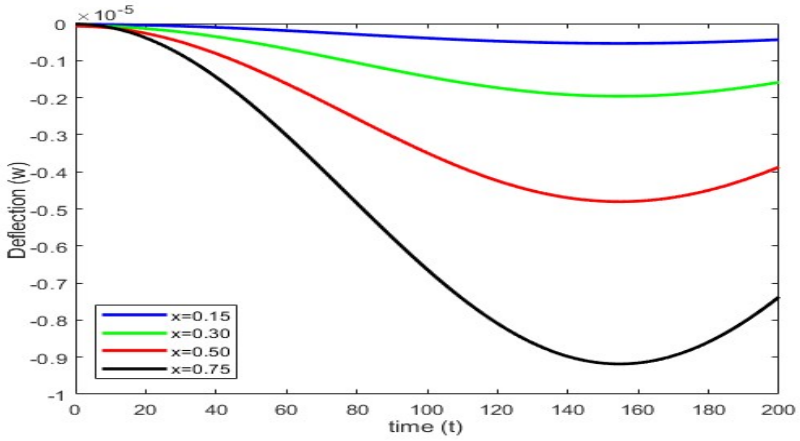

Figure 2.10: Deflection (w) in CF Viscothermoelastic beam vs time (t) at various lengths for first mode.

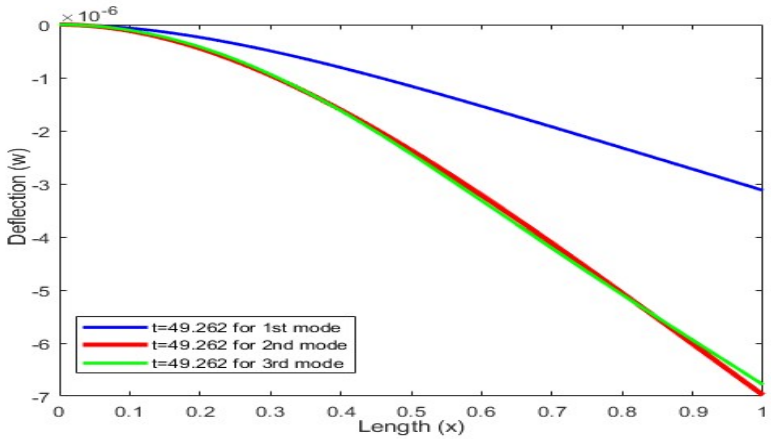

Figure 2.11: Deflection (w) in CF Viscothermoelastic beam vs length (x) for first three modes.

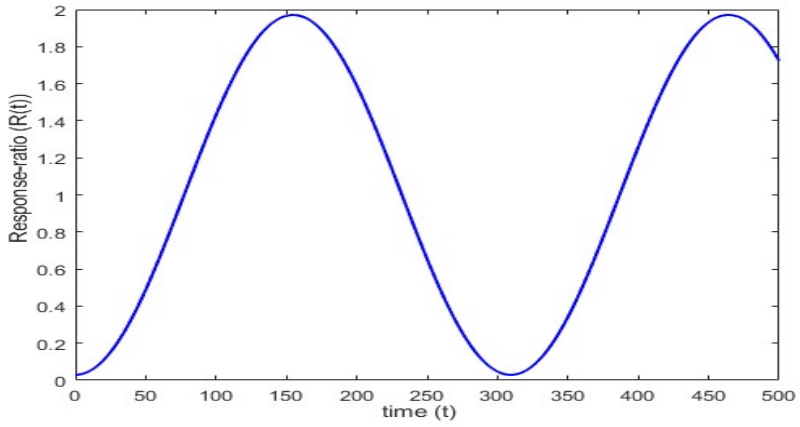

Figure 2.12: Response-ratio $(R(t))$ in CF Viscothermoelastic beam vs time (t) at mid point of beam for first mode.

2.8 Conclusion

The analytical expressions for transverse vibrations in isotropic viscothermoelastic beam under uniform load are derived. The cases of different boundary conditions CC, SS and CF has been discussed under the uniform load. It is found that for the CC and SS boundary conditions, the deflection curves are oriented symmetrically around the beam's mid point, while in CF beam, deflection is found to attain maximum value at the right end of beam. The changes in deflection is insignificant for higher nodes in all cases of boundary conditions. Oscillatory pattern is observed in response-ratio profiles at the beam's midpoint with different time period in different boundary conditions.

Electronic devices especially MEMS-based sensors and actuators will be greatly impacted by these findings as these devices require precise control of mechanical deformation. In situations where mechanical, thermal, and electrical interactions are interrelated, the study offers insightful information about optimizing the performance.

Chapter 3

Analysis of Deflection in Visco-thermoelastic Beam Resonators subjected to Harmonic Loading

3.1 Introduction

The previous chapter provides the understanding of long-term deformation due to static loading. But there are numerous resonator systems in practical applications that function under time-varying excitations, including periodic or harmonic forces. Dynamic loads induce oscillatory deflections and can profoundly affect the stability, resonance properties, and fatigue lifespan of the structure. This chapter investigates the deflection behaviour of viscothermoelastic resonators subjected to harmonic loading, utilizing the Lord–Shulman (LS) model. The LS model, which integrates a finite heat conduction speed through a thermal relaxation time, is employed to more precisely represent the transient thermal field under dynamic loading conditions.

Sharma and Kaur [44] studied the effect of harmonic concentrated load on thermoelastic beam and analysed the transverse deflection and thermal moment. Sharma and Kaur [52] discussed the influence of time varying load on homogeneous, transversely isotropic, thermoelastic micro beam resonator and explored the dynamic response by considering CC conditions at axial ends. Partap and Chugh [60] incorporated micropolar microstretch effects and investigated the flexural vibrations under the influence of time harmonic load in homogeneous isotropic thermoelastic thin beam resonators at different boundary conditions of CC, SS, or CF. In this chapter, the behaviour of homogeneous isotropic visco-thermoelastic beam is analysed when acted upon by harmonic (time varying) load and expression of transverse deflection is derived for different set of boundary conditions of CC, SS or CF.

3.2 Primary Equations

A homogeneous isotropic, viscothermoelastic beam has been considered which is initially at uniform temperature T_0 and is undeformed. The basic equation of motion has been considered in Cartesian coordinate system and is given by

$$\sigma_{ij,\ j} = \rho \frac{\partial^2 u_i}{\partial t^2}. \tag{3.1}$$

In context of Lord Shulman [5] model of generalized thermoelasticity, the equation of heat conduction along with the constitutive relations, in the absence of heat sources and body forces, which govern the displacement vector $u = (u_1, u_2, u_3)$ and temperature change $T(x,y,z,t)$ at time t are given as

$$\sigma_{ij} = \lambda^* \delta_{ij} e_{kk} + 2\mu^* e_{ij} - \beta^* T \delta_{ij}. \tag{3.2}$$

$$K\nabla^2 T = \rho C_e \left(\frac{\partial T}{\partial t} + t_0 \frac{\partial^2 T}{\partial t^2} \right) + \beta^* T_0 \left(\frac{\partial}{\partial t} + t_0 \frac{\partial^2}{\partial t^2} \right) \nabla . u, \tag{3.3}$$

where

$$\lambda^* = \lambda \left(1 + \alpha_0 \frac{\partial}{\partial t} \right) \qquad \mu^* = \mu \left(1 + \alpha_1 \frac{\partial}{\partial t} \right),$$

$$\beta^* = \beta \left(1 + \beta_0 \frac{\partial}{\partial t} \right) \qquad \beta_0 = (3\lambda\alpha_0 + 2\mu\alpha_1) \frac{\alpha_T}{\beta}. \tag{3.4}$$

3.3 Modelling of Beam Structure

We consider a homogeneous isotropic, viscothermoelastic beam of length L, width b, and thickness h, where $(0 \le x \le L), \left(\frac{-b}{2} \le y \le \frac{b}{2} \right), \left(\frac{-h}{2} \le z \le \frac{h}{2} \right)$. In equilibrium, the beam is under zero stress, zero strain and also kept at stable temperature T_0. In accordance with Euler-Bernoulli assumptions, the displacement vector u and temperature function T are given as:

$$u_1 = -z \frac{\partial w}{\partial x},\ u_2 = 0,\ u_3 = w(x,t),\ T = T(x,z,t). \tag{3.5}$$

Now by inserting the equation (3.5) in equations (3.2) and (3.3), we get the following set of equations:

$$\sigma_{xx} = (\lambda + 2\mu) \left(-z \frac{\partial^2 w}{\partial x^2} \right) + (\lambda\alpha_0 + 2\mu\alpha_1) \left(-z \frac{\partial^3 w}{\partial t \partial x^2} \right) - \beta \left(T + \beta_0 \frac{\partial T}{\partial t} \right). \tag{3.6}$$

$$K\left(\frac{\partial^2 T}{\partial x^2}+\frac{\partial^2 T}{\partial z^2}\right)=\rho C_e\left(\frac{\partial T}{\partial t}+t_0\frac{\partial^2 T}{\partial t^2}\right)-\beta^* z T_0\left(\frac{\partial^3 w}{\partial x^2\partial t}+t_0\frac{\partial^4 w}{\partial x^2\partial t^2}\right). \tag{3.7}$$

Also, the flexural moment of cross section $M(x,t)$ is represented as:

$$M(x,t)=-\int_{-h/2}^{h/2} b\sigma_{xx} z dz.$$

Using equation (3.6)

$$M(x,t)=(\lambda+2\mu)\frac{\partial^2 w}{\partial x^2}I+(\lambda\alpha_0+2\mu\alpha_1)\frac{\partial^3 w}{\partial t\partial x^2}I+\beta\left(M_T+\beta_0\frac{\partial M_T}{\partial t}\right), \tag{3.8}$$

where $I=\dfrac{bh^3}{12}$ and $M_T=\displaystyle\int_{-h/2}^{h/2} bTzdz$ represents moment of inertia of the cross section and moment of beam due to thermal effects respectively. Now taking up the equation of transverse motion of beam

$$\frac{\partial^2 M}{\partial x^2}+\rho A\frac{\partial^2 w}{\partial t^2}=q(x,t), \tag{3.9}$$

where $A=bh$ represents area of the cross-section and $q(x,t)$ represents harmonic loading on beam. So the equation of motion of beam reduces to:

$$(\lambda+2\mu)I\frac{\partial^4 w}{\partial x^4}+(\lambda\alpha_0+2\mu\alpha_1)I\frac{\partial^5 w}{\partial t\partial x^4}+\beta\left(\frac{\partial^2 M_T}{\partial x^2}+\beta_0\frac{\partial^3 M_T}{\partial t\partial x^2}\right)+\rho A\frac{\partial^2 w}{\partial t^2}=q(x,t). \tag{3.10}$$

Considering non-dimensional quantities

$$x'=\frac{x}{L},\ w'=\frac{w}{h},\ z'=\frac{z}{h},\ t'=\frac{c_1}{L}t,\ {t_0}'=\frac{c_1}{L}t_0,\ T'=\frac{T}{T_0}.$$

Using the non-dimensional quantities in equations (3.7) and (3.10), we get

$$\frac{1}{12{A_R}^2}\left(\frac{\partial^4 w}{\partial x^4}+\frac{{\delta_1}^2 c_1}{L}\frac{\partial^5 w}{\partial t\partial x^4}\right)+\bar{\beta}\left(\frac{\partial^2 M_T}{\partial x^2}+\frac{c_1\beta_0}{L}\frac{\partial^3 M_T}{\partial t\partial x^2}\right)+\frac{\partial^2 w}{\partial t^2}=q, \tag{3.11}$$

$$\text{where}\quad M_T=\int_{-1/2}^{1/2} Tzdz.$$

$$\left(\frac{\partial^2 T}{\partial x^2}+{A_R}^2\frac{\partial^2 T}{\partial z^2}\right)=\frac{\rho C_e c_1 L}{K}\left(\frac{\partial T}{\partial t}+t_0\frac{\partial^2 T}{\partial t^2}\right)-\frac{zh^2 c_1\beta}{LK}\left(1+\frac{\beta_0 c_1}{L}\frac{\partial}{\partial t}\right)\left(\frac{\partial^3 w}{\partial x^2\partial t}+t_0\frac{\partial^4 w}{\partial x^2\partial t^2}\right), \tag{3.12}$$

where

$$A_R = \frac{L}{h}, {c_1}^2 = \frac{\lambda + 2\mu}{\rho}, {c_2}^2 = \frac{\mu}{\rho}, {c_3}^2 = \frac{\lambda\alpha_0 + 2\mu\alpha_1}{\rho}, \delta^2 = \frac{{c_2}^2}{{c_1}^2}, {\delta_1}^2 = \frac{{c_3}^2}{{c_1}^2}, \bar{\beta} = \frac{\beta T_0}{\rho {c_1}^2}, q' = \frac{qL^2}{Ah\rho {c_1}^2}. \tag{3.13}$$

(Ignoring the primes for the sake of convenience.)

3.4 Initial and Boundary Conditions

A beam whose edges are either CC, SS or CF has been considered and the following conditions have been taken into account. We consider the initial conditions to be:

$$w(x,0) = \left(\frac{\partial w(x,t)}{\partial t}\right)_{t=0} = 0, \left(\frac{\partial^2 w(x,t)}{\partial t^2}\right)_{t=0} = k(\text{constant}), T(x,z,0) = \left(\frac{\partial T(x,z,t)}{\partial t}\right)_{t=0} = 0.$$

Boundary conditions from [8] are considered as:

Case I: For CC beam

$$w(0,t) = \left(\frac{\partial w(x,t)}{\partial x}\right)_{x=0} = 0 \quad \text{and} \quad w(1,t) = \left(\frac{\partial w(x,t)}{\partial x}\right)_{x=1} = 0, \tag{3.14}$$

Case II: For SS beam

$$w(0,t) = \left(\frac{\partial^2 w(x,t)}{\partial x^2}\right)_{x=0} = 0 \quad \text{and} \quad w(1,t) = \left(\frac{\partial^2 w(x,t)}{\partial x^2}\right)_{x=1} = 0, \tag{3.15}$$

Case III: For CF beam

$$w(0,t) = \left(\frac{\partial w(x,t)}{\partial x}\right)_{x=0} = 0 \quad \text{and} \quad \left(\frac{\partial^2 w(x,t)}{\partial x^2}\right)_{x=1} = \left(\frac{\partial^3 w(x,t)}{\partial x^3}\right)_{x=1} = 0. \tag{3.16}$$

3.5 Laplace Transform Approach

We apply L.T. to the equations (3.11) and (3.12) w.r.t the time domain, defined as:

$$W(x,s) = \int_0^\infty e^{-st} w(x,t)\, dt \qquad \text{and} \qquad \Theta(x,z,s) = \int_0^\infty e^{-st} T(x,z,t)\, dt.$$

$$\frac{1}{12{A_R}^2}\left(1 + \frac{{\delta_1}^2 c_1 s}{L}\right)\frac{\partial^4 W}{\partial x^4} + \bar{\beta}\left(1 + \frac{c_1\beta_0 s}{L}\right)\frac{\partial^2 M_\Theta}{\partial x^2} + s^2 W = Q. \tag{3.17}$$

$$\left(\frac{\partial^2 \Theta}{\partial x^2} + {A_R}^2 \frac{\partial^2 \Theta}{\partial z^2}\right) = \frac{\rho C_e c_1 L s \gamma_0}{K}\Theta - \frac{z h^2 c_1 \beta \gamma_0 \gamma_1 s}{LK}\frac{\partial^2 W}{\partial x^2}, \tag{3.18}$$

where

$$1+st_0=\gamma_0,\quad 1+\frac{sc_1\beta_0}{L}=\gamma_1,\quad M_\Theta=\int_{-1/2}^{1/2}\Theta z dz. \tag{3.19}$$

$Q(x,s)$ is the L.T. of load $q(x,t)$.
Solving equation (3.18) under the conditions that thers is no heat transfer across the top and bottom surfaces of beam, i.e., for

$$z=\pm\frac{1}{2},\quad \frac{\partial\Theta}{\partial z}=0.$$

Using above conditions, we get

$$\Theta(x,z,s)=\frac{h^2\beta\gamma_1}{C_eL^2\rho}\left(z-\frac{\sin pz}{p\cos\left(\frac{p}{2}\right)}\right)\frac{\partial^2W}{\partial x^2}, \tag{3.20}$$

where

$$p^2=-\frac{\rho C_e c_1 Ls\gamma_0}{K{A_R}^2}.$$

Using equation (3.19) to find M_Θ and differentiating twice w.r.t. x

$$\frac{\partial^2M_\Theta}{\partial x^2}=\frac{h^2\beta\gamma_1}{12C_eL^2\rho}(1+f(p))\frac{\partial^4W}{\partial x^4}, \tag{3.21}$$

where

$$f(p)=\frac{24}{p^3}\left(\frac{p}{2}-\tan\left(\frac{p}{2}\right)\right).$$

Using the equation (3.21) in (3.17)

$$F_s\frac{\partial^4W}{\partial x^4}+s^2W=Q.$$

$$\frac{\partial^4W}{\partial x^4}-\zeta^4W=\frac{Q}{F_s}, \tag{3.22}$$

where

$$\zeta^4=-\frac{s^2}{F_s},\quad F_s=\frac{1}{12{A_R}^2}\left(1+\frac{c_1s{\delta_1}^2}{L}+(1+f(p))\frac{\beta\bar{\beta}{\gamma_1}^2}{\rho C_e}\right).$$

Considering harmonic loading on beam $q(x,t)=q_0\sin\omega t$, so

$$Q(s,t)=\frac{q_0\omega}{s^2+\omega^2}.$$

Applying L.T. with respect to space domain defined as $\bar{W}(\xi,s)=\int_0^\infty e^{-\xi x}W(x,s)\,dx$ equation (3.22) reduces to

$$\left[\xi^4\bar{W}-\xi^3W(0,s)-\xi^2W'(0,s)-\xi^3W''(0,s)-W'''(0,s)\right]-\zeta^4\bar{W}=\frac{q_0\omega}{F_s\,(s^2+\omega^2)\,\xi}. \tag{3.23}$$

Using the boundary conditions at $x=0$ defined by equations $(3.14)-(3.16)$ and applying inverse L.T. w.r.t. space domain

Case I

$$W=\frac{c_1C(\zeta x)}{2\zeta^2}+\frac{c_2S(\zeta x)}{2\zeta^3}+\frac{q_0\omega}{F_s\,(s^2+\omega^2)}\frac{\bar{C}(\zeta x)-2}{2\zeta^4}, \tag{3.24}$$

Case II

$$W=\frac{c_3\bar{S}(\zeta x)}{2\zeta}+\frac{c_4S(\zeta x)}{2\zeta^3}+\frac{q_0\omega}{F_s\,(s^2+\omega^2)}\frac{\bar{C}(\zeta x)-2}{2\zeta^4}, \tag{3.25}$$

Case III

$$W=\frac{c_5C(\zeta x)}{2\zeta^2}+\frac{c_6S(\zeta x)}{2\zeta^3}+\frac{q_0\omega}{F_s\,(s^2+\omega^2)}\frac{\bar{C}(\zeta x)-2}{2\zeta^4}, \tag{3.26}$$

where

$$C(\zeta x)=\cosh(\zeta x)-\cos(\zeta x),\ S(\zeta x)=\sinh(\zeta x)-\sin(\zeta x),$$

$$\bar{C}(\zeta x)=\cosh(\zeta x)+\cos(\zeta x),\ \bar{S}(\zeta x)=\sinh(\zeta x)+\sin(\zeta x).$$

Using the boundary conditions at $x=1$ defined by equations $(3.14)-(3.16)$, a set of non-homogeneous linear equations is obtained and the condition for existence of infinite solutions is

Case I

$$\cos\zeta\cosh\zeta=1, \tag{3.27}$$

Case II

$$\sin\zeta\sinh\zeta=0, \tag{3.28}$$

Case III

$$\cos\zeta\cosh\zeta=-1. \tag{3.29}$$

The respective roots of the equations $(3.27)-(3.29)$ are given by:

$$\textbf{Case I}: \quad \zeta_1=4.730,\ \zeta_2=7.8532,\ \zeta_k=\left(k+\frac{1}{2}\right)\pi, k\geq 3,$$

$$\textbf{Case II}: \quad \zeta_1=3.1416,\ \zeta_2=6.2832,\ \zeta_k=k\pi, k\geq 3,$$

$$\textbf{Case III}: \quad \zeta_1=1.8751,\ \zeta_2=4.6941,\ \zeta_k=\left(k-\frac{1}{2}\right)\pi, k\geq 3, \tag{3.30}$$

and solutions for three cases of boundary conditions are given by

Case I

$$W = \frac{q_0\omega}{2\zeta^4 F_s\left(s^2+\omega^2\right)}\left(\frac{A_1(\zeta)C(\zeta x)+B_1(\zeta)S(\zeta x)+G_1(\zeta)\left(\bar{C}(\zeta x)-2\right)}{G_1(\zeta)}\right), \quad (3.31)$$

Case II

$$W = \frac{q_0\omega}{4\zeta^4 F_s\left(s^2+\omega^2\right)}\left(\frac{A_2(\zeta)\bar{S}(\zeta x)+B_2(\zeta)S(\zeta x)+2G_2(\zeta)\left(\bar{C}(\zeta x)-2\right)}{G_2(\zeta)}\right), \quad (3.32)$$

Case III

$$W = \frac{q_0\omega}{2\zeta^4 F_s\left(s^2+\omega^2\right)}\left(\frac{A_3(\zeta)C(\zeta x)+B_3(\zeta)S(\zeta x)+G_3(\zeta)\left(\bar{C}(\zeta x)-2\right)}{G_3(\zeta)}\right). \quad (3.33)$$

where

$A_1(\zeta) = \cosh\zeta - \cos\zeta - \sinh\zeta\sin\zeta, B_1(\zeta) = \sinh\zeta\left(\cos\zeta-1\right)+\sin\zeta\left(\cosh\zeta-1\right),$

$A_2(\zeta) = \sinh\zeta\left(1-\cos\zeta\right)+\sin\zeta\left(1-\cosh\zeta\right),$

$B_2(\zeta) = \sinh\zeta\left(\cos\zeta-1\right)+\sin\zeta\left(1-\cosh\zeta\right),$

$A_3(\zeta) = \sinh\zeta\sin\zeta, B_3(\zeta) = -\left(\cosh\zeta\sin\zeta+\sinh\zeta\cos\zeta\right),$

$G_1(\zeta) = 1-\cosh\zeta\cos\zeta, G_2(\zeta) = \sinh\zeta\sin\zeta, G_3(\zeta) = \cosh\zeta\cos\zeta+1.$

Taking Inverse L.T. w.r.t. time domain using method of residues [6] defined as

$$w(x,t) = \sum \text{Residues of } e^{st}W(x,s). \quad (3.34)$$

Making the use of following notations,

$r = \sqrt{1+\omega^2 t_0{}^2},\ R = \frac{1}{A_R}\sqrt{\frac{\rho C_e L c\omega r}{K}},\ \theta = \tan^{-1}\left(\frac{1}{\omega t_0}\right)$

$f_R = \frac{12\cos\theta}{R^2} - \frac{24}{R^3}\left[\frac{\cos\left(\frac{3\theta}{2}\right)\sin(R\cos\theta)+\sin\left(\frac{3\theta}{2}\right)\sinh(R\sin\theta)}{\cos(R\cos\theta)+\cosh(R\sin\theta)}\right],$

$f_I = \frac{12\sin\theta}{R^2} - \frac{24}{R^3}\left[\frac{\sin\left(\frac{3\theta}{2}\right)\sin(R\cos\theta)-\cos\left(\frac{3\theta}{2}\right)\sinh(R\sin\theta)}{\cos(R\cos\theta)+\cosh(R\sin\theta)}\right],$

$\zeta_R = \sqrt[4]{12}\sqrt{A_R\omega}\left[1-\frac{\beta\bar{\beta}}{4\rho C_e}\left(\left(1-\left(\frac{tc\beta_0}{L}\right)^2\right)(1+f_R)-\frac{2tc\beta_0}{L}f_I\right)\right],$

$\zeta_I = \sqrt[4]{12}\sqrt{A_R t}\left[-\frac{\delta_1^2 ct}{4L}-\frac{\beta\bar{\beta}}{4\rho C_e}\left(\left(1-\left(\frac{tc\beta_0}{L}\right)^2\right)f_I+\frac{2t\beta_0 c}{L}(1+f_R)\right)\right]$

where f_R, f_I are the real and imaginary parts of $f(p)$ and ζ_R, ζ_I are the real and imaginary parts of ζ respectively at $s = \pm\iota\omega$.

Case I

$s = 0$ is removable singularity, Residue = 0.

$s = \pm\iota\omega$ are simple poles and their residues are conjugates of each other, So sum of

residues is twice the real part of residue of $e^{st}W(x,s)$ at $s=\imath\omega$.

Sum of residues at $s=\pm\imath\omega$ is

$$\frac{q_0}{2\omega^2}\left(\sin(\omega t)\left(\frac{T(P+R)+U(Q+S)}{T^2+U^2}+V\right)+\cos(\omega t)\left(\frac{T(Q+S)-U(P+R)}{T^2+U^2}+Y\right)\right), \tag{3.35}$$

where

$$\begin{aligned}
P = {} & (\cosh\zeta_R\cos\zeta_I-\cos\zeta_R\cosh\zeta_I-\sinh\zeta_R\cos\zeta_I\sin\zeta_R\cosh\zeta_I \\
& +\cosh\zeta_R\sin\zeta_I\cos\zeta_R\sinh\zeta_I)\times \\
& (\cosh\zeta_R x\cos\zeta_I x-\cos\zeta_R x\cosh\zeta_I x)-(\sinh\zeta_R x\sin\zeta_I x+\sin\zeta_R x\sinh\zeta_I x)\times \\
& (\sinh\zeta_R\sin\zeta_I+\sin\zeta_R\sinh\zeta_I-\sinh\zeta_R\cos\zeta_I\cos\zeta_R\sinh\zeta_I \\
& -\cosh\zeta_R\sin\zeta_I\sin\zeta_R\cosh\zeta_I),
\end{aligned}$$

$$\begin{aligned}
Q = {} & (\cosh\zeta_R\cos\zeta_I-\cos\zeta_R\cosh\zeta_I-\sinh\zeta_R\cos\zeta_I\sin\zeta_R\cosh\zeta_I \\
& +\cosh\zeta_R\sin\zeta_I\cos\zeta_R\sinh\zeta_I)\times \\
& (\sinh\zeta_R x\sin\zeta_I x+\sin\zeta_R x\sinh\zeta_I x)+(\cosh\zeta_R x\cos\zeta_I x-\cos\zeta_R x\cosh\zeta_I x)\times \\
& (\sinh\zeta_R\sin\zeta_I+\sin\zeta_R\sinh\zeta_I-\sinh\zeta_R\cos\zeta_I\cos\zeta_R\sinh\zeta_I \\
& -\cosh\zeta_R\sin\zeta_I\sin\zeta_R\cosh\zeta_I),
\end{aligned}$$

$$\begin{aligned}
R = {} & (\sinh\zeta_R x\cos\zeta_I x-\sin\zeta_R x\cosh\zeta_I x)\times[\sinh\zeta_R\cos\zeta_I(\cos\zeta_R\cosh\zeta_I-1)+ \\
& \cosh\zeta_R\sin\zeta_I\sin\zeta_R\sinh\zeta_I+\sin\zeta_R\cosh\zeta_I(\cosh\zeta_R\cos\zeta_I-1) \\
& -\cos\zeta_R\sinh\zeta_I\sinh\zeta_R\sin\zeta_I] \\
& -(\cosh\zeta_R x\sin\zeta_I x-\cos\zeta_R x\sinh\zeta_I x)\times[(\cosh\zeta_R\sin\zeta_I)(\cos\zeta_R\cosh\zeta_I-1)- \\
& (\sinh\zeta_R\cos\zeta_I\sin\zeta_R\sinh\zeta_I)+(\sin\zeta_R\cosh\zeta_I\sinh\zeta_R\sin\zeta_I) \\
& +(\cos\zeta_R\sinh\zeta_I)(\cosh\zeta_R\cos_I-1)],
\end{aligned}$$

$$\begin{aligned}
S = {} & (\cosh\zeta_R x\sin\zeta_I x-\cos\zeta_R x\sinh\zeta_I x)\times[(\sinh\zeta_R\cos\zeta_I)(\cos\zeta_R\cosh\zeta_I-1)+ \\
& (\cosh\zeta_R\sin\zeta_I\sin\zeta_R\sinh\zeta_I)+(\cosh\zeta_R\cos\zeta_I-1)(\sin\zeta_R\cosh\zeta_I) \\
& -(\cos\zeta_R\sinh\zeta_I\sinh\zeta_R\sin\zeta_I)] \\
& +(\sinh\zeta_R x\cos\zeta_I x-\sin\zeta_R x\cosh\zeta_I x)\times[(\cosh\zeta_R\sin\zeta_I)(\cos\zeta_R\cosh\zeta_I-1)- \\
& (\sinh\zeta_R\cos\zeta_I\sin\zeta_R\sinh\zeta_I)+(\sin\zeta_R\cosh\zeta_I\sinh\zeta_R\sin\zeta_I) \\
& +(\cos\zeta_R\sinh\zeta_I)(\cosh\zeta_R\cos_I-1)],
\end{aligned}$$

$$\begin{aligned}
T &= 1-\cos\zeta_R\cosh\zeta_I\cosh\zeta_R\cos\zeta_I-\sin\zeta_R\sinh\zeta_I\sinh\zeta_R\sin\zeta_I, \\
U &= \sin\zeta_R\sinh\zeta_I\cosh\zeta_R\cos\zeta_I-\cos\zeta_R\cosh\zeta_I\sinh\zeta_R\sin\zeta_I, \\
V &= \cosh\zeta_R x\cos\zeta_I x+\cos\zeta_R x\cosh\zeta_I x-2, \\
Y &= \sinh\zeta_R x\sin\zeta_I x-\sin\zeta_R x\sinh\zeta_I x.
\end{aligned}$$

Singularity corresponding to $G_1(\zeta)=0$ given by equation (3.30) are simple poles, using equation (3.22),

$$s = \pm\iota {\zeta_k}^2\sqrt{F_s} = \pm i s_k,\ s_k = s_0\left(1+\frac{{\delta_1}^2 c s_0}{2L}+\frac{\beta\bar{\beta}}{2\rho C_e}\left(1+\frac{s_0\beta_0 c}{L}\right)^2\left(1+f_{p0}\right)\right)$$

where $s_0 = \frac{{\zeta_k}^2}{2\sqrt{3}{A_R}^2},\ P^2 = \frac{\rho C_e c L s_0 \gamma_0}{K{A_R}^2},\ 1+f_{p0} = 1-\frac{12}{P^2}+\frac{24\tanh\left(\frac{P}{2}\right)}{P^3}$

sum of the residues at $s = \pm\iota s_k$ is

$$= \frac{4q_0F_s\omega\cos(s_k t)}{\zeta_k\left(\omega^2-s_k^2\right)}\left(\frac{A_1(\zeta_k)C(\zeta_k x)+B_1(\zeta_k)S(\zeta_k x)+\left(\bar{C}(\zeta_k x)-2\right)G_1(\zeta_k)}{(\sin\zeta_k\cosh\zeta_k-\cos\zeta_k\sinh\zeta_k)}\right)\times$$

$$\left[-2s_kF_s+s_k^2\left(\frac{\delta_1^2c_1}{L}\right)+\left(\frac{2\beta\beta_0\bar{\beta}c_1\left(1+\frac{s_k\beta_0c_1}{L}\right)(1+f(p))}{\rho C_eL}\right)\right.$$
$$\left.+\left(\frac{\beta\bar{\beta}c_1L\left(1+\left(\frac{s_k\beta_0c}{L}\right)^2\right)(1+2s_kt_0)\left(\left(\frac{12\left(1+\sec^2\left(\frac{p}{2}\right)\right)}{p^4}\right)-\left(\frac{36\tanh\left(\frac{p}{2}\right)}{p^5}\right)\right)}{KA_R^2}\right)\right]^{-1}. \tag{3.36}$$

Case II

$s = 0$ is removable singularity, Residue = 0.

$s = \pm\iota\omega$ are simple poles and their residues are conjugates of each other, So sum of residues is twice the real part of residue of $e^{st}W(x,s)$ at $s = \iota\omega$.

Sum of residues at $s = \pm\iota\omega$ is

$$\frac{q_0}{4\omega^2}\left(\sin(\omega t)\left(\frac{T(P+R)+U(Q+S)}{T^2+U^2}+2V\right)+\cos(\omega t)\left(\frac{T(Q+S)-U(P+R)}{T^2+U^2}+2Y\right)\right), \tag{3.37}$$

where

$$\begin{aligned}P = {} & [\sinh\zeta_R\cos\zeta_I(1-\cos\zeta_R\cosh\zeta_I)+\sin\zeta_R\cosh\zeta_I(1-\cosh\zeta_R\cos\zeta_I)\\ & -\cosh\zeta_R\sin\zeta_I\sin\zeta_R\sinh\zeta_I+\\ & \cos\zeta_R\sinh\zeta_I\sinh\zeta_R\sin\zeta_I]\times(\sinh\zeta_Rx\cos\zeta_Ix+\sin\zeta_Rx\cosh\zeta_Ix)\\ & -[\sinh\zeta_R\cos\zeta_I\sin\zeta_R\sinh\zeta_I+\cosh\zeta_R\sin\zeta_I(1-\cos\zeta_R\cosh\zeta_I)\\ & -\sin\zeta_R\cosh\zeta_I\sinh\zeta_R\sin\zeta_I+\\ & \cos\zeta_R\sinh\zeta_I(1-\cosh\zeta_R\cos\zeta_I)]\times(\cosh\zeta_Rx\sin\zeta_Ix+\cos\zeta_Rx\sinh\zeta_Ix),\end{aligned}$$

$$\begin{aligned}Q = {} & [\sinh\zeta_R\cos\zeta_I(1-\cos\zeta_R\cosh\zeta_I)+\sin\zeta_R\cosh\zeta_I(1-\cosh\zeta_R\cos\zeta_I)\\ & -\cosh\zeta_R\sin\zeta_I\sin\zeta_R\sinh\zeta_I+\\ & \cos\zeta_R\sinh\zeta_I\sinh\zeta_R\sin\zeta_I]\times(\cosh\zeta_Rx\sin\zeta_Ix+\cos\zeta_Rx\sinh\zeta_Ix)\\ & +[\sinh\zeta_R\cos\zeta_I\sin\zeta_R\sinh\zeta_I+\cosh\zeta_R\sin\zeta_I(1-\cos\zeta_R\cosh\zeta_I)\\ & -\sin\zeta_R\cosh\zeta_I\sinh\zeta_R\sin\zeta_I+\\ & \cos\zeta_R\sinh\zeta_I(1-\cosh\zeta_R\cos\zeta_I)]\times(\sinh\zeta_Rx\cos\zeta_Ix+\sin\zeta_Rx\cosh\zeta_Ix),\end{aligned}$$

$$
\begin{aligned}
R = [&\sinh\zeta_R\cos\zeta_I\,(\cos\zeta_R\cosh\zeta_I - 1) + \sin\zeta_R\cosh\zeta_I\,(1 - \cosh\zeta_R\cos\zeta_I) \\
&+ \cosh\zeta_R\sin\zeta_I\sin\zeta_R\sinh\zeta_I + \\
&\cos\zeta_R\sinh\zeta_I\sinh\zeta_R\sin\zeta_I] \times (\sinh\zeta_R x\cos\zeta_I x + \sin\zeta_R x\cosh\zeta_I x) - \\
&[-\sinh\zeta_R\cos\zeta_I\sin\zeta_R\sinh\zeta_I + \cosh\zeta_R\sin\zeta_I\,(\cos\zeta_R\cosh\zeta_I - 1) \\
&- \sin\zeta_R\cosh\zeta_I\sinh\zeta_R\sin\zeta_I + \\
&\cos\zeta_R\sinh\zeta_I\,(1 - \cosh\zeta_R\cos\zeta_I)] \times (\cosh\zeta_R x\sin\zeta_I x - \cos\zeta_R x\sinh\zeta_I x)\,,
\end{aligned}
$$

$$
\begin{aligned}
S = [&\sinh\zeta_R\cos\zeta_I\,(\cos\zeta_R\cosh\zeta_I - 1) + \sin\zeta_R\cosh\zeta_I\,(1 - \cosh\zeta_R\cos\zeta_I) \\
&+ \cosh\zeta_R\sin\zeta_I\sin\zeta_R\sinh\zeta_I + \\
&\cos\zeta_R\sinh\zeta_I\sinh\zeta_R\sin\zeta_I] \times (\cosh\zeta_R x\sin\zeta_I x - \cos\zeta_R x\sinh\zeta_I x) + \\
&[-\sinh\zeta_R\cos\zeta_I\sin\zeta_R\sinh\zeta_I + \cosh\zeta_R\sin\zeta_I\,(\cos\zeta_R\cosh\zeta_I - 1) \\
&- \sin\zeta_R\cosh\zeta_I\sinh\zeta_R\sin\zeta_I + \\
&\cos\zeta_R\sinh\zeta_I\,(1 - \cosh\zeta_R\cos\zeta_I)] \times (\sinh\zeta_R x\cos\zeta_I x + \sin\zeta_R x\cosh\zeta_I x)\,,
\end{aligned}
$$

$$
\begin{aligned}
T &= \sinh\zeta_R\cos\zeta_I\sin\zeta_R\cosh\zeta_I - \cosh\zeta_R\sin\zeta_I\cos\zeta_R\sinh\zeta_I, \\
U &= \sinh\zeta_R\cos\zeta_I\cos\zeta_R\sinh\zeta_I + \cosh\zeta_R\sin\zeta_I\sin\zeta_R\cosh\zeta_I, \\
V &= \cosh\zeta_R x\cos\zeta_I x + \cos\zeta_R x\cosh\zeta_I x - 2, \\
Y &= \sinh\zeta_R x\sin\zeta_I x - \sin\zeta_R x\sinh\zeta_I x.
\end{aligned}
$$

Singularity corresponding to $G_2(\zeta) = 0$ given by equation (3.30) are simple poles, using equation (3.22),

$s = \pm\iota{\zeta_k}^2\sqrt{F_s},\ s_k = \pm\iota s_0\left(1 + \frac{{\delta_1}^2 c s_0}{2L} + \frac{\beta\bar{\beta}}{2\rho C_e}\left(1 + \frac{s_0\beta_0 c}{L}\right)^2\left(1 + f_{p0}\right)\right)$,

where $s_0 = \frac{{\zeta_k}^2}{2\sqrt{3}A_R},\ P^2 = \frac{\rho C_e c L s_0\gamma_0}{K{A_R}^2},\ 1 + f_{p0} = 1 - \frac{12}{P^2} + \frac{24\tanh\left(\frac{p}{2}\right)}{P^3}$

sum of the residues at $s = \pm\iota s_k$ is

$$
\begin{aligned}
&= \frac{2q_0F_s\omega\cos(s_k t)}{\zeta_k\left(\omega^2 - s_k^2\right)}\left(\frac{A_2(\zeta)\bar{S}(\zeta_k x) + B_2(\zeta_k)S(\zeta_k x) + 2\left(\bar{C}(\zeta_k x) - 2\right)G_2(\zeta_k)}{(\sinh\zeta_k\cos\zeta_k + \cosh\zeta_k\sin\zeta_k)}\right)\times \\
&\left[-2s_kF_s + s_k^2\left(\frac{\delta_1^2 c_1}{L}\right) + \left(\frac{2\beta\beta_0\bar{\beta}c_1\left(1 + \frac{s_k\beta_0 c_1}{L}\right)(1 + f(p))}{\rho C_e L}\right)\right. \\
&\left. + \left(\frac{\beta\bar{\beta}c_1 L\left(1 + \left(\frac{s_k\beta_0 c}{L}\right)^2\right)(1 + 2s_k t_0)\left(\left(\frac{12\left(1+\sec^2\left(\frac{p}{2}\right)\right)}{p^4}\right) - \left(\frac{36\tanh\left(\frac{p}{2}\right)}{p^5}\right)\right)}{KA_R^2}\right)\right]^{-1}.
\end{aligned}
\tag{3.38}
$$

Case III

$s = 0$ is removable singularity, Residue = 0.

$s = \pm\iota\omega$ are simple poles and their residues are conjugates of each other, So sum of residues is twice the real part of residue of $e^{st}W(x,s)$ at $s = \iota\omega$.
Sum of residues at $s = \pm\iota\omega$ is

$$\frac{q_0}{2\omega^2}\left(\sin(\omega t)\left(\frac{T(P+R)+U(Q+S)}{T^2+U^2}+V\right)+\cos(\omega t)\left(\frac{T(Q+S)-U(P+R)}{T^2+U^2}+Y\right)\right), \tag{3.39}$$

where

$$\begin{aligned}P = {} & (\sinh\zeta_R\cos\zeta_I\sin\zeta_R\cosh\zeta_I - \cosh\zeta_R\sin\zeta_I\sinh\zeta_I\cos\zeta_R)(\cosh\zeta_R x\cos\zeta_I x \\ & - \cos\zeta_R x\cosh\zeta_I x) \\ & - (\sinh\zeta_R\cos\zeta_I\cos\zeta_R\sinh\zeta_I + \cosh\zeta_R\sin\zeta_I\sin\zeta_R\cosh\zeta_I)(\sinh\zeta_R x\sin\zeta_I x \\ & + \sin\zeta_R x\sinh\zeta_I x),\end{aligned}$$

$$\begin{aligned}Q = {} & (\sinh\zeta_R\cos\zeta_I\sin\zeta_R\cosh\zeta_I - \cosh\zeta_R\sin\zeta_I\sinh\zeta_I\cos\zeta_R)(\sinh\zeta_R x\sin\zeta_I x \\ & + \sin\zeta_R x\sinh\zeta_I x) \\ & + (\sinh\zeta_R\cos\zeta_I\cos\zeta_R\sinh\zeta_I + \cosh\zeta_R\sin\zeta_I\sin\zeta_R\cosh\zeta_I)(\cosh\zeta_R x\cos\zeta_I x \\ & - \cos\zeta_R x\cosh\zeta_I x),\end{aligned}$$

$$\begin{aligned}R = {} & -[(\cosh\zeta_R\cos\zeta_I\sin\zeta_R\cosh\zeta_I - \sinh\zeta_R\sin\zeta_I\cos\zeta_R\sinh\zeta_I) \\ & + (\sinh\zeta_R\cos\zeta_I\cos\zeta_R\cosh\zeta_I + \\ & \cosh\zeta_R\sin\zeta_I\sin\zeta_R\sinh\zeta_I)] \times (\sinh\zeta_R x\cos\zeta_I x - \sin\zeta_R x\cosh\zeta_I x) + \\ & [\cosh\zeta_R\cos\zeta_I\cos\zeta_R\sinh\zeta_I + \sinh\zeta_R\sin\zeta_I\sin\zeta_R\cosh\zeta_I - \sinh\zeta_R\cos\zeta_I\sin\zeta_R\sinh\zeta_I \\ & + \\ & \cosh\zeta_R\sin\zeta_I\cos\zeta_R\cosh\zeta_I] \times (\cosh\zeta_R x\sin\zeta_I x - \cos\zeta_R x\sinh\zeta_I x),\end{aligned}$$

$$\begin{aligned}S = {} & -[(\cosh\zeta_R\cos\zeta_I\sin\zeta_R\cosh\zeta_I - \sinh\zeta_R\sin\zeta_I\cos\zeta_R\sinh\zeta_I) \\ & + (\sinh\zeta_R\cos\zeta_I\cos\zeta_R\cosh\zeta_I + \\ & \cosh\zeta_R\sin\zeta_I\sin\zeta_R\sinh\zeta_I)] \times (\cosh\zeta_R x\sin\zeta_I x - \cos\zeta_R x\sinh\zeta_I x) - \\ & [\cosh\zeta_R\cos\zeta_I\cos\zeta_R\sinh\zeta_I + \sinh\zeta_R\sin\zeta_I\sin\zeta_R\cosh\zeta_I - \sinh\zeta_R\cos\zeta_I\sin\zeta_R\sinh\zeta_I \\ & + \\ & \cosh\zeta_R\sin\zeta_I\cos\zeta_R\cosh\zeta_I] \times (\sinh\zeta_R x\cos\zeta_I x - \sin\zeta_R x\cosh\zeta_I x),\end{aligned}$$

$$\begin{aligned}T &= \cosh\zeta_R\cos\zeta_I\cos\zeta_R\cosh\zeta_I + \sinh\zeta_R\sin\zeta_I\sin\zeta_R\sinh\zeta_I + 1, \\ U &= -\cosh\zeta_R\cos\zeta_I\sin\zeta_R\sinh\zeta_I + \sinh\zeta_R\sin\zeta_I\cos\zeta_R\cosh\zeta_I, \\ V &= \cosh\zeta_R x\cos\zeta_I x + \cos\zeta_R x\cosh\zeta_I x - 2, \\ Y &= \sinh\zeta_R x\sin\zeta_I x - \sin\zeta_R x\sinh\zeta_I x.\end{aligned}$$

Singularity corresponding to $G_3(\zeta) = 0$ given by equation (3.30) are simple poles, using equation (3.22)
$s = \pm\iota{\zeta_k}^2\sqrt{F_s},\ s_k = \pm\iota s_0\left(1+\frac{{\delta_1}^2 c s_0}{2L}+\frac{\beta\bar{\beta}}{2\rho C_e}\left(1+\frac{s_0\beta_0 c}{L}\right)^2\left(1+f_{p0}\right)\right)$

where $s_0 = \frac{{\zeta_k}^2}{2\sqrt{3}A_R}$, $P^2 = \frac{\rho C_e c L s_0 \gamma_0}{K {A_R}^2}$, $1 + f_{p0} = 1 - \frac{12}{P^2} + \frac{24\tanh\left(\frac{P}{2}\right)}{P^3}$.
Sum of the residues at $s = \pm \imath s_k$ is

$$= \frac{4q_0 F_s \omega \cos(s_k t)}{\zeta_k\left(\omega^2 - s_k^2\right)} \left(\frac{A_3(\zeta) C(\zeta_k x) + B_3(\zeta_k) S(\zeta_k x) + \left(\bar{C}(\zeta_k x) - 2\right) G_3(\zeta_k)}{(\sinh\zeta_k \cos\zeta_k - \cosh\zeta_k \sin\zeta_k)} \right) \times$$

$$\left[-2 s_k F_s + s_k^2 \left(\frac{\delta_1^2 c_1}{L} \right) + \left(\frac{2\beta\beta_0\bar{\beta} c_1 \left(1 + \frac{s_k \beta_0 c_1}{L}\right)(1 + f(p))}{\rho C_e L} \right) \right.$$
$$\left. + \left(\frac{\beta\bar{\beta} c_1 L \left(1 + \left(\frac{s_k \beta_0 c}{L}\right)^2\right)(1 + 2 s_k t_0) \left(\left(\frac{12\left(1 + \sec^2\left(\frac{p}{2}\right)\right)}{p^4} \right) - \left(\frac{36\tanh\left(\frac{p}{2}\right)}{p^5} \right) \right)}{K A_R^2} \right) \right]^{-1} . \tag{3.40}$$

3.6 Numerical Results and Graphical Explanations

Consider viscothermoelastic solid like magnesium with the physical specifications from [36] as given below:

$C_e = 1.04 \times 10^3 J\, Kg^{-1}\, deg^{-1}$, $T_0 = 298^o K$, $\alpha_0 = \alpha_1 = 0.779 \times 10^{-9}$, $\alpha_T = 25 \times 10^{-6}$,

$\beta = 2.68 \times 10^6$, $q_0 = 2 \times 10^{-7}$

The frequency ω is 0.1076 Hz. Dimensions of the beam are taken as $L = 200\mu m$, $b = 35\mu m$ and $h = 30\mu m$. The non-dimensional value of relaxation time for CC, SS, CF beams are computed from relation $t_0 = s_0^{-1}$. So the values are given as $t_0 = 1.0322, 2.34, 6.5683$ for the first mode and $t_0 = 0.3744, 0.585, 1.0481$ for the second mode for CC, SS and CF beam respectively. Using equations $(3.34) - (3.40)$, the dimensionless deflection has been evaluated.

Fig.$[3.1 - 3.3]$ represents the transition of deflection for viscothermoelastic beam for different boundary condition as CC, SS, CF under the effect of harmonic load w.r.t length (x) at different time (t) for first and second mode. From Fig.$[3.1 - 3.3]$ The magnitude of deflection has been observed to increase with time except for cantilever beam at $t = 21$. Also from Fig. $[3.1 - 3.2]$ deflection curve is symmetrical about the middle point of beam. Also, the deflections near the axial ends are more forceful for clamped beam in comparison to simple supported beam. The figures reveal that the deflection is minimum at the restrained edges in all cases. The CF beam, being most flexible,

displays steadily increasing deflection from the clamped to the free end, with the tip showing the highest displacement. From a design standpoint, this indicates that greater flexibility or weaker supports lead to enhanced bending, implying that cantilever configurations require careful damping and material selection to prevent excessive vibration or fatigue during cyclic thermal-mechanical loading.

Fig.$[3.4-3.6]$ depicts the transition of deflection for viscothermoelastic beam for different boundary condition as CC, SS, CF under the effect of harmonic load w.r.t time (t) at various values of length (x) for first mode. From Fig.$[3.4-3.5]$, it has been remarked that maxima of deflection occurs at middle spot of beam and it reduces as it shifts away from it in either direction. Whereas, from Fig.[3.6], the deflection increases with the increase in length (x) in case of cantilever beam. On analyzing the amplitude of maximum value of deflection, it is observed that $w_{CC} \geq w_{CF} \geq w_{SS}$. These figures depict that the non-dimensional deflection gradually increases with time. This behaviour arises from the combined effects of viscous damping and thermal relaxation inherent in visco-thermoelastic materials leading to time-dependent deformation. Among the three boundary conditions, the SS beam demonstrates the largest amplitude growth, indicating that weaker constraints permit greater energy transfer from the applied harmonic load into structural deformation. In real applications, such as MEMS/NEMS beam resonators or thin mechanical sensors, this behaviour highlights the importance of accounting for long-term deformation and frequency drift when the component operates in thermally varying environments.

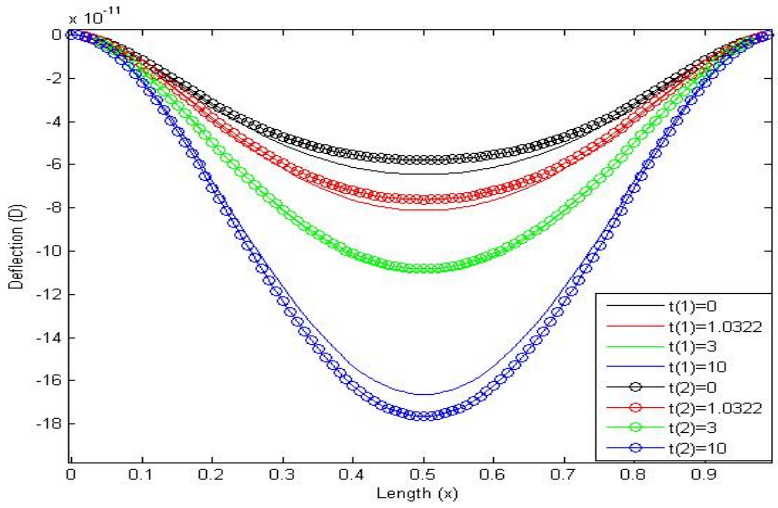

Figure 3.1: Deflection (w) in CC Viscothermoelastic beam vs length (x) at different times for first and second mode.

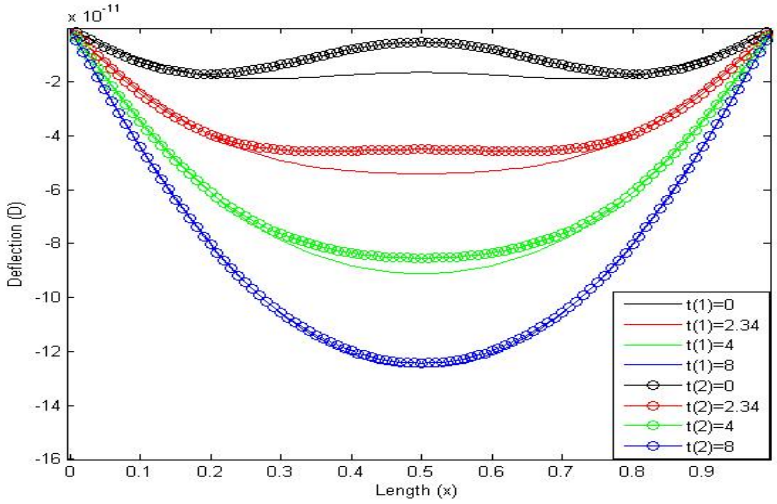

Figure 3.2: Deflection (w) in SS Viscothermoelastic beam vs length (x) at different times for first and second mode.

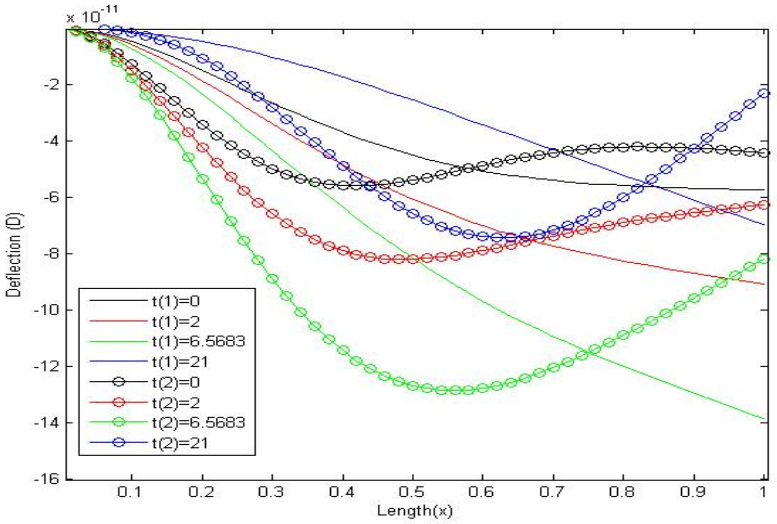

Figure 3.3: Deflection (w) in CF Viscothermoelastic beam vs length (x) at different times for first and second mode.

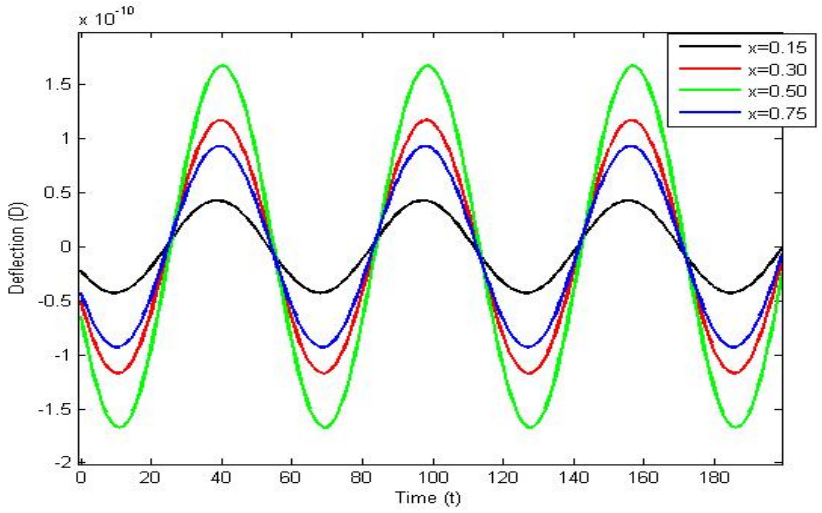

Figure 3.4: Deflection (w) in CC Viscothermoelastic beam vs time (t) at different lengths for first mode.

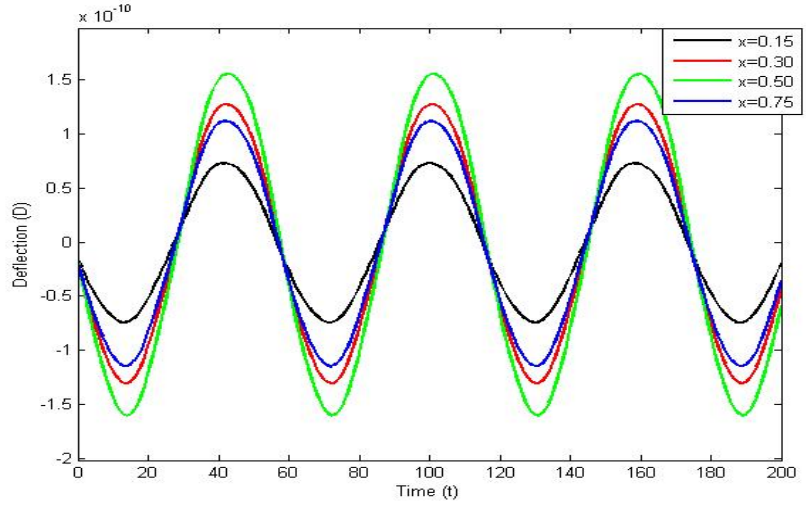

Figure 3.5: Deflection (w) in SS Viscothermoelastic beam vs time (t) at different lengths for first mode.

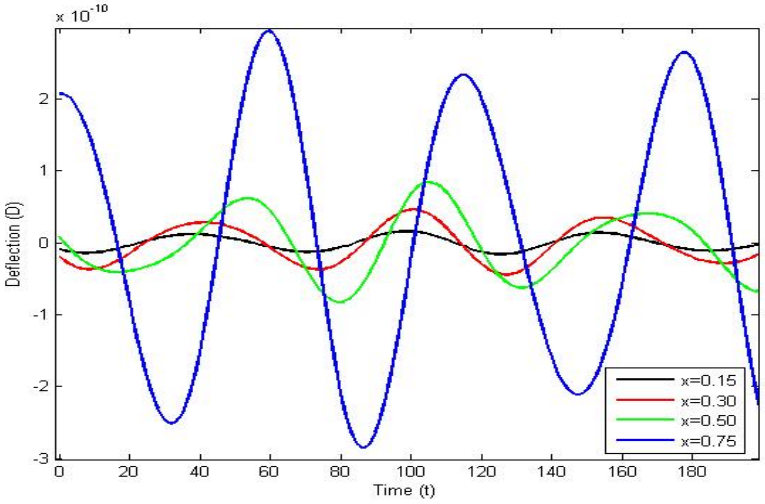

Figure 3.6: Deflection (w) in CF Viscothermoelastic beam vs time (t) at different lengths for first mode.

3.7 Conclusion

The dynamic response of homogeneous isotropic viscothermoelastic beam under the influence of harmonic loading has been studied. The L.T. technique has been used twice with respect to time and spatial domain. It is inferred that

- The deflection likewise increases with time in case of CC, SS, CF except for CF beam at relaxation time $t = 21$.
- The deflection curve is symmetrical about the middle spot of beam for CC and SS beam.
- Maxima of deflection occurs at middle spot of beam and it reduces as it shifts away from it in either direction.

Acknowledgement

The authors are grateful for the valuable discussion of Dr. Deepak Grover on this research work.

Chapter 4

Visco-thermoelastic Rectangular Plate under Uniform Loading: A Study of Deflection

4.1 Introduction

The previous two chapters discusses the analysis of deflection in beam structure which provides a fundamental understanding of one-dimensional deflection profile. There are real world applications like sensor membranes, microscale resonators which involve the multidirectional deformation. This chapter extends the study to analysis of deflection in two-dimensional structures like rectangular plates. The interplay of in-plane and out-of-plane stresses adds complexity to the analysis of deflection in rectangular plates. This chapter examines how a viscothermoelastic rectangular plate responds to uniform transverse loading under different set of boundary conditions.

Sharma and Grover [36] studied thermoelastic damping in MEMS/NEMS thin plates with voids to derive the expressions for deflection, frequency shift under different boundary conditions. Lal and Kumar [40] studied the free transverse vibration of thin rectangular plates of linearly varying thickness using two-dimensional characteristic orthogonal polynomial. Rana and Robin [55] analysed the effect on damping due to non-homogeneity in a rectangular plate of parabolically varying thickness resting on elastic foundation. Partap and Chugh [61] incorporated the microstretch, micropolar effects and investigated the expressions for thermoelastic damping, temperature distribution, deflection in micro-scale, generalized thermoelastic thin plate. Grover [86] studied the thermoelastic damping in piezothermoelastic plate resonators with voids by developing a model incorporating mechanical, thermal, and piezoelectric effects. The author derived the expressions for displacements, electric potential change, frequency shift, and thermoelastic damping under CS and SS boundary conditions and also emphasized the impact of coupling parameters and voids on the structure's resonance properties.

4.2 Primary Equations

Considering a homogeneous, isotropic, thermally conductive viscothermoelastic rectangular plate, which is initially undeformed and at temperature T_0. The basic equation of motion has been considered in Cartesian coordinate system from [31].

$$\sigma_{ij} = \lambda^* \delta_{ij} e_{kk} + 2\mu^* e_{ij} - \beta^* T \delta_{ij}. \tag{4.1}$$

In view of Lord Shulman [5] model of generalized thermoelasticity the equation of heat conduction along with the constitutive relations, in the absence of heat sources and body forces, which govern the displacement vector $u = (u_1, u_2, u_3)$ and temperature change $T(x, y, z, t)$ at time t are given as

$$(\lambda^* + 2\mu^*) \nabla (\nabla . u) - \mu^* \nabla \times (\nabla \times u) - \beta^* \nabla T = \rho \frac{\partial^2 u}{\partial t^2}. \tag{4.2}$$

$$K \nabla^2 T = \rho C_e \left(\frac{\partial T}{\partial t} + t_0 \frac{\partial^2 T}{\partial t^2} \right) + \beta^* T_0 \left(\frac{\partial}{\partial t} + t_0 \frac{\partial^2}{\partial t^2} \right) \nabla . u. \tag{4.3}$$

4.3 Modelling of Rectangular Plate Structure

A homogeneous isotropic, viscothermoelastic rectangular plate of length L, width b, and thickness h, where $(0 \leq x \leq L)$, $\left(\frac{-b}{2} \leq y \leq \frac{b}{2} \right)$, $\left(\frac{-h}{2} \leq z \leq \frac{h}{2} \right)$ is considered for the studying transverse deflection induced due to loading. In equilibrium, the plate is at stable temperature T_0, is under no stress and unstrained. In accordance with Kirchhoff-Love plate theory assumptions [22], the displacement vector u and temperature function T are given as

$$u_1 = -z \frac{\partial w}{\partial x},\ u_2 = -z \frac{\partial w}{\partial y},\ u_3 = w(x, y, t).$$

Using the above displacement vector values, equation $(4.1) - (4.3)$ reduces to

$$\left.\begin{aligned}
\sigma_{xx} &= (\lambda + 2\mu) \left(-z \tfrac{\partial^2 w}{\partial x^2} \right) + \lambda \left(-z \tfrac{\partial^2 w}{\partial y^2} \right) + (\lambda \alpha_0 + 2\mu \alpha_1) \left(-z \tfrac{\partial^3 w}{\partial t \partial x^2} \right) + \lambda \alpha_0 \left(-z \tfrac{\partial^3 w}{\partial t \partial y^2} \right) \\
&\quad -\beta \left(T + \beta_0 \tfrac{\partial T}{\partial t} \right), \\
\sigma_{yy} &= (\lambda + 2\mu) \left(-z \tfrac{\partial^2 w}{\partial y^2} \right) + \lambda \left(-z \tfrac{\partial^2 w}{\partial x^2} \right) + (\lambda \alpha_0 + 2\mu \alpha_1) \left(-z \tfrac{\partial^3 w}{\partial t \partial y^2} \right) + \lambda \alpha_0 \left(-z \tfrac{\partial^3 w}{\partial t \partial x^2} \right) \\
&\quad -\beta \left(T + \beta_0 \tfrac{\partial T}{\partial t} \right), \\
\sigma_{xy} &= -2\mu z \left(\tfrac{\partial^2 w}{\partial x \partial y} + \alpha_1 \tfrac{\partial^3 w}{\partial t \partial x \partial y} \right).
\end{aligned}\right\} \tag{4.4}$$

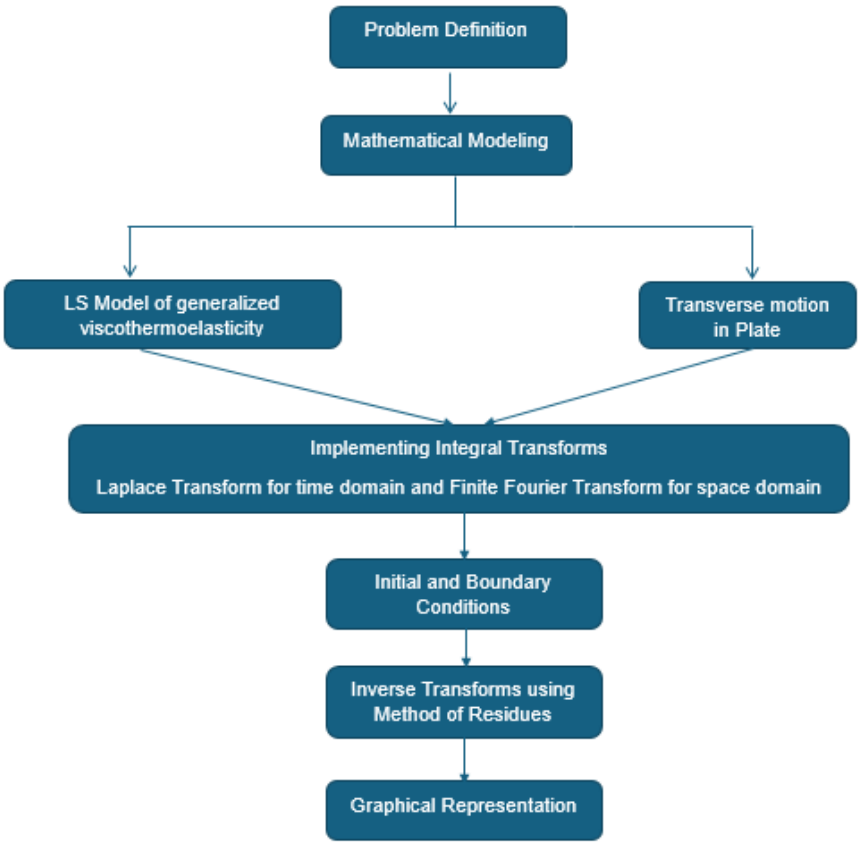

Figure 4.1: Flowchart for the modeling of the viscothermoelastic Rectangular Plate

$$\left.\begin{aligned}
&-z(\lambda+2\mu)\left(\frac{\partial^3 w}{\partial x^3}+\frac{\partial^3 w}{\partial x\partial y^2}\right)-z(\lambda\alpha_0+2\mu\alpha_1)\left(\frac{\partial^4 w}{\partial t\partial x^3}+\frac{\partial^4 w}{\partial t\partial x\partial y^2}\right)-\beta\left(\frac{\partial T}{\partial x}+\beta_0\frac{\partial^2 T}{\partial x\partial t}\right)\\
&\quad=-\rho z\frac{\partial^3 w}{\partial x\partial t^2},\\
&-z(\lambda+2\mu)\left(\frac{\partial^3 w}{\partial y^3}+\frac{\partial^3 w}{\partial y\partial x^2}\right)-z(\lambda\alpha_0+2\mu\alpha_1)\left(\frac{\partial^4 w}{\partial t\partial y\partial x^2}+\frac{\partial^4 w}{\partial t\partial y^3}\right)-\beta\left(\frac{\partial T}{\partial y}+\beta_0\frac{\partial^2 T}{\partial y\partial t}\right)\\
&\quad=-\rho z\frac{\partial^3 w}{\partial y\partial t^2},\\
&-\lambda\left(\frac{\partial^2 w}{\partial x^2}+\frac{\partial^2 w}{\partial y^2}\right)-\lambda\alpha_0\left(\frac{\partial^3 w}{\partial t\partial x^2}+\frac{\partial^3 w}{\partial t\partial y^2}\right)-\beta\left(\frac{\partial T}{\partial z}+\beta_0\frac{\partial^2 T}{\partial z\partial t}\right)=\rho\frac{\partial^2 w}{\partial t^2}.
\end{aligned}\right\} \tag{4.5}$$

$$K\nabla^2 T=\rho C_e\left(\frac{\partial T}{\partial t}+t_0\frac{\partial^2 T}{\partial t^2}\right)-\beta z T_0\left(1+\beta_0\frac{\partial}{\partial t}\right)\left(\frac{\partial}{\partial t}+t_0\frac{\partial^2}{\partial t^2}\right)\nabla_1^2 w. \tag{4.6}$$

Here $\nabla^2=\left(\frac{\partial^2}{\partial x^2}+\frac{\partial^2}{\partial y^2}+\frac{\partial^2}{\partial z^2}\right)$ and $\nabla_1^2=\left(\frac{\partial^2}{\partial x^2}+\frac{\partial^2}{\partial y^2}\right)$.

The bending moments per unit length M_{xx}, M_{yy} are induced in viscothermoelastic plate due to normal stresses σ_{xx}, σ_{yy} and the twisting moment per unit length M_{xy} is induced due to the shearing stresses σ_{xy}, σ_{yx} and are given as

$$M_{xx}=\int_{-h/2}^{h/2}\sigma_{xx}z\,dz,\quad M_{yy}=\int_{-h/2}^{h/2}\sigma_{yy}z\,dz,\quad M_{xy}=\int_{-h/2}^{h/2}\sigma_{xy}z\,dz.$$

Using the stress components from (4.4), we get

$$\left.\begin{aligned} M_{xx} &= -\tfrac{h^3}{12}\left[(\lambda+2\mu)\,\tfrac{\partial^2 w}{\partial x^2}+\lambda\,\tfrac{\partial^2 w}{\partial y^2}+(\lambda\alpha_0+2\mu\alpha_1)\,\tfrac{\partial^3 w}{\partial t\partial x^2}+\lambda\alpha_0\tfrac{\partial^3 w}{\partial t\partial y^2}\right]-\beta\left[M_T+\beta_0\tfrac{\partial M_T}{\partial t}\right],\\ M_{yy} &= -\tfrac{h^3}{12}\left[(\lambda+2\mu)\,\tfrac{\partial^2 w}{\partial y^2}+\lambda\,\tfrac{\partial^2 w}{\partial x^2}+(\lambda\alpha_0+2\mu\alpha_1)\,\tfrac{\partial^3 w}{\partial t\partial y^2}+\lambda\alpha_0\tfrac{\partial^3 w}{\partial t\partial x^2}\right]-\beta\left[M_T+\beta_0\tfrac{\partial M_T}{\partial t}\right],\\ M_{xy} &= -2\mu\tfrac{h^3}{12}\left(\tfrac{\partial^2 w}{\partial x\partial y}+\alpha_1\tfrac{\partial^3 w}{\partial t\partial x\partial y}\right). \end{aligned}\right\} \tag{4.7}$$

where $M_T=\int_{-h/2}^{h/2} Tz\,dz$ represents moment of plate due to thermal effects.
Now taking up the equation of transverse motion in plate

$$\frac{\partial^2 M_{xx}}{\partial x^2}+2\frac{\partial^2 M_{xy}}{\partial x\partial y}+\frac{\partial^2 M_{yy}}{\partial y^2}=-q\,(x,y,t)+\rho h\frac{\partial^2 w}{\partial t^2}. \tag{4.8}$$

where $q\,(x,y,t)$ represents loading on plate.
Taking uniform loading under consideration, i.e., $q\,(x,y,t)=-q_0$.
Using the equation (4.7) in (4.8), we get

$$-\frac{h^3}{12}\left[(\lambda+2\mu)\,\nabla_1^2\left(\nabla_1^2 w\right)+(\lambda\alpha_0+2\mu\alpha_1)\,\frac{\partial}{\partial t}\nabla_1^2\left(\nabla_1^2 w\right)\right]-\beta\nabla_1^2\left(M_T+\beta_0\frac{\partial M_T}{\partial t}\right)=q_0+\rho h\frac{\partial^2 w}{\partial t^2}. \tag{4.9}$$

Considering non-dimensional quantities

$$x'=\frac{x}{L},\ y'=\frac{y}{L},\ w'=\frac{w}{h},\ z'=\frac{z}{h},\ t'=\frac{c_1}{L}t,\ t_0{}'=\frac{c_1}{L}t_0,\ T'=\frac{T-T_0}{T_0}.$$

Using the non-dimensional quantities in equations (4.6) and (4.9), we get

$$\left.\begin{aligned} &\tfrac{1}{12A_R^2}\left[(\lambda+2\mu)\,\nabla_1^2\left(\nabla_1^2 w\right)+(\lambda\alpha_0+2\mu\alpha_1)\,\tfrac{c_1}{L}\tfrac{\partial}{\partial t}\nabla_1^2\left(\nabla_1^2 w\right)\right]+\\ &\qquad \beta T_0\nabla_1^2\left(M_T+\tfrac{c_1\beta_0}{L}\tfrac{\partial M_T}{\partial t}\right)+\rho c_1^2\tfrac{\partial^2 w}{\partial t^2}=-q_0A_R^2,\\ &\left[\tfrac{\partial^2 T}{\partial x^2}+\tfrac{\partial^2 T}{\partial y^2}+A_R^2\tfrac{\partial^2 T}{\partial z^2}\right]=\tfrac{\rho C_e c_1 L}{K}\left(\tfrac{\partial T}{\partial t}+t_0\tfrac{\partial^2 T}{\partial t^2}\right)-\tfrac{c_1\beta z h^2}{KL}\left(1+\tfrac{\beta_0 c_1}{L}\tfrac{\partial}{\partial t}\right)\left(\tfrac{\partial}{\partial t}+t_0\tfrac{\partial^2}{\partial t^2}\right)\nabla_1^2 w, \end{aligned}\right\} \tag{4.10}$$

$$\text{where } M_T=\int_{-1/2}^{1/2} Tz\,dz.$$

(Ignoring the primes for the sake of convenience.)

4.4 Initial and Boundary Conditions

A rectangular plate whose, either all the edges are subjected to simply supported conditions (SSSS) or horizontal edges are subjected to simply supported and vertical edges as clamped (CSCS), is considered. The initial conditions in rectangular plate [36] are

considered as:

$$w(x,y,0)=\left(\frac{\partial w}{\partial t}\right)_{t=0}=\left(\frac{\partial^2 w}{\partial t^2}\right)_{t=0}=0,\ T(x,y,z,0)=\left(\frac{\partial T}{\partial t}\right)_{t=0}=0. \tag{4.11}$$

The first condition on the deflection ensure that the plate is in undeformed position initially and the other two conditions signify that no external momentum or force is acting initially. The first condition on $T(x,y,z,t)$ means that change in temperature from initial temperature T_0 is zero in the beginning. The other condition states that temperature gradient is zero initially. and the following boundary conditions [68] are taken into account.

Case I: For simply supported plate SSSS

$$\left.\begin{array}{l} w(0,y,t)=w(1,y,t)=0 \quad \text{and} \quad w(x,0,t)=w(x,\hat{b},t)=0, \\ \left(\frac{\partial^2 w}{\partial x^2}\right)_{x=0}=\left(\frac{\partial^2 w}{\partial x^2}\right)_{x=1}=0 \quad \text{and} \quad \left(\frac{\partial^2 w}{\partial y^2}\right)_{y=0}=\left(\frac{\partial^2 w}{\partial y^2}\right)_{y=\hat{b}}=0. \end{array}\right\} \tag{4.12}$$

Case II: For clamped-simply supported plate CSCS

$$\left.\begin{array}{l} w(0,y,t)=w(1,y,t)=0 \quad \text{and} \quad w(x,0,t)=w(x,\hat{b},t)=0, \\ \left(\frac{\partial w}{\partial x}\right)_{x=0}=\left(\frac{\partial w}{\partial x}\right)_{x=1}=0 \quad \text{and} \quad \left(\frac{\partial^2 w}{\partial y^2}\right)_{y=0}=\left(\frac{\partial^2 w}{\partial y^2}\right)_{y=\hat{b}}=0. \end{array}\right\} \tag{4.13}$$

With all the edges under simply supported condition state that the plate is rigid at the edges and is not allowing the vertical movement but is free to rotate with zero resistance to bending at the boundaries when external load is applied. The other boundary condition of CSCS signify that all the edges are restricting the vertical movement but rotation is restricted only at vertical edges.

Also, there is no heat transfer through the top and bottom surface of viscothermoelastic rectangular plate, i.e., $\frac{\partial T}{\partial z}=0 \quad \text{at} \quad z=\pm\frac{1}{2}$.

4.5 Solution along thickness direction

Laplace Transform technique

The differential equations given in (4.10) are analysed using the L.T. technique. L.T. converts time-domain problems into complex frequency-domain. The transform converts the time derivatives into algebraic equations, which makes it easier to solve. We apply L.T. to the equations w.r.t the time domain, defined as

$$\mathscr{L}\left(w(x,y,t)\right)=\bar{w}(x,y,s)=\int_0^\infty e^{-st}w(x,y,t)\,dt.$$

$$\mathscr{L}\left(T\left(x,y,z,t\right)\right)=\Theta\left(x,y,z,s\right)=\int_0^\infty e^{-st}T\left(x,y,z,t\right)dt.$$

On applying L.T., under the initial conditions given by (4.11), we get

$$\begin{cases}\mathscr{L}\left(\frac{\partial w}{\partial t}\right)=s\bar{w},\ \mathscr{L}\left(\frac{\partial^2 w}{\partial t^2}\right)=s^2\bar{w},\\ \mathscr{L}\left(\frac{\partial T}{\partial t}\right)=s\Theta.\end{cases}$$

Using above expressions, set of equations in (4.10) reduce to

$$\begin{aligned}&\frac{1}{12A_R^2}\left[\left(\lambda+2\mu\right)\nabla_1^2\left(\nabla_1^2\bar{w}\right)+\left(\lambda\alpha_0+2\mu\alpha_1\right)\frac{c_1 s}{L}\nabla_1^2\left(\nabla_1^2\bar{w}\right)\right]\\&+\beta T_0\left(1+\frac{c_1\beta_0 s}{L}\right)\nabla_1^2 M_\Theta+\rho c_1^2 s^2\bar{w}=-\frac{q_0A_R^2}{s}.\end{aligned}\tag{4.14}$$

$$\left[\frac{\partial^2\Theta}{\partial x^2}+\frac{\partial^2\Theta}{\partial y^2}+A_R^2\frac{\partial^2\Theta}{\partial z^2}\right]=\frac{\rho C_e c_1 L s\gamma_0\Theta}{K}-\frac{c_1\beta z h^2}{KL}s\gamma_0\gamma_1\nabla_1^2\bar{w},\tag{4.15}$$

where $1+st_0=\gamma_0,\ 1+\frac{sc_1\beta_0}{L}=\gamma_1$ and

$$M_\Theta=\int_{-1/2}^{1/2}\Theta z dz.\tag{4.16}$$

Under the conditions that no heat flows through upper and lower surfaces of rectangular plate and considering the fact that thermal gradients are much larger along thickness direction than in the plane of cross section, ie., $\nabla_1^2\Theta << \frac{\partial^2\Theta}{\partial z^2}$, so the solution of equation (4.15) is obtained as follows:

$$\Theta\left(x,y,z,s\right)=\frac{\beta\gamma_1}{\rho C_e A_R^2}\left(z-\frac{\sin pz}{p\cos\left(p/2\right)}\right)\nabla_1^2\bar{w}\qquad\text{where}\quad p^2=-\frac{\rho C_e s\gamma_0\gamma_1}{K}.\tag{4.17}$$

Using the equation (4.16) to find M_Θ, we get

$$\nabla_1^2 M_\Theta=\frac{\beta\gamma_1}{12\rho C_e A_R^2}\left[1+\frac{24}{p^3}\left(\frac{p}{2}-\tan\left(\frac{p}{2}\right)\right)\right]\nabla_1^2\left(\nabla_1^2\bar{w}\right).\tag{4.18}$$

Using the above expression, equation (4.14) reduces to

$$\frac{1}{12A_R^2}\left[1+\varepsilon_0 s+\varepsilon_1\gamma_1^2\left(1+f\left(p\right)\right)\right]\nabla_1^2\left(\nabla_1^2\bar{w}\right)+s^2\bar{w}=-\frac{q_0A_R^2}{\rho c_1^2 s},\tag{4.19}$$

where $\varepsilon_0 = \frac{(\lambda\alpha_0+2\mu\alpha_1)c_1}{(\lambda+2\mu)L}$, $\varepsilon_1 = \frac{\beta^2 T_0}{\rho^2 C_e c_1^2}$, $(\lambda+2\mu) = \rho c_1^2$.
Re-writing the above expression, we get

$$G_s\nabla_1^2\left(\nabla_1^2\bar{w}\right) + s^2\bar{w} = -\frac{Q}{s}.$$

$$\nabla_1^2\left(\nabla_1^2\bar{w}\right) - \eta^4\bar{w} = -\frac{Q}{sG_s}. \tag{4.20}$$

where $Q = \frac{qA_R^2}{\rho c_1^2}$ and

$$G_s = \frac{1}{12A_R^2}\left[1+\varepsilon_0 s+\varepsilon_1\gamma_1^2\left(1+f\left(p\right)\right)\right], \eta^4 = -\frac{s^2}{G_s}. \tag{4.21}$$

Fourier Transform Technique

The Finite Fourier Sine Transform (FFST) method is used to investigate the differential equations mentioned in (4.20). In general, the Fourier transform makes it easier to analyse wave-like behaviour by converting functions from the spatial domain to the wavenumber domain. In particular, partial differential equations (PDEs) can be simplified by converting them into ordinary differential equations (ODEs) using the Finite Fourier Sine Transform. This transformation is especially helpful when the function is zero at the domain boundaries and fulfills homogeneous Dirichlet boundary constraints. The FFST greatly reduces computer complexity by breaking down the differential equation into a sequence of sine components by eliminating spatial derivatives. This method is useful for studying wave propagation, thermal conduction, and structural vibrations since it also sheds light on the system's inherent frequencies and mode shapes.
We apply Finite Fourier sine transform to the equation (4.20) w.r.t y, defined as:

$$\mathscr{W}\left(x,n,s\right) = \mathscr{F}\left(\bar{w}\left(x,y,s\right)\right) = \int_0^{\hat{b}} \bar{w}\left(x,y,s\right)\sin\left(\frac{n\pi y}{\hat{b}}\right)dy.$$

Using the boundary conditions from equations (4.12)-(4.13) along y, we get

$$\begin{cases} \mathscr{F}\left(\frac{\partial^2\bar{w}}{\partial y^2}\right) = -\frac{n^2\pi^2}{\hat{b}^2}\mathscr{W}, \\ \mathscr{F}\left(\frac{\partial^4\bar{w}}{\partial y^4}\right) = \frac{n^4\pi^4}{\hat{b}^4}\mathscr{W}. \end{cases} \tag{4.22}$$

Using the above expressions, equation (4.20) reduces to non-homogeneous differential equation with constant coefficients as following:

$$\left[\left(D^2-\frac{n^2\pi^2}{\hat{b}^2}\right)^2-\eta^4\right]\mathscr{W}=-\frac{Q\hat{b}\,(1-\cos n\pi)}{sG_s n\pi}. \tag{4.23}$$

where $D\equiv\frac{\partial}{\partial x}$

Solving the above differential equation, we get

$$\mathscr{W}=A\cosh m_1x+B\sinh m_1x+C\cos m_2x+D\sin m_2x-\frac{1}{\left(\frac{n^4\pi^4}{\hat{b}^4}-\eta^4\right)}.\left(\frac{Q\hat{b}\,(1-\cos n\pi)}{sG_s n\pi}\right). \tag{4.24}$$

Here $m_1=\sqrt{\eta^2+\frac{n^2\pi^2}{\hat{b}^2}}$, $m_2=\sqrt{\eta^2-\frac{n^2\pi^2}{\hat{b}^2}}$.
Using the boundary conditions along x from (4.12), (4.13), solution of (4.24) is obtained as follows:

Case I: For simply supported plate SSSS

$$\mathscr{W}=\left(\frac{Q\hat{b}\,(1-\cos n\pi)}{n\pi s\left(s^2+\frac{n^4\pi^4}{\hat{b}^4}G_s\right)}\right)\times\left[\frac{A_1(m_1,m_2)\cosh m_1x+B_1(m_1,m_2)\sinh m_1x+C_1(m_1,m_2)\cos m_2x+D_1(m_1,m_2)\sin m_2x}{H_1(m_1,m_2)}-1\right]. \tag{4.25}$$

Case II: For simply supported-clamped plate CSCS

$$\mathscr{W}=\left(\frac{Q\hat{b}\,(1-\cos n\pi)}{n\pi s\left(s^2+\frac{n^4\pi^4}{\hat{b}^4}G_s\right)}\right)\times\left[\frac{A_2(m_1,m_2)\cosh m_1x+B_2(m_1,m_2)\sinh m_1x+C_2(m_1,m_2)\cos m_2x+D_2(m_1,m_2)\sin m_2x}{H_2(m_1,m_2)}-1\right], \tag{4.26}$$

where

$A_1(m_1,m_2)=m_2^2\sinh m_1\sin m_2,\ B_1(m_1,m_2)=m_2^2(1-\cosh m_1)\sin m_2,$
$C_1(m_1,m_2)=m_1^2\sin m_2\sinh m_1,$
$D_1(m_1,m_2)=m_1^2(1-\cos m_2)\sinh m_1,\ H_1(m_1,m_2)=2\eta^2\sinh m_1\sin m_2,$
$A_2(m_1,m_2)=m_1m_2(1-\cos m_2)(\cosh m_1+1)-m_2^2\sinh m_1\sin m_2,$
$B_2(m_1,m_2)=m_2^2\sin m_2(\cosh m_1-1)-m_1m_2\sinh m_1(1-\cos m_2),$

$C_2(m_1,m_2) = m_1^2 \sinh m_1 \sin m_2 - m_1 m_2 (1+\cos m_2)(\cosh m_1 - 1)$,
$D_2(m_1,m_2) = m_1^2 \sinh m_1 (1-\cos m_2) - m_1 m_2 \sin m_2 (\cosh m_1 - 1)$,
$H_2(m_1,m_2) = 2m_1 m_2 (1-\cosh m_1 \cos m_2) + \left(m_1^2 - m_2^2\right) \sinh m_1 \sin m_2$.
Taking Inverse Finite Fourier sine transform of (4.25)-(4.26) w.r.t. y

$$\bar{w} = \frac{2}{\hat{b}} \sum_{n=1}^{\infty} \mathscr{W}(x,n,s) \sin \frac{n\pi y}{\hat{b}}.$$

Using method of residues for finding Inverse L.T. defined as:

$$\mathscr{L}^{-1}(\bar{w}(x,y,s)) = w(x,y,t) = \sum \text{Residues of } e^{st}\bar{w}(x,y,s). \tag{4.27}$$

Case I: For simply supported plate SSSS
$s = 0$ is pole of order 2 and residue is 0.
$s = \pm\iota \frac{n^2\pi^2}{\hat{b}^2}\sqrt{G_s} = \pm\iota s_1$ are simple poles.

Residues at $s = \pm\iota s_1$ is

$$\left[\frac{A_1(m_{11},m_{12})\cosh m_{11}x + B_1(m_{11},m_{12})\sinh m_{11}x + C_1(m_{11},m_{12})\cos m_{12}x + D_1(m_{11},m_{12})\sin m_{12}x}{H_1(m_{11},m_{12})}\right.$$

$$\left. - 1\right] \times \frac{Q\hat{b}e^{\pm\iota s_1 t}(\cos n\pi - 1)}{2n\pi s_1^2}$$

Singularities w.r.t $H_1(m_1,m_2) = 0, i.e.$, the auxiliary roots are given by Rao [68] as
$m_1 = \iota k\pi = m_{1k},\ m_2 = k\pi = m_{2k}; k = 1,2,3,\ldots$ are simple poles.
Using $m_{1k}^2 = \eta_{1k}^2 + \frac{n^2\pi^2}{\hat{b}^2},\ m_{2k}^2 = \eta_{2k}^2 - \frac{n^2\pi^2}{\hat{b}^2},\ s_{1k} = \pm\iota\eta_{1k}^2\sqrt{G_s},\ s_{2k} = \pm\iota\eta_{2k}^2\sqrt{G_s}$.

Residue at $s = s_{1k}$ is
$$\frac{Q\hat{b}e^{s_{1k}t}(1-\cos n\pi)}{n\pi s_{1k}\left(\frac{n^4\pi^4}{\hat{b}^4}G_s + s_{1k}^2\right)}\left[\frac{A_1(m_1,m_2)\cosh m_1x + B_1(m_1,m_2)\sinh m_1x + C_1(m_1,m_2)\cos m_2x + D_1(m_1,m_2)\sin m_2x}{2\eta_{1k}^2\frac{dH_1}{ds}}\right]_{m_1=m_{1k}}.$$

Residue at $s = s_{2k}$ is
$$\frac{Q\hat{b}e^{s_{2k}t}(1-\cos n\pi)}{n\pi s_{2k}\left(\frac{n^4\pi^4}{\hat{b}^4}G_s + s_{2k}^2\right)}\left[\frac{A_1(m_1,m_2)\cosh m_1x + B_1(m_1,m_2)\sinh m_1x + C_1(m_1,m_2)\cos m_2x + D_1(m_1,m_2)\sin m_2x}{2\eta_{2k}^2\frac{dH_1}{ds}}\right]_{m_2=m_{2k}}.$$

Case II: For simply supported-clamped plate CSCS
$s = 0$ is pole of order 2 and residue is 0.
$s = \pm\iota \frac{n^2\pi^2}{\hat{b}^2}\sqrt{G_s} = \pm\iota s_1$ are simple poles.

Residues at $s = \pm \iota s_1$ is

$$\left[\frac{A_2(m_{11},m_{12})\cosh m_{11}x + B_2(m_{11},m_{12})\sinh m_{11}x + C_2(m_{11},m_{12})\cos m_{12}x + D_2(m_{11},m_{12})\sin m_{12}x}{H_2(m_{11},m_{12})} - 1\right] \times \frac{Q\hat{b}e^{\pm \iota s_1 t}(\cos n\pi - 1)}{2n\pi s_1^2}$$

Singularities w.r.t $H_2(m_1,m_2) = 0, i.e.$, the auxiliary roots are given by Rao [68] as $m_1 = \iota\left(k+\frac{1}{2}\right)\pi = m_{1k},\ m_2 = \left(k+\frac{1}{2}\right)\pi = m_{2k}; k = 1,2,3,...$ are simple poles. Using $m_{1k}^2 = \eta_{1k}^2 + \frac{n^2\pi^2}{\hat{b}^2},\ m_{2k}^2 = \eta_{2k}^2 - \frac{n^2\pi^2}{\hat{b}^2},\ s_{1k} = \pm\iota\eta_{1k}^2\sqrt{G_s},\ s_{2k} = \pm\iota\eta_{2k}^2\sqrt{G_s}$.

Residue at $s = s_{1k}$ is

$$\frac{Q\hat{b}e^{s_{1k}t}(1-\cos n\pi)}{n\pi s_{1k}\left(\frac{n^4\pi^4}{\hat{b}^4}G_s + s_{1k}^2\right)}\left[\frac{A_2(m_1,m_2)\cosh m_1x + B_2(m_1,m_2)\sinh m_1x + C_2(m_1,m_2)\cos m_2x + D_2(m_1,m_2)\sin m_2x}{2\eta_{1k}^2\frac{dH_2}{ds}}\right]_{m_1=m_{1k}}.$$

Residue at $s = s_{2k}$ is

$$\frac{Q\hat{b}e^{s_{2k}t}(1-\cos n\pi)}{n\pi s_{2k}\left(\frac{n^4\pi^4}{\hat{b}^4}G_s + s_{2k}^2\right)}\left[\frac{A_2(m_1,m_2)\cosh m_1x + B_2(m_1,m_2)\sinh m_1x + C_2(m_1,m_2)\cos m_2x + D_2(m_1,m_2)\sin m_2x}{2\eta_{2k}^2\frac{dH_2}{ds}}\right]_{m_2=m_{2k}}.$$

where $s_1 = s_0\left[1 + \frac{\varepsilon_0 s_0}{2} + \frac{\beta^2\gamma_{10}^2 T_0}{2\rho^2 c_1^2 C_e}(1+fp_0)\right],\ s_0 = \frac{1}{2\sqrt{3}A_R}\frac{n^2\pi^2}{\hat{b}^2},\ \gamma_{10} = 1 + \frac{s_0\beta_0 c_1}{L},$
$P_0^2 = \frac{\rho C_e c_1 L s_0(1+s_0 t_0)}{KA_R^2},\ fp_0 = -\frac{12}{P_0^2} + \frac{24}{P_0^3}\tanh\left(\frac{P_0}{2}\right),\ \gamma_1 = 1 \pm \iota\frac{s_1\beta_0 c_1}{L},\ P_1^2 = \frac{\pm\iota s_1\rho C_e c_1 L(1\pm\iota s_1 t_0)}{KA_R^2},$
$fp_1 = -\frac{12}{P_1^2} + \frac{24}{P_1^3}\tanh\left(\frac{P_1}{2}\right),\ \eta_1^2 = 2\sqrt{3}A_R s_1\left(1 \mp \iota\frac{\varepsilon_0 s_1}{2} - \frac{\varepsilon_1\gamma_1^2}{2}(1+fp_1)\right),$
$m_{11} = \sqrt{\left(\eta_1^2 + \frac{n^2\pi^2}{\hat{b}^2}\right)},\ m_{12} = \sqrt{\left(\eta_1^2 - \frac{n^2\pi^2}{\hat{b}^2}\right)}.$

4.6 Numerical Results and Graphical Discussion

Consider viscothermoelastic solid like magnesium with the physical specifications from [36] as given below:
$\lambda = 9.4\times10^{10}N/m^2;\ \mu = 4.0\times10^{10}N/m^2;\ \rho = 1.74\times10^3 Kg/m^3;$
$C_e = 1.04\times10^3 JKg^{-1}deg^{-1};\ T_0 = 298^o\text{K};\ \alpha_0 = \alpha_1 = 0.779\times10^{-9};$
$K = 1.7\times10^6 Wm^{-1}deg^{-1};\ q_0 = 2\times10^{-7}$
Dimensions of the rectangular plate are taken as: $L = 500\mu m, h = 50\mu m, b = 100\mu m.$

Non-dimensional deflection has been computed for different modes in view of equation (4.27). Fig.$[4.2-4.9]$ represents variation in deflection along the dimensions of plate for different modes (1, 1), (1, 2), (2, 1) and (2, 2) for SSSS and CSCS plate under the uniform load. Numerical simulations utilizing MATLAB software programming were conducted for a material analogous to magnesium. Graphical representations of the computer-simulated outcomes were provided, depicting diverse boundary conditions.

The deflection plot clearly signifies the zero deflection at all the four edges. In case of Fig.$[4.6-4.9]$, the clamped edges are observed to be flat which signifies that rotation is restricted around these edges. While, in case of Fig.$[4.2-4.5]$, the absence of flatness in simply supported edges signify that bending of edges is allowed here. It has been remarked that the degree of deflection is greatest at the plate's centre and diminishes as we move away from it in either direction. The symmetric deflection profile depicts the uniform loading on the plate. It has been noted that, even as the mode indices increase, the plate continues to deform in one dominant direction under uniform load. Physically, this behaviour confirms that the uniform load excites a centrally concentrated bending field.

Also it is observed that $w_{11} < w_{12} < w_{21} < w_{22}$ in case of SSSS plate, but the values are in different order in case of CSCS plate $w_{12} < w_{22} < w_{11} < w_{21}$. The change in deflection due to different mode is found to be more forceful in SSSS plate than CSCS plate. The deflection is observed to be high in magnitude in SSSS as compared to CSCS. These results confirm that even limited clamping provides an effective means of reducing deflection without altering the plate geometry, making CSCS configurations advantageous in visco-thermoelastic components.

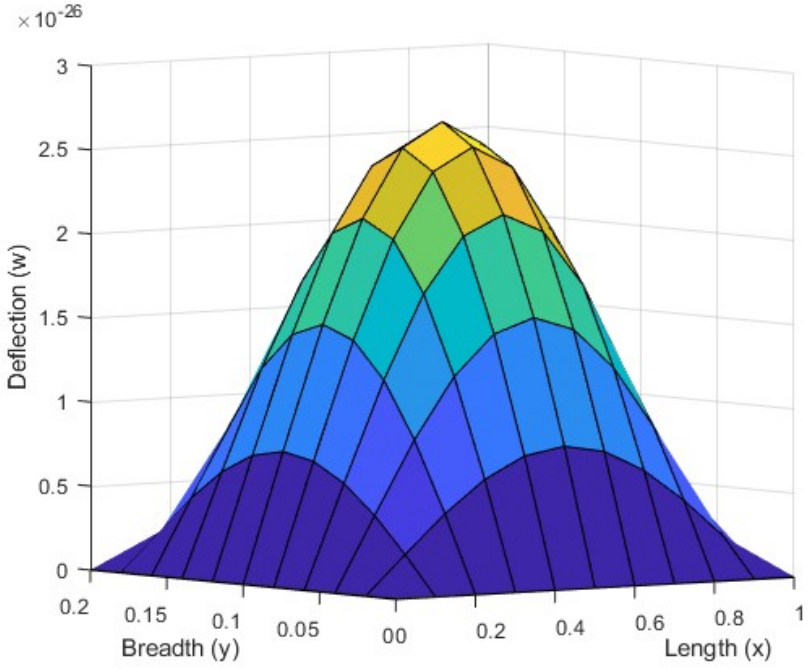

Figure 4.2: Variation of deflection for (1,1) mode in viscothermoelastic SSSS plate under uniform load along the (x,y) dimensions at $t = 30$

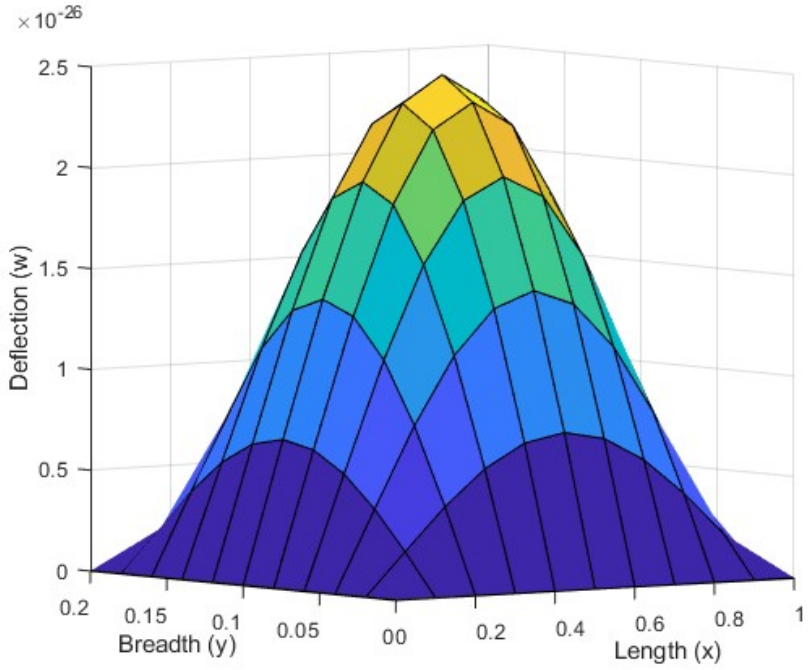

Figure 4.3: Variation of deflection for (1,2) mode in viscothermoelastic SSSS plate under uniform load along the (x,y) dimensions at $t = 30$.

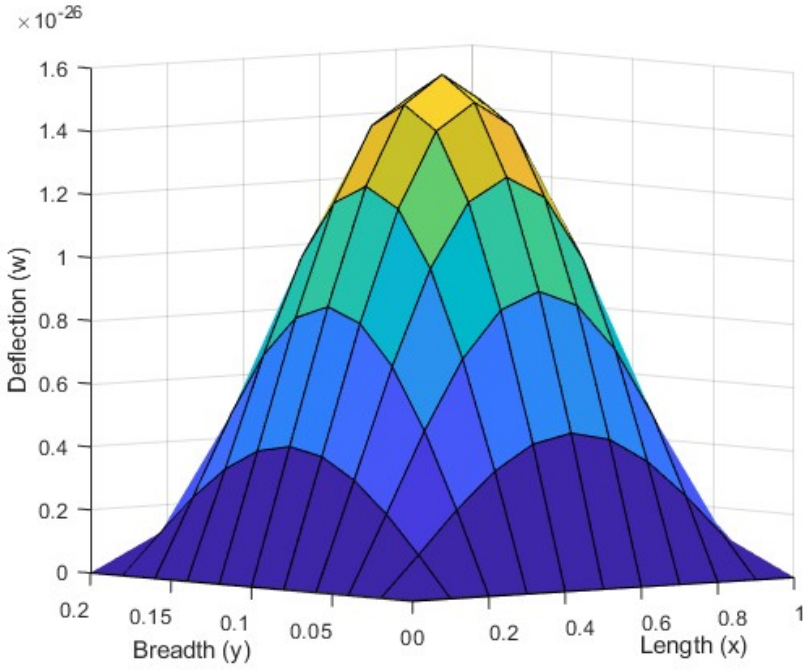

Figure 4.4: Variation of deflection for (2,1) mode in viscothermoelastic SSSS plate under uniform load along the (x,y) dimensions at $t = 30$.

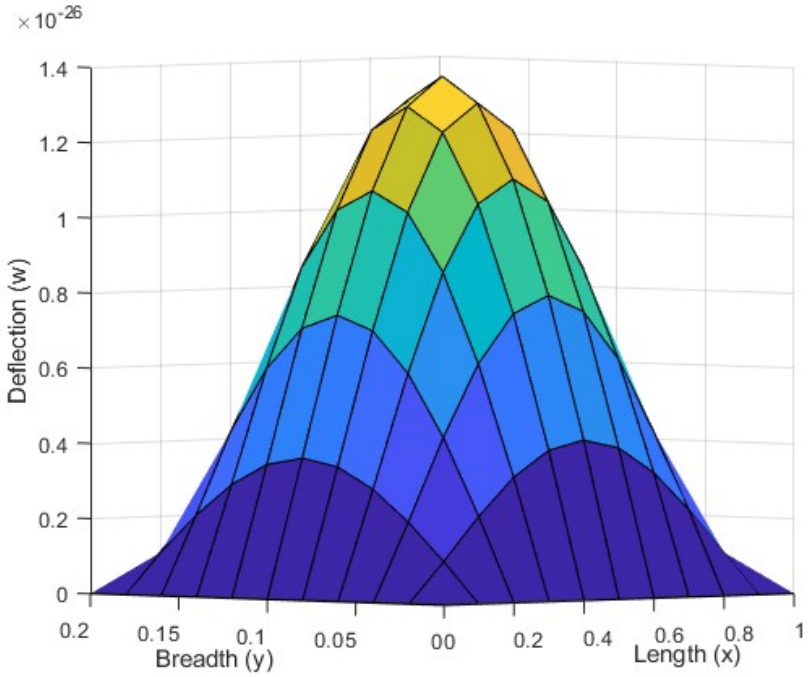

Figure 4.5: Variation of deflection for (2,2) mode in viscothermoelastic SSSS plate under uniform load along the (x,y) dimensions at $t = 30$.

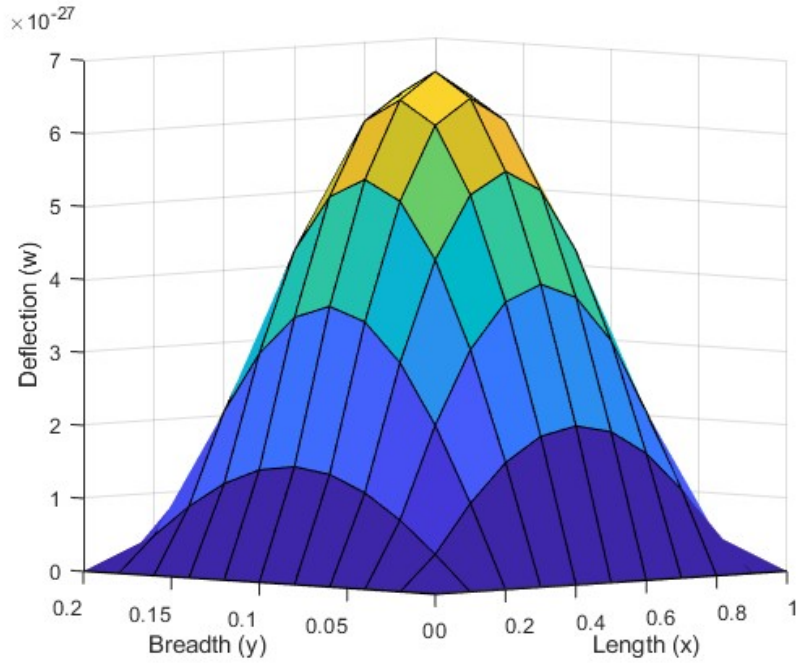

Figure 4.6: Variation of deflection for (1,1) mode in viscothermoelastic CSCS plate under uniform load along the (x,y) dimensions at $t = 30$.

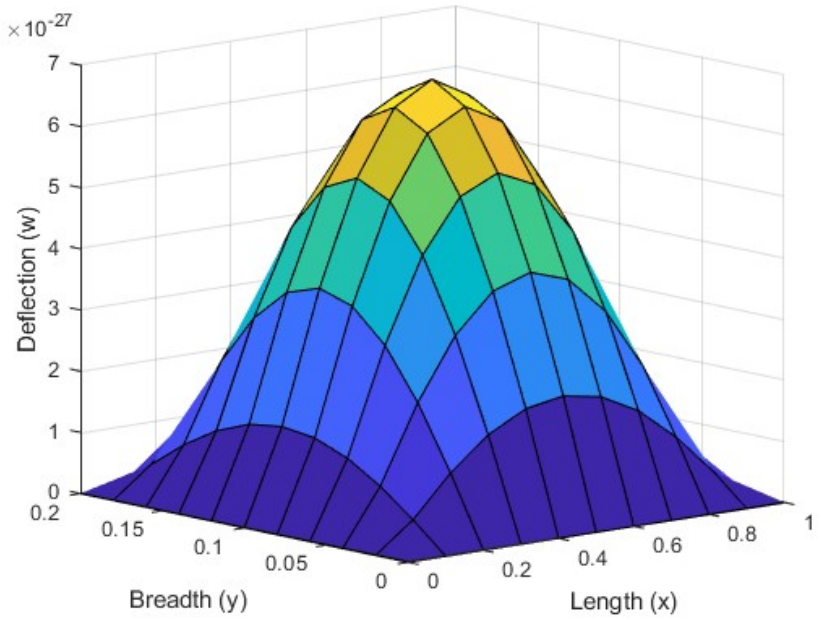

Figure 4.7: Variation of deflection for (1,2) mode in viscothermoelastic CSCS plate under uniform load along the (x,y) dimensions at $t = 30$.

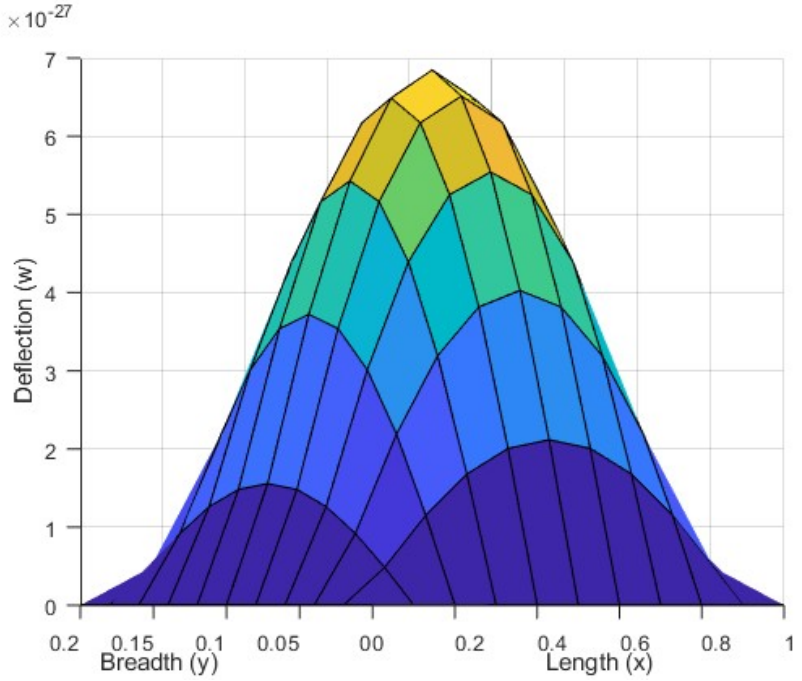

Figure 4.8: Variation of deflection for (2,1) mode in viscothermoelastic CSCS plate under uniform load along the (x,y) dimensions at $t = 30$.

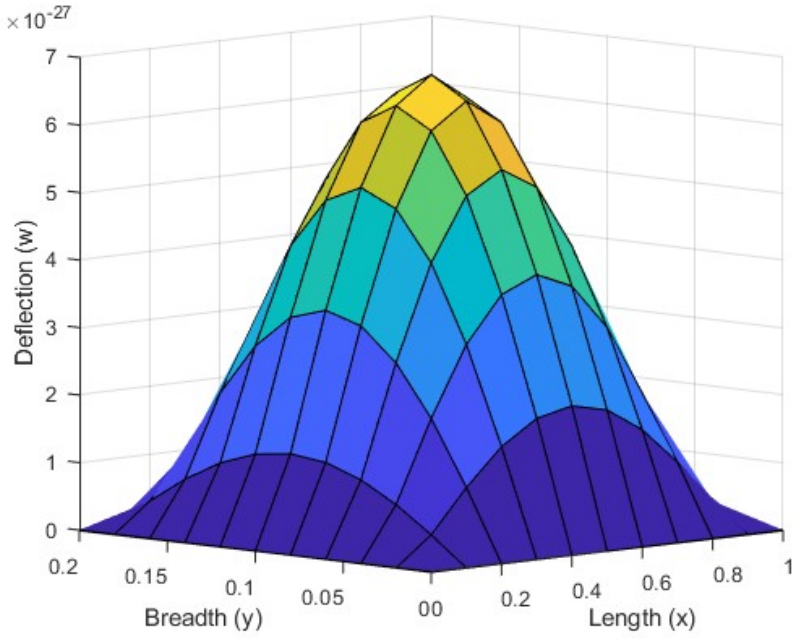

Figure 4.9: Variation of deflection for (2,2) mode in viscothermoelastic CSCS plate under uniform load along the (x, y) dimensions at $t = 30$.

4.7 Conclusion

An investigation was conducted into the dynamic behaviour of a uniform, isotropic viscothermoelastic rectangular plate subjected to uniform loading. The L.T. technique and FFST has been used w.r.t. time and spatial domain respectively. It is inferred that

1. The magnitude of deflection is more in SSSS as compared to CSCS.
2. The deflection curve is symmetrical about the centre of plate. The deflection is found to be more symmetrical along both the dimensions in case of SSSS as compared to CSCS.
3. Maxima of deflection occurs at the centre of plate and its magnitude diminishes progressively as it moves further away in either direction.
4. The change in deflection due to different mode is found to be more pronounced in SSSS plate than CSCS plate.

Chapter 5

Modeling and Analysis of Transverse Vibrations in Visco-thermoelastic Rectangular Plate of Silicon Nitride due to Harmonic Loading

5.1 Introduction

This chapter examines the dynamic response of viscothermoelastic rectangular plates under harmonic (time-periodic) transverse loading, following the investigation of deflection under uniform loading. Real life applications like panels, MEMS devices involve the oscillatory loads which makes it important to the study the deflection in viscothermoelastic rectangular plate under harmonic loading. These applications involve time-dependent inertia effects and resonance.

Li et al [35] presented an analytical model for the thermoelastic damping in the fully clamped and simply supported rectangular and circular microplates and derived the expression for quality factor using the energy dissipated over the volume of microplate per cycle of vibration. Lal and Saini [50] analysed the transverse vibration in thin rectangular plates of linearly varying thickness using generalized differential quadrature method. Grover [48] studied the effect of fixed aspect ratio and fixed dimensions on thermoelastic damping of out of plane vibrations in visco thermoelastic circular plate resonator. Grover and Seth [66] analysed the effect of time delay and mechanical relaxation time on thermoelastic damping using generalized dual-phase-lagging model. Liu et al [63] has studied the effect of size and shape on thermoelastic damping and out-of-plane vibration of the laminated rectangular plate. Youssef and El-Bary [81] derived the mathematical model for a circular microplate with boundaries under the effect of ramp heating in view of Kirchhoff's Love plate theory and dual-phase-lagging model and made the significant observations on damage parameters and the thickness of the resonator.

5.2 Primary Equations

The present problem examines about deflection induced in a rectangular plate when subjected to harmonic loading on the edges. A homogeneous, isotropic, thermally conductive viscothermoelastic rectangular undeformed plate is taken under consideration and is initially at temperature T_0. The fundamental equation governing its movement has been analysed within a Cartesian coordinate framework.

$$\sigma_{ij} = \lambda^* \delta_{ij} e_{kk} + 2\mu^* e_{ij} - \beta^* T \delta_{ij}. \tag{5.1}$$

Following Lord Shulman's generalized thermoelasticity model [5], the equations governing heat conduction, along with the constitutive relations, in the absence of heat sources and body forces, which dictate the displacement vector $u = (u_1, u_2, u_3)$ and temperature variation $T(x, y, z, t)$ at time t, are expressed as:

$$(\lambda^* + 2\mu^*) \nabla (\nabla . u) - \mu^* \nabla \times (\nabla \times u) - \beta_1^* \nabla T = \rho \frac{\partial^2 \nu}{\partial t^2}. \tag{5.2}$$

$$K \nabla^2 T = \rho C_e \left(\frac{\partial T}{\partial t} + t_0 \frac{\partial^2 T}{\partial t^2} \right) + \beta_1^* T_0 \left(\frac{\partial}{\partial t} + t_0 \frac{\partial^2}{\partial t^2} \right) \nabla . u. \tag{5.3}$$

5.3 Modelling of the problem

A homogeneous, isotropic, and viscothermoelastic rectangular plate is subjected to a loading condition that induces transverse deflection. The dimensions of plate are considered as length $L\,(0 \leq x \leq L)$, width $b\left(\frac{-b}{2} \leq y \leq \frac{b}{2}\right)$, and thickness $h\left(\frac{-h}{2} \leq z \leq \frac{h}{2}\right)$. This problem examines the resulting displacement and temperature distribution within the plate. Initially, the plate is in a state of equilibrium at a stable temperature T_0 with no applied stress or strain. In accordance with Kirchhoff-Love plate theory [22] assumptions,

1. No deformation occurs along the length of normal material line.
2. The normal material line continues to be straight, and the orthogonality property also remains preserved after deformation.

As a consequence of second assumption, the vertical shear strain $\gamma_{xz},\ \gamma_{yz}$ are insignificant. Also normal strain e_{zz} can be ignored since the deflection is primarily due to bending strains. The displacement vector u, temperature function T are the primary variables of interest in this problem. These variables describe the plate's mechanical

and thermal response, respectively, under the given loading and boundary conditions. Using the above assumptions, the relation between strain and displacement can be reduced to

$$e_{xx} = \frac{\partial v_1}{\partial x},\ e_{yy} = \frac{\partial u_2}{\partial y},\ e_{xy} = \frac{1}{2}\left(\frac{\partial u_1}{\partial y} + \frac{\partial u_2}{\partial x}\right). \tag{5.4}$$

$$e_{zz} = \frac{\partial u_3}{\partial z} = 0, \tag{5.5}$$

which implies that $u_3 = w(x,y,t)$.
Also $e_{xz} = \frac{1}{2}\left(\frac{\partial u_1}{\partial z} + \frac{\partial u_3}{\partial x}\right) = 0,\ e_{yz} = \frac{1}{2}\left(\frac{\partial u_2}{\partial z} + \frac{\partial u_3}{\partial y}\right) = 0.$
Keeping first assumption in mind and using above expressions, the displacement vector u is given as:

$$u_1 = -z\frac{\partial w}{\partial x},\ u_2 = -z\frac{\partial w}{\partial y},\ u_3 = w(x,y,t). \tag{5.6}$$

Using the above displacement vector values, equation (5.1) – (5.3) reduces to

$$\left.\begin{aligned}
\sigma_{xx} &= -z\lambda\left(\left(\tfrac{\partial^2 w}{\partial x^2} + \tfrac{\partial^2 w}{\partial y^2}\right) + \alpha_0\left(\tfrac{\partial^3 w}{\partial t\partial x^2} + \tfrac{\partial^3 w}{\partial t\partial y^2}\right)\right) - 2z\mu\left(\left(\tfrac{\partial^2 w}{\partial x^2} + \alpha_1\tfrac{\partial^3 w}{\partial t\partial x^2}\right)\right) - \beta\left(T + \beta_0\tfrac{\partial T}{\partial t}\right),\\
\sigma_{yy} &= -z\lambda\left(\left(\tfrac{\partial^2 w}{\partial x^2} + \tfrac{\partial^2 w}{\partial y^2}\right) + \alpha_0\left(\tfrac{\partial^3 w}{\partial t\partial x^2} + \tfrac{\partial^3 w}{\partial t\partial y^2}\right)\right) - 2z\mu\left(\left(\tfrac{\partial^2 w}{\partial y^2} + \alpha_1\tfrac{\partial^3 w}{\partial t\partial y^2}\right)\right) - \beta\left(T + \beta_0\tfrac{\partial T}{\partial t}\right),\\
\sigma_{xy} &= -2\mu z\left(\tfrac{\partial^2 w}{\partial x\partial y} + \alpha_1\tfrac{\partial^3 w}{\partial t\partial x\partial y}\right).
\end{aligned}\right\} \tag{5.7}$$

$$\left.\begin{aligned}
&-z(\lambda+2\mu)\left(\tfrac{\partial^3 w}{\partial x^3} + \tfrac{\partial^3 w}{\partial x\partial y^2}\right) - z(\lambda\alpha_0 + 2\mu\alpha_1)\left(\tfrac{\partial^4 w}{\partial t\partial x^3} + \tfrac{\partial^4 w}{\partial t\partial x\partial y^2}\right) - \beta\left(\tfrac{\partial T}{\partial x} + \beta_0\tfrac{\partial^2 T}{\partial x\partial t}\right) = -\rho z\tfrac{\partial^3 w}{\partial x\partial t^2},\\
&-z(\lambda+2\mu)\left(\tfrac{\partial^3 w}{\partial y^3} + \tfrac{\partial^3 w}{\partial y\partial x^2}\right) - z(\lambda\alpha_0 + 2\mu\alpha_1)\left(\tfrac{\partial^4 w}{\partial t\partial y\partial x^2} + \tfrac{\partial^4 w}{\partial t\partial y^3}\right) - \beta\left(\tfrac{\partial T}{\partial y} + \beta_0\tfrac{\partial^2 T}{\partial y\partial t}\right) = -\rho z\tfrac{\partial^3 w}{\partial y\partial t^2},\\
&-\lambda\left(\left(\tfrac{\partial^2 w}{\partial x^2} + \tfrac{\partial^2 w}{\partial y^2}\right) + \alpha_0\left(\tfrac{\partial^3 w}{\partial t\partial x^2} + \tfrac{\partial^3 w}{\partial t\partial y^2}\right)\right) - \beta\left(\tfrac{\partial T}{\partial z} + \beta_0\tfrac{\partial^2 T}{\partial z\partial t}\right) = \rho\tfrac{\partial^2 w}{\partial t^2}.
\end{aligned}\right\} \tag{5.8}$$

$$\begin{aligned}
K\left(\frac{\partial^2 T}{\partial x^2} + \frac{\partial^2 T}{\partial y^2} + \frac{\partial^2 T}{\partial z^2}\right) &= \rho C_e\left(\frac{\partial T}{\partial t} + t_0\frac{\partial^2 T}{\partial t^2}\right)\\
&\quad - \beta z T_0\left(1 + \beta_0\frac{\partial}{\partial t}\right)\left(\frac{\partial}{\partial t} + t_0\frac{\partial^2}{\partial t^2}\right)\left(\frac{\partial^2 w}{\partial x^2} + \frac{\partial^2 w}{\partial y^2}\right).
\end{aligned} \tag{5.9}$$

Due to the normal stresses, $\sigma_{xx},\ \sigma_{yy}$, viscothermoelastic plate experiences bending moments per unit length $M_{xx},\ M_{yy}$ and additionally due to the shearing stress σ_{xy}, it experiences twisting moment per unit length M_{xy} given by:
$M_{xx} = \int_{-h/2}^{h/2} \sigma_{xx}\, z dz,\ M_{yy} = \int_{-h/2}^{h/2} \sigma_{yy}\, z dz,\ M_{xy} = \int_{-h/2}^{h/2} \sigma_{xy}\, z dz.$

On evaluating bending moments using the stress components from (5.7), we get

$$\left.\begin{aligned} M_{xx} &= -\tfrac{h^3}{12}\left[\lambda\left(\left(\tfrac{\partial^2 w}{\partial x^2}+\tfrac{\partial^2 w}{\partial y^2}\right)+\alpha_0\left(\tfrac{\partial^3 w}{\partial t\partial x^2}+\tfrac{\partial^3 w}{\partial t\partial y^2}\right)\right)+2\mu\left(\tfrac{\partial^2 w}{\partial x^2}+\alpha_1\tfrac{\partial^3 w}{\partial t\partial x^2}\right)\right]-\beta\left[M_T+\beta_0\tfrac{\partial M_T}{\partial t}\right],\\ M_{yy} &= -\tfrac{h^3}{12}\left[\lambda\left(\left(\tfrac{\partial^2 w}{\partial x^2}+\tfrac{\partial^2 w}{\partial y^2}\right)+\alpha_0\left(\tfrac{\partial^3 w}{\partial t\partial x^2}+\tfrac{\partial^3 w}{\partial t\partial y^2}\right)\right)+2\mu\left(\tfrac{\partial^2 w}{\partial y^2}+\alpha_1\tfrac{\partial^3 w}{\partial t\partial y^2}\right)\right]-\beta\left[M_T+\beta_0\tfrac{\partial M_T}{\partial t}\right],\\ M_{xy} &= -2\mu\tfrac{h^3}{12}\left(\tfrac{\partial^2 w}{\partial x\partial y}+\alpha_1\tfrac{\partial^3 w}{\partial t\partial x\partial y}\right), \end{aligned}\right\} \tag{5.10}$$

where $M_T = \int_{-h/2}^{h/2} Tz\,dz$ is the moment generated in the plate due to thermal effects.
Now Considering equation of transverse motion in plate

$$\frac{\partial^2 M_{xx}}{\partial x^2}+2\frac{\partial^2 M_{xy}}{\partial x\partial y}+\frac{\partial^2 M_{yy}}{\partial y^2}+q(x,y,t)=\rho h\frac{\partial^2 w}{\partial t^2}, \tag{5.11}$$

where $q(x,y,t)$ represents loading on plate. Taking harmonic loading into account to study the effects; i.e.,$q(x,y,t) = -q_0(1-\cos\omega t)$ and
Putting the values of bending moments from equation (5.10) in (5.11), we get

$$\begin{aligned} &-\frac{h^3}{12}\left(\left(\frac{\partial^2}{\partial x^2}+\frac{\partial^2}{\partial y^2}\right)^2 w+\frac{\varepsilon_0 L}{c_1}\frac{\partial}{\partial t}\left(\frac{\partial^2}{\partial x^2}+\frac{\partial^2}{\partial y^2}\right)^2 w\right)\\ &-\frac{\rho C_e\varepsilon_1}{\beta T_0}\left(\frac{\partial^2}{\partial x^2}+\frac{\partial^2}{\partial y^2}\right)\left(M_T+\beta_0\frac{\partial M_T}{\partial t}\right)=\frac{q_0(1-\cos\omega t)}{\rho c_1^2}+\frac{h}{c_1^2}\frac{\partial^2 w}{\partial t^2}, \end{aligned} \tag{5.12}$$

where $(\lambda+2\mu)=\rho c_1^2,\ \frac{\lambda\alpha_0+2\mu\alpha_1}{\rho c_1 L}=\varepsilon_0,\ \frac{\beta^2 T_0}{\rho^2 C_e c_1^2}=\varepsilon_1.$
Defining non-dimensional quantities as:

$$X=\frac{x}{L},\ Y=\frac{y}{L},\ W=\frac{w}{h},\ Z=\frac{z}{h},\ \tau=\frac{c_1}{L}t,\ \tau_0=\frac{c_1}{L}t_0,\ \theta=\frac{T-T_0}{T_0},\ \Omega=\frac{L}{c_1}\omega.$$

Making use of the non-dimensional quantities in equations (5.9) and (5.12), we get

$$\left.\begin{aligned} &\tfrac{1}{12A_R^2}\left[\nabla_1^2\left(\nabla_1^2 W\right)+\varepsilon_0\tfrac{\partial}{\partial\tau}\nabla_1^2\left(\nabla_1^2 W\right)\right]+\tfrac{\rho C_e\varepsilon_1}{\beta}\nabla_1^2\left(M_\theta+\tfrac{c_1\beta_0}{L}\tfrac{\partial M_\theta}{\partial\tau}\right)+\tfrac{\partial^2 W}{\partial\tau^2}=-Q_0(1-\cos\Omega\tau),\\ &K\left[\tfrac{\partial^2\theta}{\partial X^2}+\tfrac{\partial^2\theta}{\partial Y^2}+A_R^2\tfrac{\partial^2\theta}{\partial Z^2}\right]=\rho C_e c_1 L\left(\tfrac{\partial\theta}{\partial\tau}+\tau_0\tfrac{\partial^2\theta}{\partial\tau^2}\right)-\tfrac{c_1\beta Z h^2}{L}\left(1+\tfrac{\beta_0 c_1}{L}\tfrac{\partial}{\partial\tau}\right)\left(\tfrac{\partial}{\partial\tau}+\tau_0\tfrac{\partial^2}{\partial\tau^2}\right)\nabla_1^2 W, \end{aligned}\right\} \tag{5.13}$$

where $M_\theta=\int_{-1/2}^{1/2}\theta Z\,dZ,\ A_R=\frac{L}{h},\ Q_0=\frac{q_0 A_R^2}{\rho c_1^2},\ \nabla_1^2=\left(\frac{\partial^2}{\partial X^2}+\frac{\partial^2}{\partial Y^2}\right).$

5.4 Initial and Boundary Conditions

A rectangular plate is considered under two set of boundary conditions. In one set of conditions, all the edges are taken under simply supported conditions (SSSS) and in the

other set, edges are taken under clamped and simply supported conditions alternatively (CSCS). The initial conditions in rectangular plate are considered as:

$$W(X,Y,0)=\left(\frac{\partial W}{\partial \tau}\right)_{\tau=0}=\left(\frac{\partial^2 W}{\partial \tau^2}\right)_{\tau=0}=0, \theta(X,Y,Z,0)=\left(\frac{\partial \theta}{\partial \tau}\right)_{\tau=0}=0, \quad (5.14)$$

and the following boundary conditions by Rao [68] are taken into account.

Set I: For simply supported plate SSSS

$$\left.\begin{array}{l} W(0,Y,\tau)=W(1,Y,\tau)=0 \text{ and } W(X,0,\tau)=W(X,\hat{b},\tau)=0, \\ \left(\frac{\partial^2 W}{\partial X^2}\right)_{X=0}=\left(\frac{\partial^2 W}{\partial X^2}\right)_{X=1}=0 \text{ and } \left(\frac{\partial^2 W}{\partial Y^2}\right)_{Y=0}=\left(\frac{\partial^2 W}{\partial Y^2}\right)_{Y=\hat{b}}=0. \end{array}\right\} \quad (5.15)$$

Set II: For clamped-simply supported plate CSCS

$$\left.\begin{array}{l} W(0,Y,\tau)=W(1,Y,\tau)=0 \text{ and } W(X,0,\tau)=W(X,\hat{b},\tau)=0, \\ \left(\frac{\partial W}{\partial X}\right)_{X=0}=\left(\frac{\partial W}{\partial X}\right)_{X=1}=0 \quad \text{and} \quad \left(\frac{\partial^2 W}{\partial Y^2}\right)_{Y=0}=\left(\frac{\partial^2 W}{\partial Y^2}\right)_{Y=\hat{b}}=0. \end{array}\right\} \quad (5.16)$$

Here $\hat{b}=\frac{b}{L}$.

Also, No heat flows across the lower and upper surface of rectangular plate, i.e., $\frac{\partial \theta}{\partial Z}=0$ at $Z=\pm\frac{1}{2}$.

5.5 Solution in the direction of thickness

Laplace Transform technique

Applying L.T. to the equations w.r.t the time domain, defined as:

$$\bar{W}(X,Y,s)=\int_0^\infty e^{-s\tau}W(X,Y,\tau)\,d\tau \text{ and } \Theta(X,Y,Z,s)=\int_0^\infty e^{-s\tau}\theta(X,Y,Z,\tau)\,d\tau.$$

On applying L.T., under the initial conditions given by (5.14), equations in (5.13) reduce to

$$\frac{1}{12A_R^2}\left[\nabla_1^2\left(\nabla_1^2\bar{W}\right)+\varepsilon_0 s\nabla_1^2\left(\nabla_1^2\bar{W}\right)\right]+\frac{\rho C_e\varepsilon_1}{\beta}\left(1+\frac{c_1\beta_0 s}{L}\right)\nabla_1^2 M_\Theta+s^2\bar{W}=-\frac{Q_0\Omega^2}{s\left(s^2+\Omega^2\right)}. \quad (5.17)$$

$$K\left[\frac{\partial^2\Theta}{\partial X^2}+\frac{\partial^2\Theta}{\partial Y^2}+A_R^2\frac{\partial^2\Theta}{\partial Z^2}\right]=\rho C_e c_1 Ls(1+s\tau_0)\Theta-\frac{c_1\beta Zh^2}{L}s(1+s\tau_0)\left(1+\frac{sc_1\beta_0}{L}\right)\nabla_1^2\bar{W}, \quad (5.18)$$

where

$$M_\Theta=\int_{-1/2}^{1/2}\Theta Z dZ. \quad (5.19)$$

Considering the fact that thermal gradients are considerably more pronounced along thickness direction than within the plane of cross section, i.e., $\nabla_1^2\Theta$ is negligible as compared to $\frac{\partial^2\Theta}{\partial Z^2}$, the solution of equation (5.18) is obtained as follows:

$$\Theta(X,Y,Z,s) = \frac{\beta\left(1+\frac{sc_1\beta_0}{L}\right)}{\rho C_e A_R^2}\left(Z - \frac{\sin pZ}{p\cos(p/2)}\right)\nabla_1^2\bar{W} \quad \text{where} \quad p^2 = -\frac{\rho C_e c_1 L s(1+s\tau_0)}{KA_R^2}. \tag{5.20}$$

Using the equation (5.19) to find M_Θ, we get

$$\nabla_1^2 M_\Theta = \frac{\beta\left(1+\frac{sc_1\beta_0}{L}\right)}{12\rho C_e A_R^2}\left[1+\frac{24}{p^3}\left(\frac{p}{2}-\tan\left(\frac{p}{2}\right)\right)\right]\nabla_1^2\left(\nabla_1^2\bar{W}\right). \tag{5.21}$$

Using the above expression, equation (5.17) reduces to

$$\frac{1}{12A_R^2}\left[1+\varepsilon_0 s+\varepsilon_1\gamma_1^2(1+g(p))\right]\nabla_1^2\left(\nabla_1^2\bar{W}\right)+s^2\bar{W} = -\frac{Q_0\Omega^2}{s(s^2+\Omega^2)}, \tag{5.22}$$

where $1+s\tau_0=\gamma_0,\ 1+\frac{sc_1\beta_0}{L}=\gamma_1$.
Re-writing the above expression, we get

$$D_s\nabla_1^2\left(\nabla_1^2\bar{W}\right)+s^2\bar{W} = -\frac{Q_0\Omega^2}{s(s^2+\Omega^2)}.$$

$$\nabla_1^2\left(\nabla_1^2\bar{W}\right)-\eta^4\bar{W} = -\frac{Q_0\Omega^2}{s(s^2+\Omega^2)D_s}, \tag{5.23}$$

where

$$D_s = \frac{1}{12A_R^2}\left[1+\varepsilon_0 s+\varepsilon_1\gamma_1^2(1+g(p))\right], \eta^4 = -\frac{s^2}{D_s}. \tag{5.24}$$

Fourier Transform Technique

Making use of Finite Fourier sine transform w.r.t Y, defined as:
$\mathscr{W}(X,n,s) = \mathscr{F}(\bar{W}(X,Y,s)) = \int_0^{\hat{b}} \bar{W}(X,Y,s)\sin\left(\frac{n\pi Y}{\hat{b}}\right)dY,$
and using the boundary conditions from equations (5.15)-(5.16) along Y, we get

$$\begin{cases} \mathscr{F}\left(\frac{\partial^2\bar{W}}{\partial Y^2}\right) = -\frac{n^2\pi^2}{\hat{b}^2}\mathscr{W}, \\ \mathscr{F}\left(\frac{\partial^4\bar{W}}{\partial Y^4}\right) = \frac{n^4\pi^4}{\hat{b}^4}\mathscr{W}. \end{cases} \tag{5.25}$$

Applying Finite Fourier sine Transform to eq. (5.23) and using the above values, a constant coefficient non-homogeneous differential equation is obtained as follows:

$$\left[\left(D^2-\frac{n^2\pi^2}{\hat{b}^2}\right)^2-\eta^4\right]\mathscr{W}=-\frac{Q_0\hat{b}\Omega^2\left(1-\cos n\pi\right)}{s\left(s^2+\Omega^2\right)D_s n\pi}, \tag{5.26}$$

where $D\equiv\frac{\partial}{\partial x}$.
On solving the above differential equation, we get

$$\mathscr{W}=A\cos k_1X+B\sin k_1X+C\cosh k_2X+D\sinh k_2X-\frac{1}{\left(\frac{n^4\pi^4}{\hat{b}^4}-\eta^4\right)}\left(\frac{Q_0\hat{b}\Omega^2\left(1-\cos n\pi\right)}{s\left(s^2+\Omega^2\right)D_s n\pi}\right). \tag{5.27}$$

Here $k_1=\sqrt{\eta^2-\frac{n^2\pi^2}{\hat{b}^2}}$, $k_2=\sqrt{\eta^2+\frac{n^2\pi^2}{\hat{b}^2}}$.
Using the boundary conditions along X from (5.15), (5.16), solution of (5.27) is obtained as follows:

Set I: For simply supported plate SSSS

$$\mathscr{W}=\left[\frac{A_1\left(k_1,k_2\right)\cos k_1X+B_1\left(k_1,k_2\right)\sin k_1X+C_1\left(k_1,k_2\right)\cosh k_2X+D_1\left(k_1,k_2\right)\sinh k_2X}{G_1\left(k_1,k_2\right)}-1\right]\times\left(\frac{Q_0\hat{b}\Omega^2\left(1-\cos n\pi\right)}{n\pi s\left(s^2+\Omega^2\right)\left(s^2+\frac{n^4\pi^4}{\hat{b}^4}D_s\right)}\right). \tag{5.28}$$

Set II: For simply supported-clamped plate CSCS

$$\mathscr{W}=\left[\frac{A_2\left(k_1,k_2\right)\cos k_1X+B_2\left(k_1,k_2\right)\sin k_1X+C_2\left(k_1,k_2\right)\cosh k_2X+D_2\left(k_1,k_2\right)\sinh k_2X}{G_2\left(k_1,k_2\right)}-1\right]\times\left(\frac{Q_0\hat{b}\Omega^2\left(1-\cos n\pi\right)}{n\pi s\left(s^2+\Omega^2\right)\left(s^2+\frac{n^4\pi^4}{\hat{b}^4}D_s\right)}\right), \tag{5.29}$$

where $A_1\left(k_1,k_2\right)=k_2^2\sin k_1\sinh k_2$, $B_1\left(k_1,k_2\right)=k_2^2\sinh k_2\left(1-\cos k_1\right)$,
$C_1\left(k_1,k_2\right)=k_1^2\sin k_1\sinh k_2$, $D_1\left(k_1,k_2\right)=k_1^2\sin k_1\left(1-\cosh k_2\right)$,
$G_1\left(k_1,k_2\right)=2\eta^2\sin k_1\sinh k_2$,
$A_2\left(k_1,k_2\right)=k_2^2\sin k_1\sinh k_2-k_1k_2\left(1+\cos k_1\right)\left(\cosh k_2-1\right)$,
$B_2\left(k_1,k_2\right)=k_2^2\sinh k_2\left(1-\cos k_1\right)-k_1k_2\sin k_1\left(\cosh k_2-1\right)$,
$C_2\left(k_1,k_2\right)=k_1k_2\left(1-\cos k_1\right)\left(\cosh k_2+1\right)-k_1^2\sinh k_2\sin k_1$,
$D_2\left(k_1,k_2\right)=k_1^2\sin k_1\left(\cosh k_2-1\right)-k_1k_2\sinh k_2\left(1-\cos k_1\right)$,

$G_2(k_1,k_2) = 2k_1k_2(1-\cosh k_2\cos k_1) + \left(k_2^2-k_1^2\right)\sinh k_2\sin k_1.$
Taking Inverse Finite Fourier sine transform of (5.28)-(5.29) w.r.t. Y

$$\bar{W} = \frac{2}{\hat{b}}\sum_{n=1}^{\infty} \mathscr{W}(X,n,s)\sin\frac{n\pi Y}{\hat{b}}.$$

Using method of residues for finding Inverse L.T. defined as:

$$W(X,Y,\tau) = \sum \text{Residues of } e^{s\tau}\bar{W}(X,Y,s). \tag{5.30}$$

Set I: For simply supported plate SSSS
$s=0$ is pole of order 2 and residue is 0.
$s = \pm\iota\Omega$ are simple poles and **Residue at** $s = \pm\iota\Omega$ **is**

$$-\frac{Q\hat{b}e^{\pm\iota\Omega\tau}(1-\cos n\pi)}{2n\pi\left(\frac{n^4\pi^4}{\hat{b}^4}D_s-\Omega^2\right)}\times$$

$$\left[\frac{A_1(k_{11},k_{21})\cos k_{11}X + B_1(k_{11},k_{21})\sin k_{11}X + C_1(k_{11},k_{21})\cosh k_{21}X + D_1(k_{11},k_{21})\sinh k_{21}X}{G_1(k_{11},k_{21})} - 1\right].$$

$s = \pm\iota\dfrac{n^2\pi^2}{\hat{b}^2}\sqrt{D_s} = \pm\iota s_1$ are simple poles and **Residue at** $s = \pm\iota s_1$ **is**

$$-\frac{Q\hat{b}\Omega^2e^{\pm\iota s_1\tau}(1-\cos n\pi)}{2n\pi^2s_1^2\left(\Omega^2-s_1^2\right)}\times$$

$$\left[\frac{A_1(k_{12},k_{22})\cos k_{12}X + B_1(k_{12},k_{22})\sin k_{12}X + C_1(k_{12},k_{22})\cosh k_{22}X + D_1(k_{12},k_{22})\sinh k_{22}X}{G_1(k_{12},k_{22})} - 1\right].$$

Singularities w.r.t $G_1(k_1,k_2)=0$ are given by [68] as $k_1 = m\pi = k_{1m},\ k_2 = \iota m\pi = k_{2m}; m = 1,2,3,...$ are simple poles.
Using $k_{1m}^2 = \eta_{1m}^2 - \frac{n^2\pi^2}{\hat{b}^2},\ k_{2m}^2 = \eta_{2m}^2 + \frac{n^2\pi^2}{\hat{b}^2},\ s_{1m} = \pm\iota\eta_{1m}^2\sqrt{D_s},\ s_{2m} = \pm\iota\eta_{2m}^2\sqrt{D_s}.$
Residue at $s = s_{1m}$ is

$$\frac{Q\hat{b}\Omega^2e^{s_{1m}\tau}(1-\cos n\pi)}{n\pi s_{1m}\left(s_{1m}^2+\Omega^2\right)\left(\frac{n^4\pi^4}{\hat{b}^4}D_s+s_{1m}^2\right)}\times$$

$$\left[\frac{A_1(k_1,k_2)\cosh k_1x + B_1(k_1,k_2)\sinh k_1x + C_1(k_1,k_2)\cos k_2x + D_1(k_1,k_2)\sin k_2x}{\frac{dG_1}{ds}} - 1\right]_{k_1=k_{1m}}.$$

Residue at $s = s_{2m}$ is

$$\frac{Q\hat{b}e^{s_{2m}\tau}\left(1-\cos n\pi\right)}{n\pi s_{2m}\left(s_{2m}^2+\Omega^2\right)\left(\frac{n^4\pi^4}{\hat{b}^4}D_s+s_{2m}^2\right)}\times$$

$$\left[\frac{A_1\left(k_1,k_2\right)\cosh k_1x+B_1\left(k_1,k_2\right)\sinh k_1x+C_1\left(k_1,k_2\right)\cos k_2x+D_1\left(k_1,k_2\right)\sin k_2x}{\frac{dG_1}{ds}}-1\right]_{k_2=k_{2m}}.$$

Set II: For simply supported-clamped plate CSCS

$s=0$ is pole of order 2 and residue is 0.

$s=\pm\iota\Omega$ are simple poles and **Residue at $s=\pm\iota\Omega$ is**

$$-\frac{Q\hat{b}e^{\pm\iota\Omega\tau}\left(1-\cos n\pi\right)}{2n\pi\left(\frac{n^4\pi^4}{\hat{b}^4}D_s-\Omega^2\right)}\times$$

$$\left[\frac{A_2\left(k_{11},k_{21}\right)\cos k_{11}X+B_2\left(k_{11},k_{21}\right)\sin k_{11}X+C_2\left(k_{11},k_{21}\right)\cosh k_{21}X+D_2\left(k_{11},k_{21}\right)\sinh k_{21}X}{G_2\left(k_{11},k_{21}\right)}-1\right].$$

$s=\pm\iota\frac{n^2\pi^2}{\hat{b}^2}\sqrt{D_s}=\pm\iota s_1$ are simple poles and **Residue at $s=\pm\iota s_1$ is**

$$-\frac{Q\hat{b}\Omega^2e^{\pm\iota s_1\tau}\left(1-\cos n\pi\right)}{2n\pi s_1^2\left(\Omega^2-s_1^2\right)}\times$$

$$\left[\frac{A_2\left(k_{12},k_{22}\right)\cos k_{12}X+B_2\left(k_{12},k_{22}\right)\sin k_{12}X+C_2\left(k_{12},k_{22}\right)\cosh k_{22}X+D_2\left(k_{12},k_{22}\right)\sinh k_{22}X}{G_2\left(k_{12},k_{22}\right)}-1\right].$$

Singularities w.r.t $G_2\left(k_1,k_2\right)=0$ are given by [68] as $k_1=\left(m+\frac{1}{2}\right)\pi=k_{1m},\ k_2=\iota\left(m+\frac{1}{2}\right)\pi=k_{2m};k=1,2,3,...$ are simple poles. Using $k_{1m}^2=\eta_{1m}^2+\frac{n^2\pi^2}{\hat{b}^2},\ k_{2m}^2=\eta_{2m}^2-\frac{n^2\pi^2}{\hat{b}^2},\ s_{1m}=\pm\iota\eta_{1m}^2\sqrt{D_s}$,
$s_{2m}=\pm\iota\eta_{2m}^2\sqrt{D_s}$.

Residue at $s=s_{1m}$ is

$$\frac{Q\hat{b}e^{s_{1m}t}\left(1-\cos n\pi\right)}{n\pi s_{1m}\left(s_{1m}^2+\Omega^2\right)\left(\frac{n^4\pi^4}{\hat{b}^4}D_s+s_{1m}^2\right)}\times$$

$$\left[\frac{A_2\left(k_1,k_2\right)\cosh k_1x+B_2\left(k_1,k_2\right)\sinh k_1x+C_2\left(k_1,k_2\right)\cos k_2x+D_2\left(k_1,k_2\right)\sin k_2x}{\frac{dG_2}{ds}}-1\right]_{k_1=k_{1m}}.$$

Residue at $s=s_{2m}$ is

$$\frac{Q\hat{b}e^{s_{2m}t}\left(1-\cos n\pi\right)}{n\pi s_{2m}\left(s_{2m}^2+\Omega^2\right)\left(\frac{n^4\pi^4}{\hat{b}^4}D_s+s_{2m}^2\right)}\times$$

$$\left[\frac{A_2(k_1,k_2)\cosh k_1x+B_2(k_1,k_2)\sinh k_1x+C_2(k_1,k_2)\cos k_2x+D_2(k_1,k_2)\sin k_2x}{\frac{dG_2}{ds}}-1\right]_{k_2=k_{2m}}.$$

Here, for singularity $s=\pm\iota\Omega$

$\eta_1^2=\left(\frac{\Omega}{\sqrt{D_s}}\right)_{s=\pm\iota\Omega}$, $k_{11}=\sqrt{\left(\eta_1^2-\frac{n^2\pi^2}{\hat{b}^2}\right)}$, $k_{21}=\sqrt{\left(\eta_1^2+\frac{n^2\pi^2}{\hat{b}^2}\right)}$

and for $s=\pm\iota s_1$

$\eta_2^2=\left(\frac{s_1}{\sqrt{D_s}}\right)_{s=\pm\iota s_1}$, $k_{12}=\sqrt{\left(\eta_2^2-\frac{n^2\pi^2}{\hat{b}^2}\right)}$, $k_{22}=\sqrt{\left(\eta_2^2+\frac{n^2\pi^2}{\hat{b}^2}\right)}$,

$s_1=s_0\left[1+\frac{\varepsilon_0 s_0}{2}+\frac{\varepsilon_1\gamma_0^2}{2}(1+g_0)\right]$, $s_0=\frac{1}{2\sqrt{3}A_R}\frac{n^2\pi^2}{\hat{b}^2}$, $\gamma_0=1+\frac{s_0\beta_0c_1}{L}$,

$P_0^2=\frac{\rho C_e c_1 L s_0(1+s_0t_0)}{KA_R^2}$, $g_0=-\frac{12}{P_0^2}+\frac{24}{P_0^3}\tanh\left(\frac{P_0}{2}\right)$, $\gamma_1=1\pm\iota\frac{s_1\beta_0c_1}{L}$,

$P_1^2=\frac{\pm\iota s_1\rho C_e c_1 L(1\pm\iota s_1t_0)}{KA_R^2}$, $g_{p_1}=-\frac{12}{P_1^2}+\frac{24}{P_1^3}\tanh\left(\frac{P_1}{2}\right)$.

5.6 Numerical Results and Graphical Discussion

To validate the theoretical findings presented earlier, numerical simulations are conducted. The simulations utilized properties of viscothermoelastic material silicon nitride. Silicon nitride's high stiffness, low density, compatibility with semiconductor and minimal damping are ideal for achieving stable resonant frequencies in resonator devices. These properties make silicon nitride resonators essential components in MEMS, enabling integration with other microscale devices.

Physical parameters for the silicon nitride were adopted based on data provided by [82] as:

$\lambda=2.17\times10^{11};\mu=1.08\times10^{11};\rho=3.20\times10^{3};C_e=630J/Kgdeg;T_0=296^oK;$

$K=43.5;\alpha_0=\alpha_1=6.89\times10^{-13};\beta=2.71\times10^{6};q_0=2\times10^{-7};\omega=1.076Hz$

Dimensions of the rectangular plate are taken as: $L=500\mu m;h=25\mu m,b=250\mu m;$

Non-dimensional deflection has been computed for various modes as per equation (5.30). Figures. $[5.1-5.8]$ illustrate the deflection profiles across the plate dimensions for modes (1, 1), (1, 2), (2, 1), and (2, 2) under harmonic loading conditions. The simulations were performed using MATLAB software, modeling a material silicon nitride. The graphical representations offered visual insights into the effects of different boundary conditions on dimensionless deflection for different modes.

It has been noted that the deflection magnitude is greatest at the centre of the plate and decreases as we move away from the centre in either direction. Additionally, for an SSSS plate, the deflection values follow the pattern $W_{22} < W_{12} = W_{21} < W_{11}$. In contrast, for a CSCS plate, the values are ordered differently as $W_{21} < W_{11} = W_{22} < W_{12}$. The variation in deflection due to different modes is more pronounced in the SSSS plate compared to the CSCS plate.

Figures. $5.9\,[a-b]$ illustrate the front view of deflection profile at the clamped edges and simply supported edges in CSCS plate resp. and Figures. $5.10\,[a-b]$ illustrate the front view of deflection profile at all simply supported edges in SSSS plate. The presence of flatness near the clamped edges in Figures. $5.9\,[a]$ signify zero slope and hence zero rotation, while in case of simple supported edges in Figures. $5.9\,[b]\,, 5.10\,[a-b]$, the absence of flatness clearly depict that bending is allowed here. Also, Figures. $[5.11-5.12]$ illustrate the deflection profile in CSCS and SSSS plate for various time instants. The plots illustrate the system's harmonic oscillations and the response's periodicity. The variation in amplitude over time highlights the effects of viscous damping and thermal relaxation. For practical applications, these findings imply that careful tuning of material damping and excitation frequency can suppress excessive oscillations, thereby enhancing the long-term reliability of MEMS-based resonant systems.

Under uniform loading in the chapter 4, the deflection pattern remains steady and symmetric, with the maximum displacement occurring at the center and gradually diminishing towards the supported or clamped edges. In contrast, harmonic loading induces a time-varying oscillatory deflection characterized by alternating peaks and troughs corresponding to the frequency of excitation. Physically, the uniform loading condition highlights the static stiffness behavior of the structure, while the harmonic loading emphasizes its dynamic resonance response.

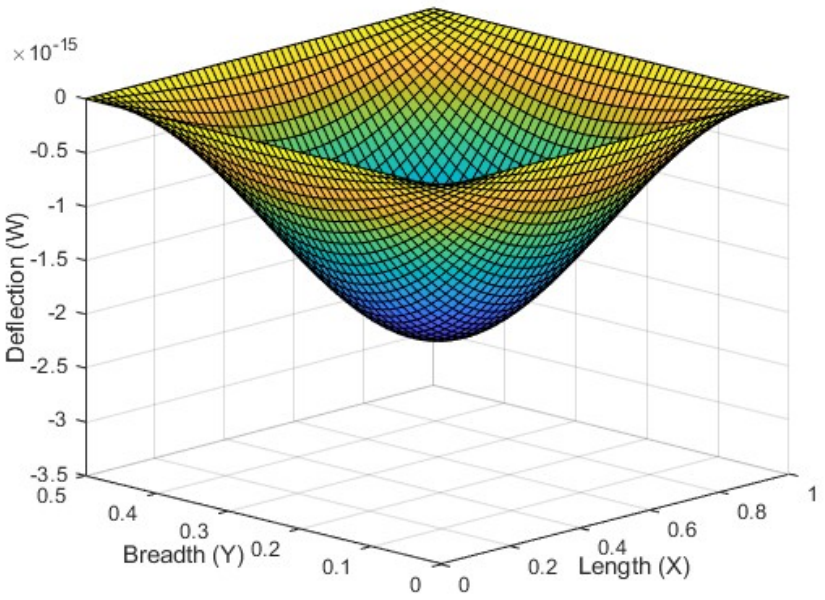

Figure 5.1: Variation of dimensionless deflection for (1,1) mode in viscothermoelastic SSSS plate under harmonic load along the (x,y) dimensions at $t = 5$

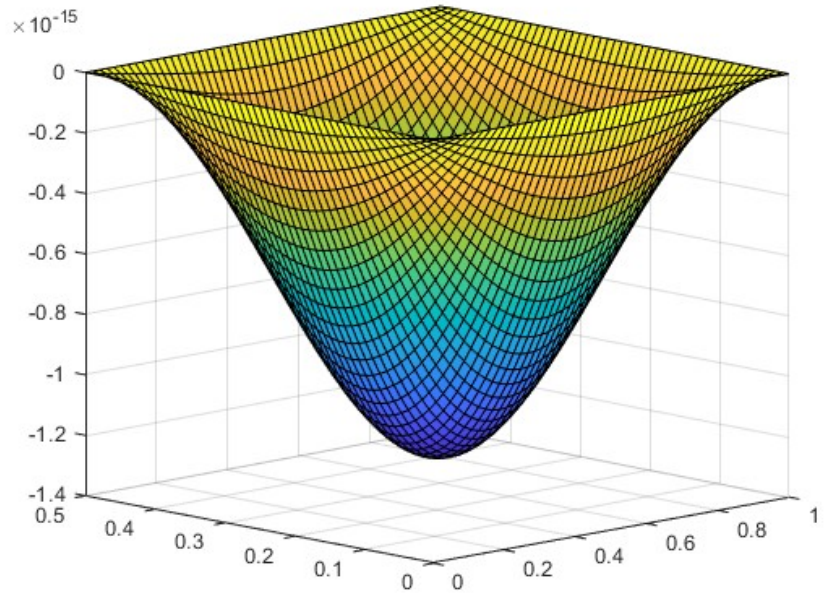

Figure 5.2: Variation of dimensionless deflection for (1,2) mode in viscothermoelastic SSSS plate under harmonic load along the (x,y) dimensions at $t = 5$

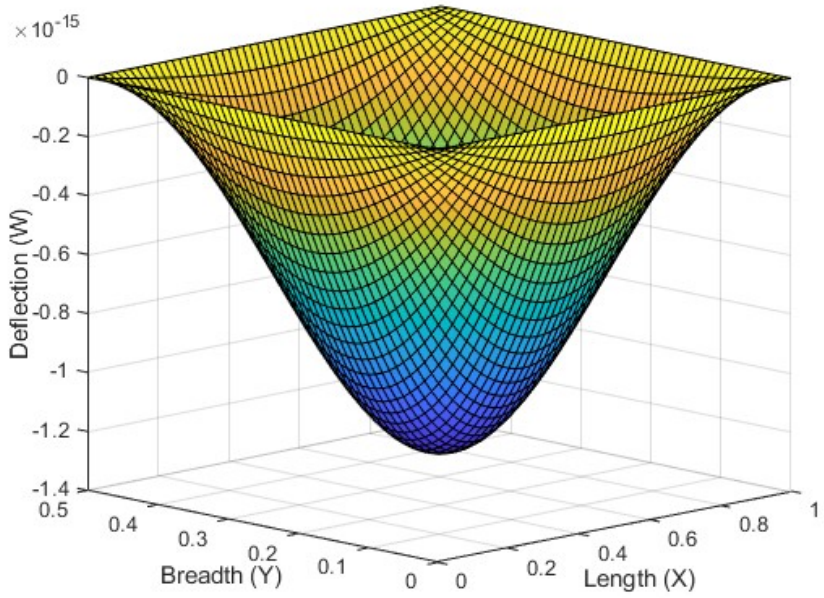

Figure 5.3: Variation of dimensionless deflection for (2,1) mode in viscothermoelastic SSSS plate under harmonic load along the (x, y) dimensions at $t = 5$

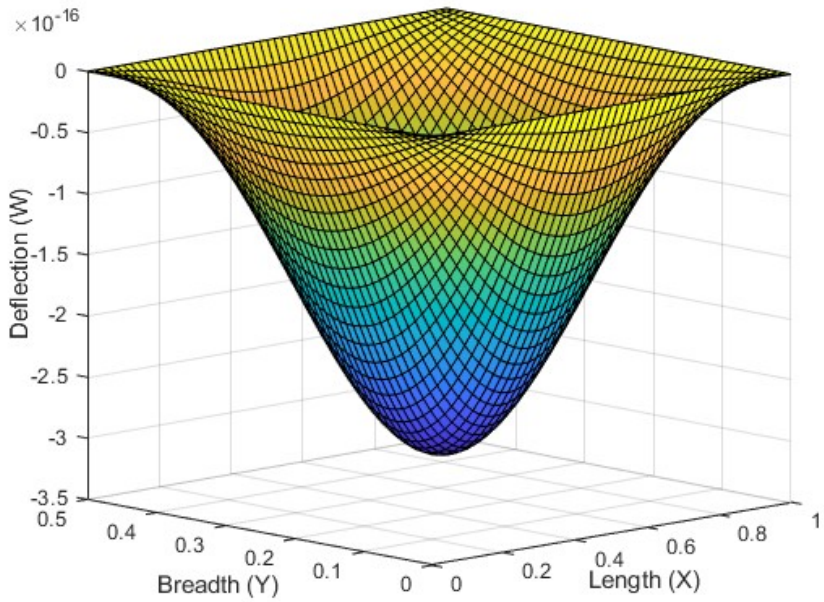

Figure 5.4: Variation of dimensionless deflection for (2,2) mode in viscothermoelastic SSSS plate under harmonic load along the (x, y) dimensions at $t = 5$

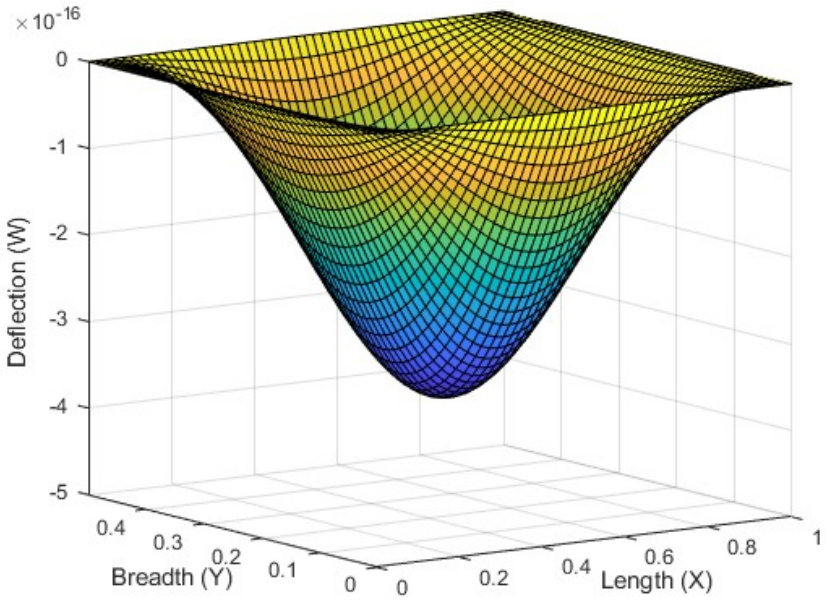

Figure 5.5: Variation of dimensionless deflection for (1,1) mode in viscothermoelastic CSCS plate under harmonic load along the (x, y) dimensions at $t = 5$

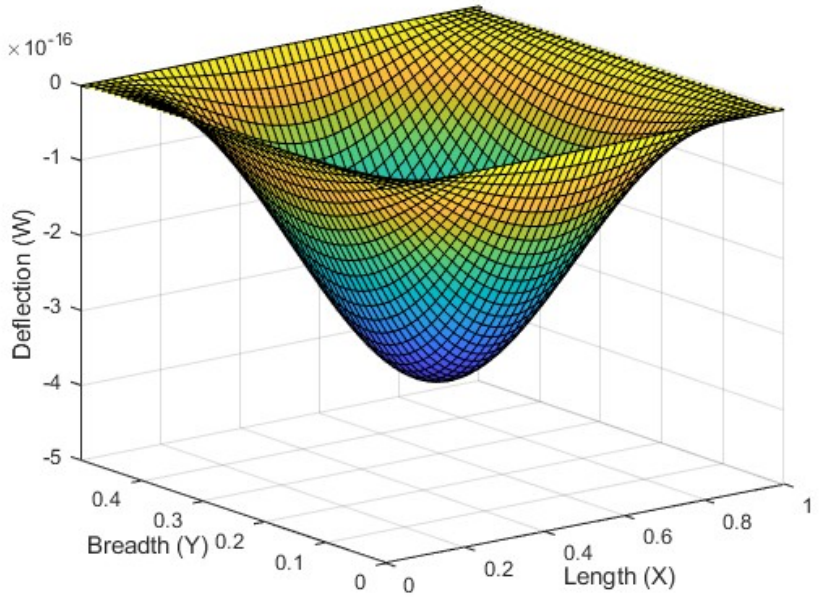

Figure 5.6: Variation of dimensionless deflection for (1,2) mode in viscothermoelastic CSCS plate under harmonic load along the (x, y) dimensions at $t = 5$

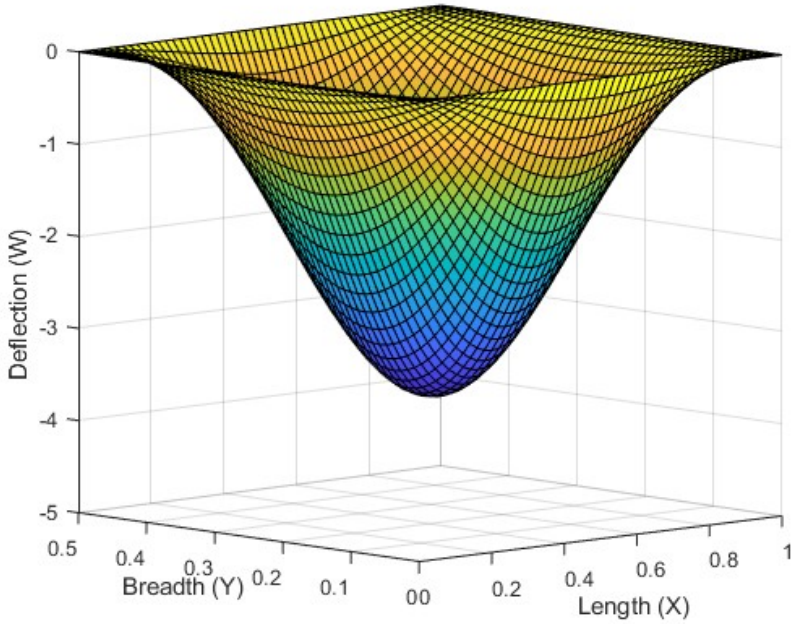

Figure 5.7: Variation of dimensionless deflection for (2,1) mode in viscothermoelastic CSCS plate under harmonic load along the (x, y) dimensions at $t = 5$

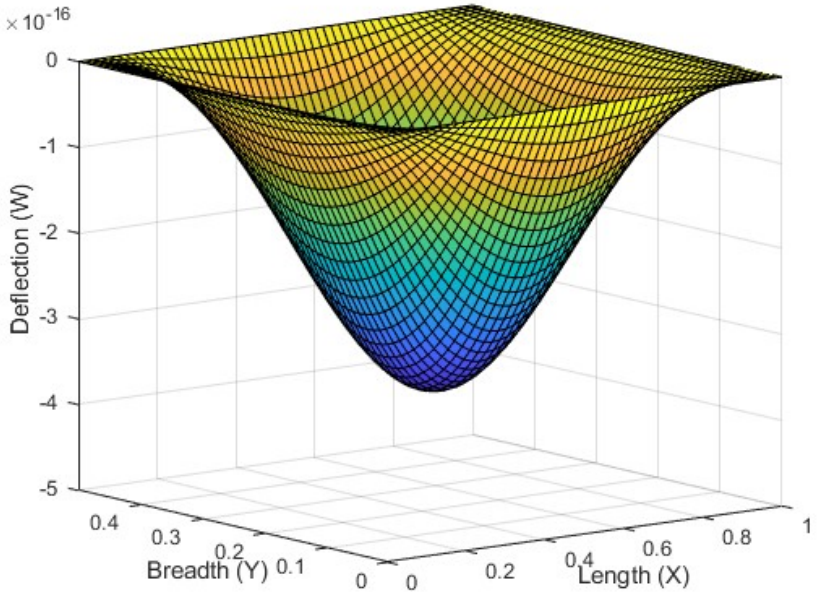

Figure 5.8: Variation of dimensionless deflection for (2,2) mode in viscothermoelastic CSCS plate under harmonic load along the (x, y) dimensions at $t = 5$

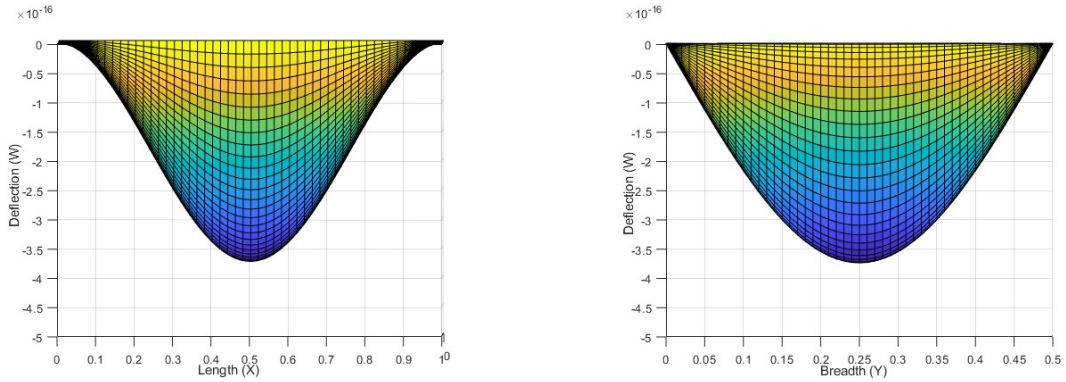

(a) Clamped edges (b) Simply supported edges

Figure 5.9: Front view of dimensionless deflection at the edges for (1,1) mode in viscothermoelastic CSCS plate.

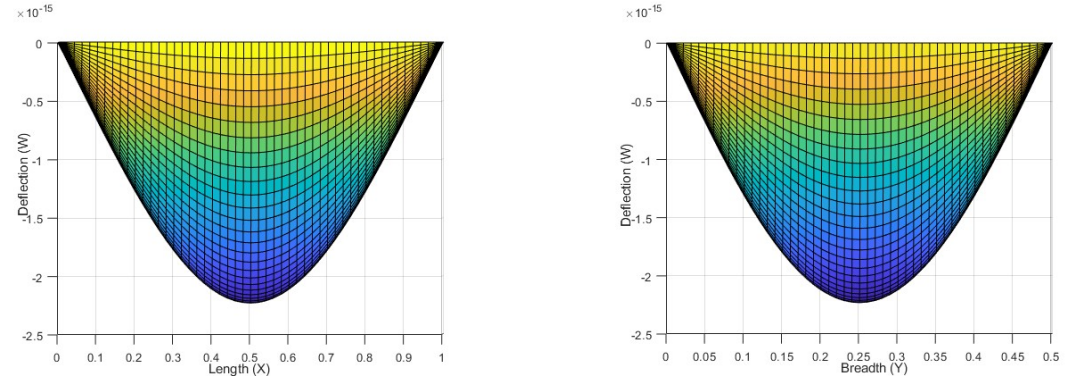

(a) (b)

Figure 5.10: Front view of dimensionless deflection at the simple supported edges for (1,1) mode in viscothermoelastic SSSS plate.

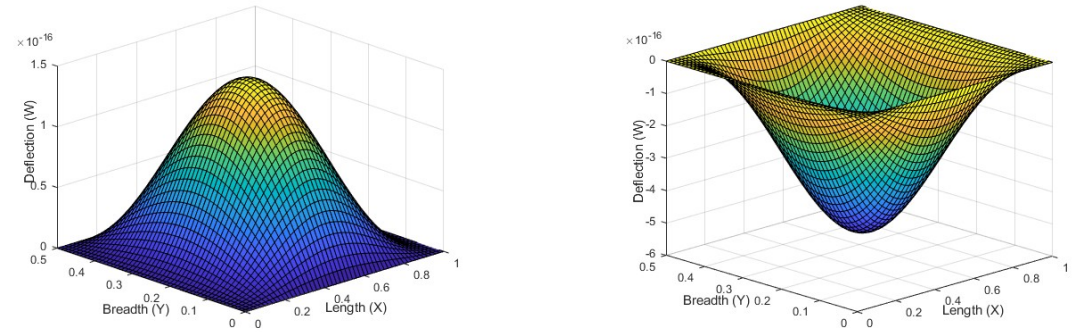

(a) t=10 (b) t=18

Figure 5.11: Variation of dimensionless deflection for (1,1) mode in viscothermoelastic CSCS plate under harmonic load along the (x, y) dimensions for various time

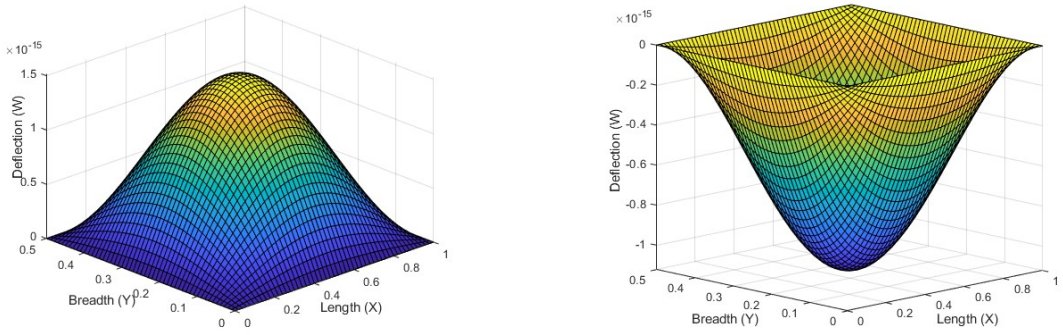

(a) t=10 (b) t=21

Figure 5.12: Variation of dimensionless deflection for (1,1) mode in viscothermoelastic SSSS plate under harmonic load along the (x, y) dimensions for various time

5.7 Conclusion

In the present problem, a study has been carried out to examine the dynamic behaviour of a uniform, isotropic, viscothermoelastic rectangular plate under harmonic loading under various boundary conditions. The analysis has employed the L.T. technique with respect to the time domain and the Finite Fourier sine transform for the space domain. It is concluded that

1. The deflection curve is symmetrical around the centre of the plate. In the case of an SSSS plate, the deflection symmetry is more pronounced along both dimensions compared to a CSCS plate.

2. The maximum deflection occurs at the plate's centre, with its magnitude decreasing gradually as it moves away from the centre in either direction.

3. The variation in deflection due to different modes is more significant in a SSSS plate than in a CSCS plate.

4. The order of deflection for different modes vary under the both set of boundary conditions.

Chapter 6

Concluding Observations

This chapter encapsulates the principal findings of the current study on visco-thermoelastic beam and plate structures subjected to various loading conditions. It emphasizes the principal contributions, indicates the limitations of the current study, and proposes opportunities for future investigation.

6.1 Summary of Findings

This thesis has contributed in study of the deflection behaviour of viscothermoelastic structures such as beams and rectangular plates. Utilizing the Lord-Shulman (LS) generalized thermoelasticity model, the study took into account various loading scenarios and boundary conditions. A combination of analytical modeling, non-dimensional formulation, and numerical evaluation has been employed. The incorporation of thermal relaxation time has resulted in noticeable variations in transient and steady-state responses, particularly discussed for uniform loading in beam. With thermal and viscous coupling, the deflection magnitude and pattern varied significantly, according to comparisons across boundary conditions. Numerical simulation and Graphical representation has demonstrated the deflection profile. Mode-wise analysis has demonstrated that the degree of significant effect on deflection pattern vary with boundary conditions and type of loading. The studies in chapter 2 and 4 confirm that uniform loading can induce dynamic-like responses due to inherent material time-dependence. The results have revealed mode-dependent deflection patterns by illustrating the interaction between loading type and structural geometry.

In Chapter 2, the a visco-thermoelastic beam subjected to uniform loading was examined. Numerical evaluation revealed that the deflection increased uniformly with load intensity, exhibiting a symmetric curvature about the midspan. The maximum non-dimensional deflection occurred at the beam center. Chapter 3 extended the analysis to the beam under harmonic loading. The time-dependent deflection profiles indicated

oscillatory behavior with periodic energy exchange between thermal and elastic fields, highlighting the dominance of dynamic visco-thermoelastic coupling. In Chapter 4, the study of a rectangular plate under uniform loading showed a steady, symmetric deflection surface with a maximum at the center of plate and diminishing smoothly toward the edges. The plate response under uniform pressure thus represents the quasi-static deformation limit of the visco-thermoelastic model. In Chapter 5, the plate under harmonic loading displayed alternating peaks and troughs in deflection consistent with the excitation frequency, reflecting dynamic resonance and energy exchange between thermal and elastic fields, while the shape retained central symmetry. The SSSS plate allowed greater rotational freedom, resulting in higher mid-span deflection and a more flexible deformation profile as compared to CSCS.

6.2 Limitations of the Present Study

While the present study has made important contributions, it is limited to the theory of small deflection and linear material behaviour, assuming the homogeneity and isotropy of the material properties, which fails to reflect actual anisotropic nature, composite or layered structures. From a theoretical perspective, the investigation strictly adhered to the Lord–Shulman model, disregarding alternative generalized thermoelastic formulations like the Green–Lindsay or dual-phase-lag theories. The analysis is restricted to structures of uniform thickness, excluding the possibilities of variable thickness in real life applications.

6.3 Future Scope

The current research can be expanded in various promising directions. Future research may integrate additional generalized thermoelastic models, including the Green–Lindsay theory and dual-phase-lag models. The analysis of deflection can be extended for circular plates, multi-layered or functionally graded materials. The impact of loading can be studied by incorporating anisotropic properties, multi-field coupling such as piezoelectric or magneto-thermoelastic. The methodology can also be extended for the materials with variable thickness to represent the real world materials better.

In conclusion, this thesis has sought to enhance the modeling of visco-thermoelastic structures by integrating thermal and viscous couplings. With appropriate extensions, the results of this work will improve the predictive capacities of visco-thermoelastic

theories and help them be applied to structural analysis and design in the real world.

Bibliography

[1] S. P. Timoshenko, *Strength of Materials, Part I: Elementary Theory and Problems*. New York: D. Van Nostrand Company, 1934.

[2] I. S. Sokolnikoff, *Mathematical Theory of Elasticity*. New York: McGraw-Hill, 1946.

[3] M. A. Biot, "Thermoelasticity and irreversible thermodynamics," *Journal of applied physics*, vol. 27, no. 3, pp. 240–253, 1956.

[4] S. Timoshenko and S. Woinowsky-Krieger, "Theory of plates and shells," 1959.

[5] H. W. Lord and Y. Shulman, "A generalized dynamical theory of thermoelasticity," *Journal of the Mechanics and Physics of Solids*, vol. 15, no. 5, pp. 299–309, 1967.

[6] R. V. Churchill *et al.*, *Operational mathematics*. McGraw-Hill New York, 1972, vol. 1.

[7] W. Nowacki, "The micropolar thermoelasticity," in *Micropolar Elasticity: Symposium Organized by the Department of Mechanics of Solids, June 1972*, Springer, 1974, pp. 105–168.

[8] K. Graff, "Wave motion in elastic solids," *Publication of: Oxford University Press*, 1975.

[9] W. Nowacki, *Dynamic Problems of Thermoelasticity*. Springer Science & Business Media, 1975.

[10] D. Chandrasekharaiah, "Thermoelasticity with second sound: A review," 1986.

[11] A. Drozdov, "A constitutive model in thermoviscoelasticity," *Mechanics research communications*, vol. 23, no. 5, pp. 543–548, 1996.

[12] R. Lifshitz and M. L. Roukes, "Thermoelastic damping in micro-and nanomechanical systems," *Physical review B*, vol. 61, no. 8, p. 5600, 2000.

[13] M. A. Ezzat and A. S. El-Karamany, "The relaxation effects of the volume properties of viscoelastic material in generalized thermoelasticity," *International journal of engineering science*, vol. 41, no. 19, pp. 2281–2298, 2003.

[14] M. A. Ezzat, A. S. El-Karamany, A. A. Samaan, and M. Zakaria, "The relaxation effects of the volume properties of viscoelastic material in generalized thermoelasticity with thermal relaxation," *Journal of thermal stresses*, vol. 26, no. 7, pp. 671–690, 2003.

[15] F. Guo and G. Rogerson, "Thermoelastic coupling effect on a micro-machined beam resonator," *Mechanics research communications*, vol. 30, no. 6, pp. 513–518, 2003.

[16] A. H. Nayfeh and M. I. Younis, "Modeling and simulations of thermoelastic damping in microplates," *Journal of micromechanics and microengineering*, vol. 14, no. 12, p. 1711, 2004.

[17] R. Kumar and S. Choudhary, "Deformation due to time harwortic source in orthotropic micropolar viscoelastic medium," *International Journal of Applied Mechanics and Engineering*, vol. 10, no. 4, pp. 617–629, 2005.

[18] R. Kumar and S. Choudhary, "Disturbance due to a time harmonic source in orthotropic micropolar viscoelastic medium," 2005.

[19] S. Vengallatore, "Analysis of thermoelastic damping in laminated composite micromechanical beam resonators," *Journal of Micromechanics and Microengineering*, vol. 15, no. 12, p. 2398, 2005.

[20] Y. Sun, D. Fang, and A. K. Soh, "Thermoelastic damping in micro-beam resonators," *International Journal of Solids and Structures*, vol. 43, no. 10, pp. 3213–3229, 2006.

[21] S. Prabhakar and S. Vengallatore, "Thermoelastic damping in bilayered micromechanical beam resonators," *Journal of Micromechanics and Microengineering*, vol. 17, no. 3, p. 532, 2007.

[22] O. A. Bauchau and J. I. Craig, *Structural analysis: with applications to aerospace structures*. Springer Science & Business Media, 2009, vol. 163.

[23] X.-X. Guo, Z.-M. Wang, Y. Wang, and Y.-F. Zhou, "Analysis of the coupled thermoelastic vibration for axially moving beam," *Journal of Sound and Vibration*, vol. 325, no. 3, pp. 597–608, 2009.

[24] S. Prabhakar, M. P. Païdoussis, and S. Vengallatore, "Analysis of frequency shifts due to thermoelastic coupling in flexural-mode micromechanical and nanomechanical resonators," *Journal of Sound and Vibration*, vol. 323, no. 1-2, pp. 385–396, 2009.

[25] Y. Sun and M. Saka, "Thermoelastic damping in micro-scale circular plate resonators," *Journal of Sound and Vibration*, vol. 329, no. 3, pp. 328–337, 2010.

[26] B. Yanping and H. Yilong, "Static deflections analysis of micro-cantilevers beam under transverse loading," in *Proceedings of the 9th WSEAS international conference on Circuits, systems, electronics, control & signal processing*, 2010, pp. 17–21.

[27] M. Pustan, S. Paquay, V. Rochus, and J.-C. Golinval, "Modeling and finite element analysis of mechanical behavior of flexible mems components," *Microsystem technologies*, vol. 17, pp. 553–562, 2011.

[28] J. Sharma and D. Grover, "Thermoelastic vibrations in micro-/nano-scale beam resonators with voids," *Journal of Sound and vibration*, vol. 330, no. 12, pp. 2964–2977, 2011.

[29] H. M. Youssef and K. A. Elsibai, "Vibration of nano beam induced by ramp type heating," *World Journal of Nano Science and Engineering*, vol. 1, no. 2, pp. 37–44, 2011.

[30] N. A. Ali and A. K. Mohammadi, "Thermoelastic damping in clamped-clamped annular microplate," *Applied Mechanics and Materials*, vol. 110, pp. 1870–1878, 2012.

[31] D. Grover, "Viscothermoelastic vibrations in micro-scale beam resonators with linearly varying thickness," *Canadian Journal of Physics*, vol. 90, no. 5, pp. 487–496, 2012.

[32] D. Grover and J. Sharma, "Transverse vibrations in piezothermoelastic beam resonators," *Journal of intelligent material systems and structures*, vol. 23, no. 1, pp. 77–84, 2012.

[33] F. Guo, G. Wang, and G. Rogerson, "Analysis of thermoelastic damping in micro- and nanomechanical resonators based on dual-phase-lagging generalized thermoelasticity theory," *International Journal of Engineering Science*, vol. 60, pp. 59–65, 2012.

[34] R. Kumar, V. Chawla, and I. A. Abbas, "Effect of viscosity on wave propagation in anisotropic thermoelastic medium with three-phase-lag model," *Theoretical and Applied Mechanics*, vol. 39, no. 4, pp. 313–341, 2012.

[35] P. Li, Y. Fang, and R. Hu, "Thermoelastic damping in rectangular and circular microplate resonators," *Journal of Sound and Vibration*, vol. 331, no. 3, pp. 721–733, 2012.

[36] J. Sharma and D. Grover, "Thermoelastic vibration analysis of mems/nems plate resonators with voids," *Acta mechanica*, vol. 223, no. 1, pp. 167–187, 2012.

[37] Y. Xu and D. Zhou, "Two-dimensional thermoelastic analysis of beams with variable thickness subjected to thermo-mechanical loads," *Applied Mathematical Modelling*, vol. 36, no. 12, pp. 5818–5829, 2012.

[38] R. M. Christensen, *Theory of viscoelasticity*. Courier Corporation, 2013.

[39] D. Grover, "Transverse vibrations in micro-scale viscothermoelastic beam resonators," *Archive of Applied Mechanics*, vol. 83, pp. 303–314, 2013.

[40] R. Lal and Y. Kumar, "Transverse vibrations of nonhomogeneous rectangular plates with variable thickness," *Mechanics of Advanced Materials and Structures*, vol. 20, no. 4, pp. 264–275, 2013.

[41] J. Sharma, D. Grover, and A. Sangal, "Viscothermoelastic waves-a statistical study," *Journal of Vibration and Control*, vol. 19, no. 8, pp. 1216–1226, 2013.

[42] F. Guo, J. Song, G. Wang, and Y. Zhou, "Analysis of thermoelastic dissipation in circular micro-plate resonators using the generalized thermoelasticity theory of dual-phase-lagging model," *Journal of Sound and Vibration*, vol. 333, no. 11, pp. 2465–2474, 2014.

[43] J. Sharma and R. Kaur, "Transverse vibrations in thermoelastic-diffusive thin micro-beam resonators," *Journal of Thermal Stresses*, vol. 37, no. 11, pp. 1265–1285, 2014.

[44] J. Sharma and R. Kaur, "Analysis of forced vibrations in micro-scale anisotropic thermo-elastic beams due to concentrated loads," *Journal of Thermal Stresses*, vol. 37, no. 1, pp. 93–116, 2014.

[45] A. M. Zenkour and A. E. Abouelregal, "Nonlocal thermoelastic vibrations for variable thermal conductivity nanobeams due to harmonically varying heat," *Journal of Vibroengineering*, vol. 16, no. 8, pp. 3665–3678, 2014.

[46] A. M. Zenkour and A. E. Abouelregal, "Vibration of fg nanobeams induced by sinusoidal pulse-heating via a nonlocal thermoelastic model," *Acta Mechanica*, vol. 225, pp. 3409–3421, 2014.

[47] I. A. Abbas, "Exact solution of thermoelastic damping and frequency shifts in a nano-beam resonator," *International Journal of Structural Stability and Dynamics*, vol. 15, no. 06, p. 1 450 082, 2015.

[48] D. Grover, "Damping in thin circular viscothermoelastic plate resonators," *Canadian Journal of Physics*, vol. 93, no. 12, pp. 1597–1605, 2015.

[49] C. M. Hoang, "Thermoelastic damping depending on vibration modes of nano beam resonator," *Commun. Phys*, vol. 25, no. 4, pp. 317–325, 2015.

[50] R. Lal and R. Saini, "Transverse vibrations of nonhomogeneous rectangular kirchhoff plates of variable thickness," in *Mathematical Analysis and its Applications: Roorkee, India, December 2014*, Springer, 2015, pp. 609–618.

[51] D. V. Parayil, S. S. Kulkarni, and D. N. Pawaskar, "Analytical and numerical solutions for thick beams with thermoelastic damping," *International Journal of Mechanical Sciences*, vol. 94, pp. 10–19, 2015.

[52] J. Sharma and R. Kaur, "Response of anisotropic thermoelastic micro-beam resonators under dynamic loads," *Applied Mathematical Modelling*, vol. 39, no. 10-11, pp. 2929–2941, 2015.

[53] A. M. Zenkour and A. E. Abouelregal, "Thermoelastic vibration of an axially moving microbeam subjected to sinusoidal pulse heating," *International Journal of Structural Stability and Dynamics*, vol. 15, no. 06, p. 1 450 081, 2015.

[54] D. R. Bland, *The theory of linear viscoelasticity*. Courier Dover Publications, 2016.

[55] U. S. Rana and Robin, "Study of damped vibration of non-homogeneous rectangular plate of variable thickness," *International Journal of Engineering and Applied Sciences*, vol. 3, no. 8, pp. 42–50, 2016.

[56] H. Zhang, T. Kim, G. Choi, and H. H. Cho, "Thermoelastic damping in micro-and nanomechanical beam resonators considering size effects," *International Journal of Heat and Mass Transfer*, vol. 103, pp. 783–790, 2016.

[57] N. Alghamdi, "Dual-phase-lagging thermoelastic damping vibration in micro-nano scale beam resonators with voids," *Int J Multidiscip Curr Res*, vol. 5, pp. 71–78, 2017.

[58] S.-R. Li, X. Xu, and S. Chen, "Analysis of thermoelastic damping of functionally graded material beam resonators," *Composite Structures*, vol. 182, pp. 728–736, 2017.

[59] D. Mashat, A. Zenkour, and A. Abouelregal, "Thermoviscoelastic vibrations of a micro-scale beam subjected to sinusoidal pulse heating," *International Journal of Acoustics and Vibration*, vol. 22, no. 2, pp. 260–269, 2017.

[60] G. Partap and N. Chugh, "Deflection analysis of micro-scale microstretch thermoelastic beam resonators under harmonic loading," *Applied Mathematical Modelling*, vol. 46, pp. 16–27, 2017.

[61] G. Partap and N. Chugh, "Thermoelastic damping in microstretch thermoelastic rectangular plate," *Microsystem Technologies*, vol. 23, pp. 5875–5886, 2017.

[62] D. Grover and R. Seth, "Viscothermoelastic micro-scale beam resonators based on dual-phase lagging model," *Microsystem Technologies*, vol. 24, pp. 1667–1672, 2018.

[63] S. Liu, J. Ma, X. Yang, Y. Sun, J. Yang, and X. Wang, "Theoretical 3d model of thermoelastic damping in laminated rectangular plate resonators," *International Journal of Structural Stability and Dynamics*, vol. 18, no. 12, p. 1 850 158, 2018.

[64] N. A. Alghamdi, "Vibration of circular micro-ceramic (si3n4) plate resonators in the context of the generalized viscothermoelastic dual-phase-lagging theory," *Advances in Mechanical Engineering*, vol. 11, no. 11, pp. 1–8, 2019.

[65] D. Grover, "Clamped-free micro-scale transversely isotropic thermoelastic beam resonators," *Microsystem Technologies*, vol. 25, no. 11, pp. 4269–4276, 2019.

[66] D. Grover and R. Seth, "Generalized viscothermoelasticity theory of dual-phase-lagging model for damping analysis in circular micro-plate resonators," *Mechanics of Time-Dependent Materials*, vol. 23, pp. 119–132, 2019.

[67] G. Partap and N. Chugh, "Study of deflection and damping in microbeam resonator based on microstretch thermoelastic theory," *Mechanics of Advanced Materials and Structures*, vol. 26, no. 2, pp. 189–197, 2019.

[68] S. S. Rao, *Vibration of continuous systems*. John Wiley & Sons, 2019.

[69] H. Zhang, S. Kim, G. Choi, D. Xie, and H. H. Cho, "Effect of temperature dependent material properties on thermoelastic damping in thin beams," *International Journal of Heat and Mass Transfer*, vol. 139, pp. 1031–1036, 2019.

[70] W. Zuo, P. Li, J. Du, and J. Huang, "Thermoelastic damping in trilayered microplate resonators," *International Journal of Mechanical Sciences*, vol. 151, pp. 595–608, 2019.

[71] A. E. Abouelregal and W. W. Mohammed, "Effects of nonlocal thermoelasticity on nanoscale beams based on couple stress theory," *Mathematical Methods in the Applied Sciences*, 2020.

[72] N. Alcheikh, L. Kosuru, S. Kazmi, and M. I. Younis, "In-plane air damping of micro-and nano-mechanical resonators," *Journal of Micromechanics and Microengineering*, vol. 30, no. 3, p. 035 007, 2020.

[73] N. A. Alghamdi, "The vibration of a viscothermoelastic nanobeam of silicon nitride based on dual-phase-lage heat conduction model and subjected to ramp-type heating," *AIP Advances*, vol. 10, no. 10, p. 105 112, 2020.

[74] E. Pierro, "Damping control in viscoelastic beam dynamics," *Journal of Vibration and Control*, vol. 26, no. 19-20, pp. 1753–1764, 2020.

[75] T. Saeed, I. Abbas, and M. Marin, "A gl model on thermo-elastic interaction in a poroelastic material using finite element method," *Symmetry*, vol. 12, no. 3, p. 488, 2020.

[76] H. M. Youssef, A. A. El-Bary, H. M. Atef, and A. H. El-Sharif, "Numerical analysis of the damage mechanics variable and vibration of a viscothermoelastic microbeam with variable thermal conductivity," *Journal of Vibroengineering*, vol. 23, no. 1, pp. 75–95, Nov. 2020.

[77] A. E. Abouelregal, "Thermoelastic fractional derivative model for exciting viscoelastic microbeam resting on winkler foundation," *Journal of vibration and control*, vol. 27, no. 17-18, pp. 2123–2135, 2021.

[78] N. Chugh and G. Partap, "Study of thermoelastic damping in microstretch thermoelastic thin circular plate," *Journal of Vibration Engineering & Technologies*, vol. 9, pp. 105–114, 2021.

[79] B. Gu and T. He, "Investigation of thermoelastic wave propagation in euler–bernoulli beam via nonlocal strain gradient elasticity and gn theory," *Journal of Vibration Engineering & Technologies*, vol. 9, no. 5, pp. 715–724, 2021.

[80] R. Kumar and R. Kumar, "Effect of two-temperature parameter on thermoelastic vibration in micro and nano beam resonator," *European Journal of Mechanics-A/Solids*, vol. 89, p. 104 310, 2021.

[81] H. M. Youssef and A. A. El-Bary, "Influence of the mechanical damage on vibration of a viscothermoelastic circular microplate resonator based on dual-phase-lag heat conduction," *Mechanics of Time-Dependent Materials*, vol. 25, no. 3, pp. 473–493, 2021.

[82] H. M. Youssef and E. A. Al-Lehaibi, "The vibration of a viscothermoelastic nanobeam of silicon nitride with variable thermal conductivity induced by ramp-type thermal loading," *Journal of Thermal Analysis and Calorimetry*, vol. 146, pp. 2387–2402, 2021.

[83] N. A. Alghamdi and A. A. Alosaimi, "The vibration of a simply supported viscothermoelastic nano-beam of silicon nitride induced by thermal shock," *Int. J. of Multidisciplinary and Current research*, vol. 10, no. 2, pp. 124–131, 2022.

[84] Z. Qi, W. Peng, and T. He, "Investigation on the thermoelastic response of a nanobeam in modified couple stress theory considering size-dependent and memory-dependent effects," *Journal of Thermal Stresses*, vol. 45, no. 10, pp. 773–792, 2022.

[85] A. E. Abouelregal and H. E. Dargail, "Memory and dynamic response of a thermoelastic functionally graded nanobeams due to a periodic heat flux," *Mechanics Based Design of Structures and Machines*, vol. 51, no. 4, pp. 2154–2176, 2023.

[86] D. Grover, "Analysis of thermoelastic damping and modeling of piezothermoelastic plate resonators with voids," *International Journal for Computational Methods in Engineering Science and Mechanics*, vol. 24, no. 3, pp. 211–226, 2023.

[87] S. Guha, A. K. Singh, and S. Singh, "Thermoelastic damping and frequency shift of different micro-scale piezoelectro-magneto-thermoelastic beams," *Physica Scripta*, vol. 99, no. 1, p. 015 203, 2023.

[88] N. Mungle, P. Singh, S. Prayagi, and D. Mate, "Determination of deflection function in a rectangular body.," *Journal of Advanced Zoology*, vol. 44, no. 5s, pp. 1726–1730, 2023.

[89] K. Singh, I. Kaur, and E.-M. Craciun, "Study of transversely isotropic viscobeam with memory-dependent derivative," *Mathematics*, vol. 11, no. 21, p. 4416, 2023.

[90] A. Srivastava and S. Mukhopadhyay, "Analysis of the dynamic responses of a piezothermoelastic microbeam resonator under dual-phase-lag heat conduction," *Waves in Random and Complex Media*, pp. 1–22, 2024.

[91] H. M. Youssef and A. A. El-Bary, "The influence of the mechanical damage on a viscothermoelastic nanobeam due to ramp-type heating under green-naghdi theory type-ii," *The Journal of Strain Analysis for Engineering Design*, vol. 59, no. 1, pp. 44–55, 2024.

[92] A. Duhan, R. K. Sahrawat, K. Kumar, and M. Kumar, "Vibrations in piezothermoelastic micro-/nanobeam with voids utilizing modified couple stress theory," *Mechanics of Advanced Materials and Structures*, vol. 32, no. 12, pp. 2718–2731, 2025.

[93] S. Mondal and A. Sur, "Piezothermoelastic vibrations of microbeam resonator with memory effects," *Mechanics of Time-Dependent Materials*, vol. 29, no. 1, pp. 1–21, 2025.

[94] S. Mondal and A. Sur, "Studies on piezoelectric vibrations in thermoelastic microbeam resonator with memory and nonlocal effects," *The Journal of Strain Analysis for Engineering Design*, vol. 60, no. 3, pp. 180–195, 2025.

[95] A. Srivastava and S. Mukhopadhyay, "Vibration analysis of a transversely isotropic piezothermoelastic beam resonators under nonlocal strain gradient theory with dpl model," *Acta Mechanica*, vol. 236, no. 2, pp. 1071–1090, 2025.

List of Publications

1. Deepti Chopra, Prince Singh, ”Analysis of Deflection in Visco-Thermoelastic Beam Resonators Subjected to Harmonic Loading”, *International Journal of Applied Mechanics and Engineering*, 27(2):35-52 2022, DOI: 10.2478/ijame-2022-0018 **(Scopus, Impact factor: 0.89, SJR: 0.225, Q4)**

2. Deepti Chopra, Prince Singh, ”Visco-thermoelastic Rectangular plate under uniform Loading: A Study of Deflection”, *Nonlinear Engineering*, **(Accepted, Scopus, Impact factor: 2.4, SJR: 0.423, Q1)**

3. Deepti Chopra, Prince Singh, ”Modeling and analysis of transverse vibrations in Visco-thermoelastic Rectangular plate of Silicon Nitride due to Harmonic loading”, *Journal of Mathematical Sciences*, **(Accepted, Scopus, SJR: 0.28, Q4)**

4. Deepti Chopra, Prince Singh, ”Static and Dynamic analysis of Uniform load on transverse vibrations in Visco-thermoelastic beam”, **(Communicated)**.

Conferences Attended/Papers Presented

1. Presented paper in Multi-disciplinary International Conference on Indian Culture, Science and Traditions held at Himalayan Forest Research Institute, Shimla from Nov 13, 2021 to Nov15, 2021.

2. Presented paper in National Conference on Frontiers in Theoretical and Experimental Physics sponsored by DBT, Govt. of India, held at DAV College Jalandhar from Sept 18, 2024 to Sept 19, 2024.